ALFRED-WEGENER-INSTITUT
HELMHOLTZ-ZENTRUM FÜR POLAR- UND MEERESFORSCHUNG

683
2014

Berichte
zur Polar- und Meeresforschung

Reports on Polar and Marine Research

The Expedition PS83 of the Research Vessel POLARSTERN to the Atlantic Ocean in 2014

Edited by
Hartwig Deneke
with contributions of the participants

HELMHOLTZ GEMEINSCHAFT

Die Berichte zur Polar- und Meeresforschung werden vom Alfred-Wegener-Institut, Helmholtz-Zentrum für Polar- und Meeresforschung (AWI) in Bremerhaven, Deutschland, in Fortsetzung der vormaligen Berichte zur Polarforschung herausgegeben. Sie erscheinen in unregelmäßiger Abfolge.

Die Berichte zur Polar- und Meeresforschung enthalten Darstellungen und Ergebnisse der vom AWI selbst oder mit seiner Unterstützung durchgeführten Forschungsarbeiten in den Polargebieten und in den Meeren.

Die Publikationen umfassen Expeditionsberichte der vom AWI betriebenen Schiffe, Flugzeuge und Stationen, Forschungsergebnisse (inkl. Dissertationen) des Instituts und des Archivs für deutsche Polarforschung, sowie Abstracts und Proceedings von nationalen und internationalen Tagungen und Workshops des AWI.

Die Beiträge geben nicht notwendigerweise die Auffassung des AWI wider.

Herausgeber
Dr. Horst Bornemann

Redaktionelle Bearbeitung und Layout
Birgit Chiaventone

Alfred-Wegener-Institut
Helmholtz-Zentrum für Polar- und Meeresforschung
Am Handeshafen 12
27570 Bremerhaven
Germany

www.awi.de
www.reports.awi.de

Der Erstautor bzw. herausgebende Autor eines Bandes der Berichte zur Polar- und Meeresforschung versichert, dass er über alle Rechte am Werk verfügt und überträgt sämtliche Rechte auch im Namen seiner Koautoren an das AWI. Ein einfaches Nutzungsrecht verbleibt, wenn nicht anders angegeben, beim Autor (bei den Autoren). Das AWI beansprucht die Publikation der eingereichten Manuskripte über sein Repositorium ePIC (electronic Publication Information Center, s. Innenseite am Rückdeckel) mit optionalem print-on-demand.

The Reports on Polar and Marine Research are issued by the Alfred Wegener Institute, Helmholtz Centre for Polar and Marine Research (AWI) in Bremerhaven, Germany, succeeding the former Reports on Polar Research. They are published at irregular intervals.

The Reports on Polar and Marine Research contain presentations and results of research activities in polar regions and in the seas either carried out by the AWI or with its support.

Publications comprise expedition reports of the ships, aircrafts, and stations operated by the AWI, research results (incl. dissertations) of the Institute and the Archiv für deutsche Polarforschung, as well as abstracts and proceedings of national and international conferences and workshops of the AWI.

The papers contained in the Reports do not necessarily reflect the opinion of the AWI.

Editor
Dr. Horst Bornemann

Editorial editing and layout
Birgit Chiaventone

Alfred-Wegener-Institut
Helmholtz-Zentrum für Polar- und Meeresforschung
Am Handeshafen 12
27570 Bremerhaven
Germany

www.awi.de
www.reports.awi.de

The first or editing author of an issue of Reports on Polar and Marine Research ensures that he possesses all rights of the opus, and transfers all rights to the AWI, inlcuding those associated with the co-authors. The non-exclusive right of use (einfaches Nutzungsrecht) remains with the author unless stated otherwise. The AWI reserves the right to publish the submitted articles in its repository ePIC (electronic Publication Information Center, see inside page of verso) with the option to "print-on-demand".

Titel: Treffen der deutschen Forschungsschiffe Polarstern (links) und Meteor (rechts) am 21. März 2014 auf dem Atlantik bei 21°N 11°W (Foto von Dominik Nachtsheim, Alfred-Wegener-Institut, von einem Schlauchboot aus aufgenommen).

Cover:Rendevouz of the German research vessels Polarstern (left) and Meteor (right) on the 21st of March 2014 on the Atlantic at 21°N 11°W (picture taken by Dominik Nachtsheim, Alfred-Wegener-Institut, from a zodiac).

The Expedition PS83 of the Research Vessel POLARSTERN to the Atlantic Ocean in 2014

Edited by

Hartwig Deneke

with contributions of the participants

Please cite or link this publication using the identifiers
hdl:10013/epic.44670 or http://hdl.handle.net/10013/epic.44670 and
doi:10.2312/BzPM_0683_2014 or http://doi.org/10.2312/BzPM_0683_2014

ISSN 1866-3192

PS83

(ANT-XXIX/10)

8 March 2014 – 14 April 2014

Cape Town – Bremerhaven

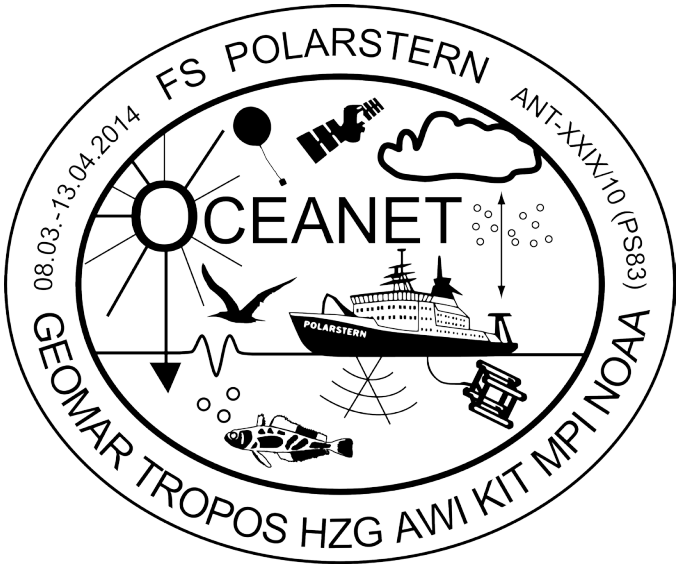

Chief scientist
Hartwig Deneke

Coordinator
Rainer Knust

Contents

1. FAHRTVERLAUF UND ZUSAMMENFASSUNG

Hartwig Deneke TROPOS

Mit dem Abschluss des Süd-Nordtransekts PS83 (ANT-XXIX/10) geht eine außergewöhnlich lange Forschungskampagne des Forschungseisbrechers *Polarstern* auf der Südhalbkugel zu Ende. Nach 1,5 Jahren inklusive Überwinterung in der Antarktis brach die *Polarstern* am 8. März 2014 gegen 22 Uhr von Kapstadt mit 28 Wissenschaftlern und 42 Besatzungsmitgliedern leicht verspätet in die Heimat auf. Am 23. März traf die *Polarstern* auf hoher See bei 11°N 34° das deutsche Forschungsschiff *Meteor*, eine willkommene Abwechslung im Forschungsalltag und die Chance, das jeweils andere Schiff zu besuchen und sich mit Kollegen auszutauschen. Bei einem Zwischenstopp in Gran Canaria am 1. April kamen weitere 13 Fahrtteilnehmer an Bord. Am 13.4. erreichte die *Polarstern* gegen 12 Uhr die Nordschleuse in Bremerhaven, um dann gegen 15 Uhr am Kai festzumachen.

Dieser letzte Fahrtabschnitt wurde wiederum für detaillierte Beobachtungen der Atmosphäre zu Aerosolpartikeln, Wolken und Spurengasen, und zur Untersuchung von Austauschprozessen zwischen Ozean und Atmosphäre im Rahmen des OCEANET Programms genutzt. Die Instrumentierung an Bord wurde erstmals durch ein Radar des NOAA Earth System Research Laboratory ergänzt, dass der Vertikalprofilierung von Wolken diente. Diese verbesserten Beobachtungsmöglichkeiten wurden zu einem Vergleich mit den Messdaten der Erdbeobachtungssatelliten Cloudsat und Calipso genutzt, die ebenfalls ein Wolkenradar und ein Aerosol- und Wolkenlidar tragen. Hierfür wurde die Route der *Polarstern* dergestalt angepasst, dass während der Überflüge eine bestmögliche Übereinstimmung des Kurses mit der Satellitenumlaufbahn erzielt wurde. Außerdem fanden zum ersten Mal spektroskopische Messungen des Gehalts von Kohlendioxid und Methan statt. Entlang des Transekts wurden des Weiteren Sichtungsdaten zur Verbreitung von Meeresvögeln und -säugern erhoben, sowie mehrere Aquarien mit Fischen aus der Antarktis nach Bremerhaven ans Alfred-Wegener-Institut überführt. Auf dem letzten Teil der Fahrt nach dem Stopp in Gran Canaria fanden mehrere Instrumentenerprobungen statt. So kam erstmalig das Schleppsystem TRIAXUS auf *Polarstern* zum Einsatz, und wurde auf seine Leistungsfähigkeit hin untersucht. Ebenso wurde ein detailliertes Testprogramm zur Abnahme des Fächerecholots Hydrosweep DS3 bearbeitet und Vergleichsmessungen des Wellenradars WaMoS II mit einer Wellenboje durchgeführt. Abschließend lässt sich festhalten, dass PS83 (ANT-XXIX/10) eine sehr erfolgreiche Fahrt war und ohne nennenswerte Probleme verlief. Im Namen aller Wissenschaftler möchte ich der Mannschaft an dieser Stelle unseren herzlichen Dank für die Unterstützung und angenehme Atmosphäre an Bord aussprechen.

CRUISE NARRATIVE AND SUMMARY

As final cruise leg, the South-North transect PS83 (ANT-XXIX/10) ended an exceptionally long research campaign in the Southern Hemisphere. After 1.5 years and overwintering in Antarctica, *Polarstern* commenced the return cruise from Cape Town to its home port on March 8, 2014, with a slight delay at approximately 10 pm. On board, there were 28 scientists and 42 crew members. On 23 March, *Polarstern* met the German research vessel *Meteor* at 21°N 11°W at high seas, a welcome break in the daily routine and a chance for scientists and crew members to visit the respective other ship and for discussions with colleagues. Another 13 cruise participants came on board in the port of Las Palmas during an intermediate stop on April 1st. On April 13, *Polarstern* reached the Northern Lock in Bremerhaven, and finally docked at the about 3 pm.

This last cruise leg was again used for detailed observations of the atmosphere, particularly aerosols, clouds and greenhouse gases, and the exchange between ocean and atmosphere in the frame of the OCEANET programme. For the first time the instrumentation on board was complemented by cloud radar from NOAA's Earth System Research Laboratory for vertical profiling of clouds. This opportunity was used for a comparison of our observations with those from the earth-observing satellites Cloudsat and Calipso, which also carry a cloud radar and aerosol-cloud lidar. For this purpose, the course of *Polarstern* was adjusted to exactly match the satellite orbits during the overflights. As further addition, spectroscopic measurements of the greenhouse gases carbon dioxide and methane were carried out during the cruise. Along the transect, observations of marine birds and mammals were made, and aquaria from Antarctica with fish captured during the previous cruise leg were transported back to the Alfred Wegner Institute. On the last part of the cruise after the stop in Gran Canaria, several instrumental tests were carried out. For the first time the towed vehicle TRIAXUS was tested on board. Detailed tests of the multibeam echo sounder Hydrosweep DS3 were carried out, and measurements of the wave radar WaMoS II were compared against results from a wave buoy. Altogether, PS83 (ANT-XXIX/10) was a very successful cruise without significant problems. On behalf of all scientists, I would like to take the opportunity here to sincerely thank the crew for their support and the pleasant atmosphere on board.

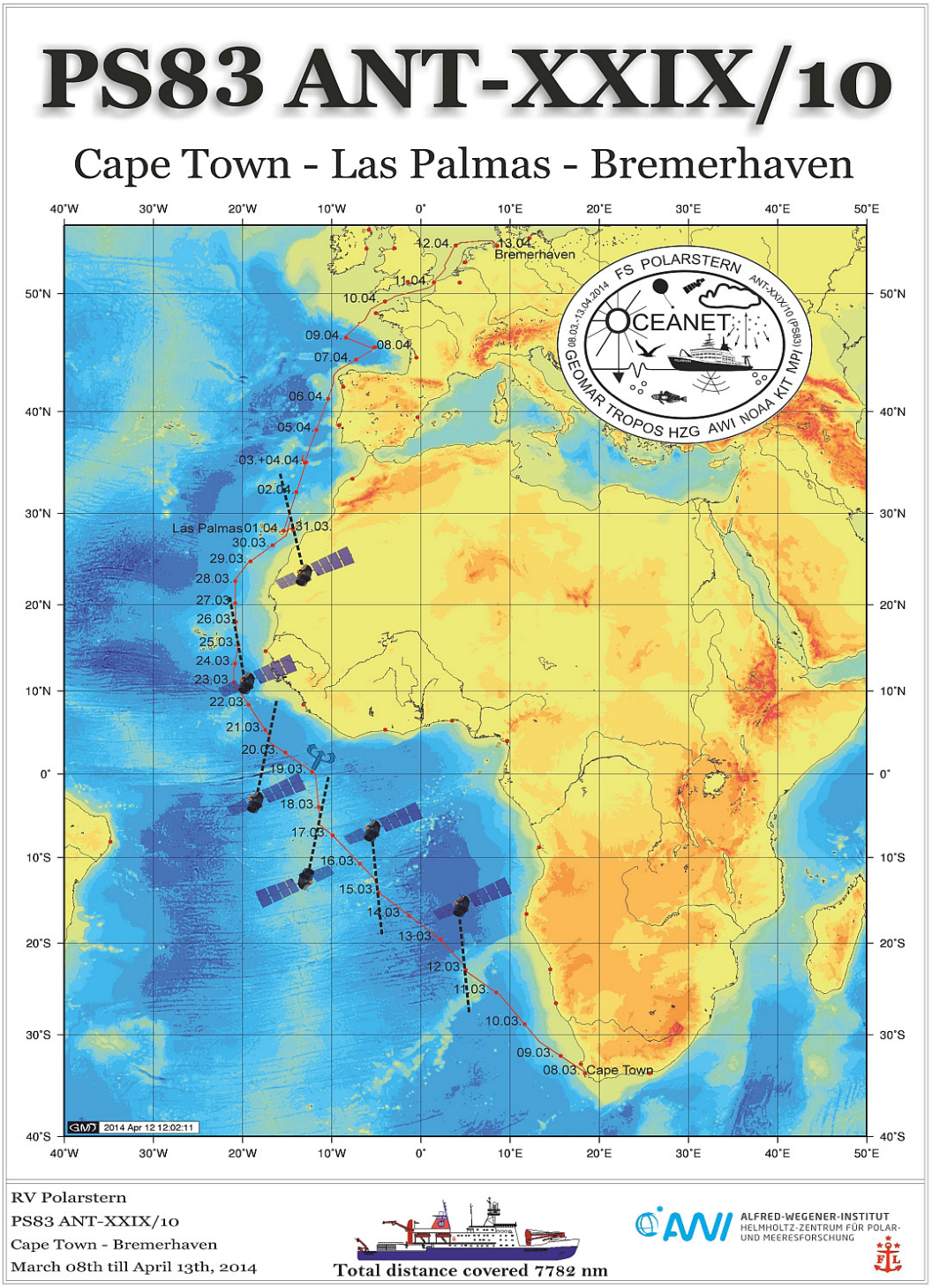

Abb. 1.1: Fahrtroute der Polarstern während der Expedition PS83 (ANT-XXIX/10) (PS83); Mastertrack s. http://doi.pangaea.de/10.1594/PANGAEA.832511

Fig. 1.1: Cruise track of Polarstern during the expedition PS83 (ANT-XXIX/10) (PS83); Mastertrack s. http://doi.pangaea.de/10.1594/PANGAEA.832511

2. WEATHER CONDITIONS

Dipl.-Met. Max Miller, DWD
Juliane Hempelt, DWD

On Saturday, March 08 2014, the local wind system “Cape Doctor” got the dominant feature at Cape Town. In the evening (11:00 pm) *Polarstern* left the harbour for the campaign PS83 (ANT-XXIX/10). South-easterly winds at Bft 6 to 7 and gusts up to 8, clear skies and 18°C were registered. The stormy tail winds (SSE 7 to 8 and swell around 4 m) continued on Sunday, caused by a strong high pressure area east of Gough Island and a secondary low over Namibia. On Monday (March 10) *Polarstern* departed from the area of strongest pressure gradient and winds abated.

From Tuesday (March 11) on we sailed the southern trade wind zone for one week. South-easterly winds at Bft 4 prevailed and increased only for short times up to Bft 5. Only isolated showers could be observed.

During the night to Wednesday (March 19) and almost at the Equator we reached the inner tropical convergence zone. While steaming the ITCZ we registered some heavy showers, but no thunderstorms. Only sheet lightning indicated stronger convection in the surrounding area.

On Friday (March 21) *Polarstern* left the ITCZ, entered the northern trade wind zone and sailed it for one week until Friday (March 28) at a prevailing wind force 5. At the end of the period winds increased up to Bft 6 and for short times Bft 7.

On Saturday (March 29) a high west of the Azores built a ridge towards Morocco. Therefore winds abated and became light and variable on Sunday (March 30).

On Monday (March 31) a low west of the Bay of Biscay got the dominant feature. It extended south and was renewed by several secondary lows. Winds veered southwest and increased Bft 5 to 6. But soon the lee of Canary Islands caused decreasing wind force.

On Tuesday morning (April 01 , 10:00 am) *Polarstern* reached Las Palmas. While staying there we measured variable winds with maximum at Bft 4. After leaving again (03:15 pm) we sailed the lee of Canary Islands for one more hour. But afterwards winds veered abruptly southwest to west and increased from Bft 4 up to Bft 7 and the expected cold front approached. On Wednesday (April 02) frequent showers were present at westerly winds Bft 6 to 7 and swell around 4 m. But south of the Azores a new high formed and built a ridge east. On Thursday (April 03) we entered the ridge west of Gibraltar and winds abated.

Near the Azores a trough approached. It moved east and caused increasing south-westerly to southerly winds along the coast of Portugal. Entering the Bay of Biscay during the night to Monday (April 07) south-westerly winds peaked at Bft 7. Around noon on Monday the cold front passed our area and winds started to abate.

On Tuesday (April 08) a high reached the Bay of Biscay and weak winds veered east.

Passing the English Channel we observed only light to moderate winds and a first cold front weakened. During the night to Sunday (April 13) another cold front crossed the German Bight southeast and westerly winds increased up to Bft 6 to 7.

On early Sunday afternoon, April 13 2014, *Polarstern* reached Bremerhaven at strong and gusty westerly winds and isolated showers.

For further statistics see Fig. 2.1 – Fig. 2.3.

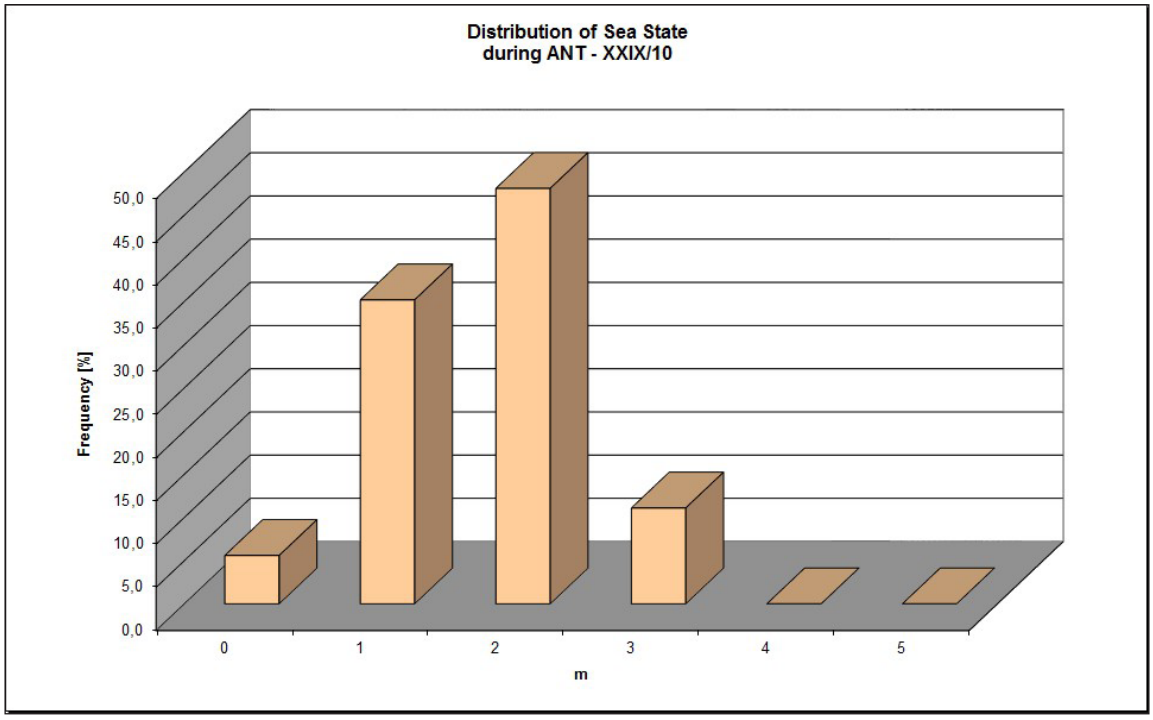

Fig. 2.1: Distribution of sea state during PS83 (ANT-XXIX/10)

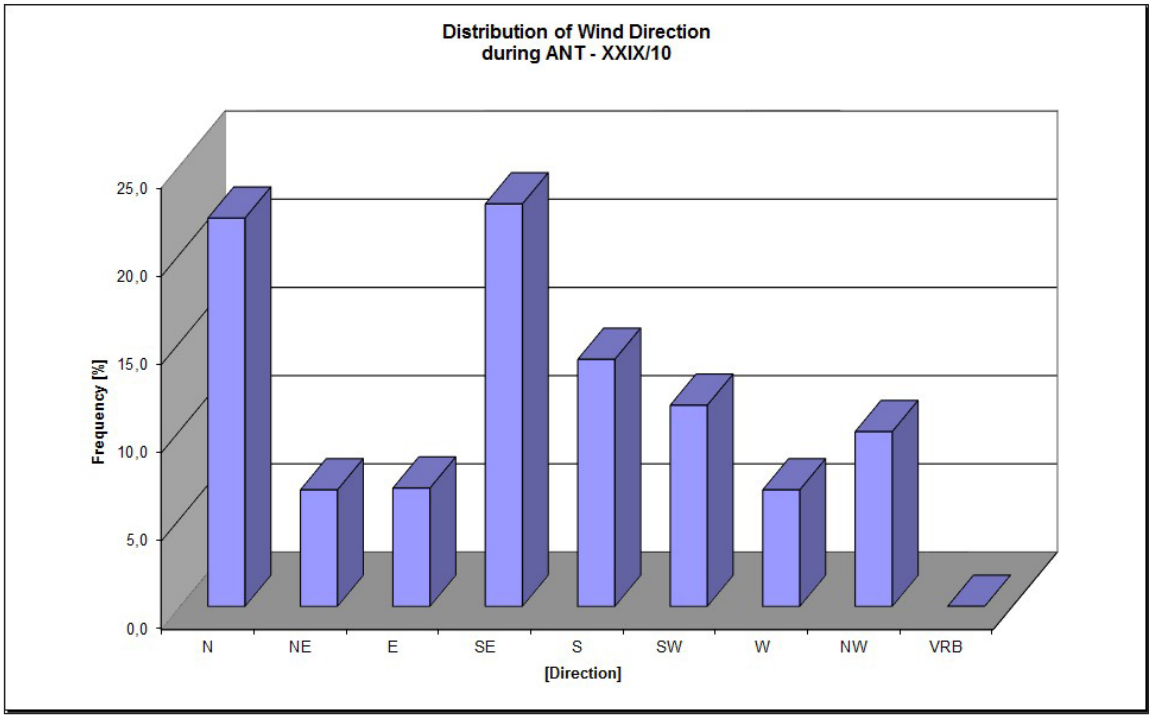

Fig. 2.2: Distribution of wind direction during PS83 (ANT-XXIX/10)

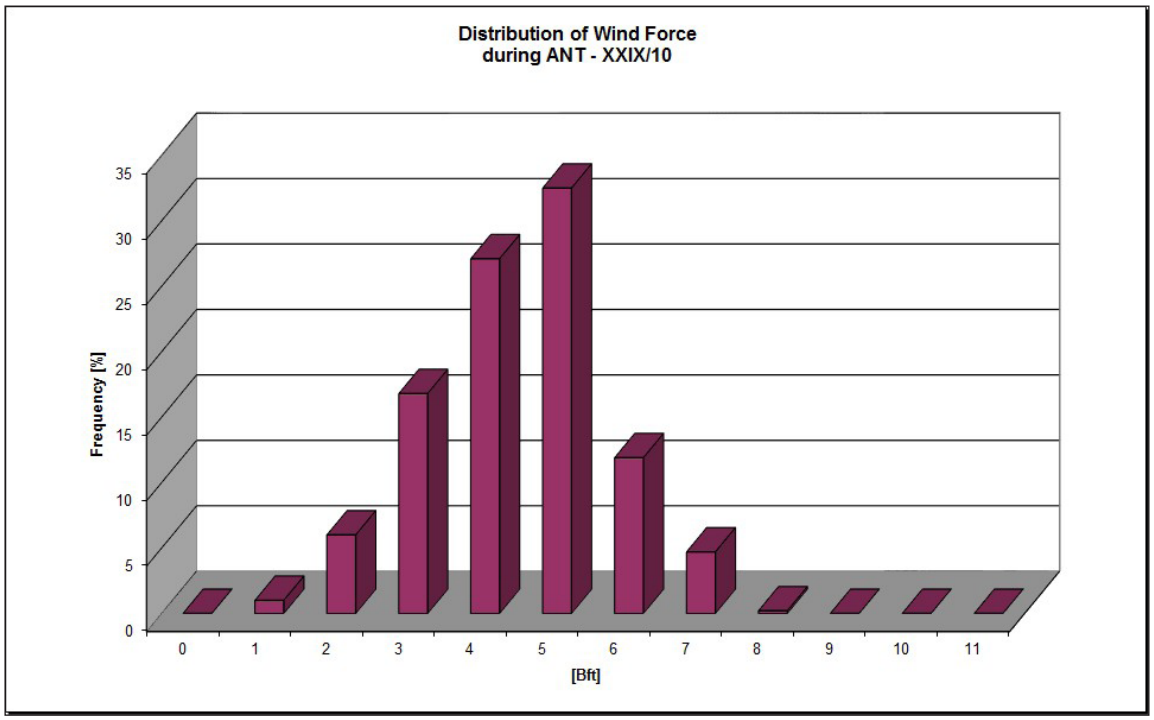

Fig. 2.3: Distribution of wind force during PS83 (ANT-XXIX/10)

3. OCEANET: TROPOSPHERIC PROFILING OF CLOUDS, AEROSOL, TEMPERATURE AND WATER VAPOR USING AN AUTONOMOUS MEASUREMENT PLATFORM

Sebastian Bley[1], Andreas Foth[2],
not on board: Ronny Engelmann[1], Andreas Macke[1], Bernhard Pospichal[2]

[1] TROPOS
[2] Uni Leipzig

Objectives

Convective clouds still pose significant challenges for numerical models and our understanding of the underlying physical processes as well as the coupled atmosphere-ocean climate system. This includes the characterization of aerosol particles, their vertical distribution in the atmosphere and their interaction with clouds.

The net radiation budget at the surface is the driving force for most physical processes in the climate system. The changes of irradiance from aerosol-radiation effects (direct aerosol forcing) and from aerosol-cloud interactions (indirect aerosol forcing) can be described by the radiative forcing (Boucher et al., 2013). These direct and indirect effects are mainly determined by the complex spatial distribution of temperature, humidity, hydrometeors and aerosol particles. The project aims at observing both the radiation budget and the state of the cloudy atmosphere as accurate as possible to provide realistic atmosphere-radiation relationships for comparison with climate models and observations in remote sensing.

In the framework of the OCEANET programme, detailed observations of these quantities will be carried out targeting aerosols and clouds. For the first time, the exact course of *Polarstern* will be adjusted to match the ship track to overflights of the A-Train satellite constellation, which contains among other instruments the space-born cloud and aerosol lidar CALIOP and the cloud radar CLOUDSAT. This offers the unique opportunity to intercompare vertical profiles of clouds and aerosols taken from the ground and space.

A multichannel microwave radiometer is used for continuous observations of temperature and humidity profiles as well as cloud liquid water path and integrated water vapor content over the ocean. Time series of these profiles can be compared to results from previous cruises in order to determine characteristic values and to identify interesting variations. As additional benefit of this transfer cruise, it is possible to investigate the variability of these measurements across several climate zones.

The lidar system PollyXT, a semi-autonomous multi-wavelength polarization Raman lidar is operated inside the OCEANET container to measure vertically resolved profiles of aerosol particles, clouds, and water vapor. The lidar is able to independently measure profiles of particle backscatter at three wavelengths and extinction at two wavelengths, which allows identifying particle type, size, and concentration. Additionally particle depolarization is measured in order to discriminate between spherical and non-spherical particles, e.g. biomass-burning smoke vs. mineral dust or water clouds vs. ice clouds. The determined height-resolved aerosol extinction completes the radiation measurements. In this way, the radiative influence of aerosol particles or clouds can be calculated with radiation-transport models.

Work at sea

The OCEANET container was located on the helicopter deck on port side. As in previous *Polarstern* cruises continuous measurements were carried out by using two pyranometers, one pyrgeometer and a full sky imager that took one digital picture every 15 seconds. Additionally a scaled weather station mast was situated on top of the container.

A multi-channel microwave radiometer (HATPRO) was utilized for continuous measurements of atmospheric temperature and humidity profiles as well as the vertical integrated water vapour content (IWV) and liquid water path (LWP). Due to the rolling and pitching of the ship the radiometer was adjusted only for vertical measurements. As first step the radiometer had been calibrated with liquid nitrogen in the harbour of Cape Town. After a rough sea the rain sensor which is mounted on the radiometer cover had to be cleaned to avoid misclassifications of the weather conditions.

The lidar system PollyXT was running every night with pre-defined settings of the grey filters. For daytime measurements of the vertical distribution of water vapour the grey filter of the water vapour channel had been changed to a higher optical thickness on particular days. Due to the accumulation of sea salt on the half domes of the pyrano-, pyrgeometer and full sky imager as well as the outlet and inlet window for the lidar beam were cleaned every day. During the time when *Polarstern* had passed low latitudes PollyXT had been turned off to avoid a direct downward radiation of the sun into the telescope. The lidar system was running for all satellite overflights of Calipso.

Preliminary (expected) results

With the microwave radiometer the IWV can be well retrieved. Fig. 3.1 shows the IWV along the whole ship track until April 7, 2014. As expected the highest values were reached in the tropics and lower values in higher latitudes. Unfortunately, the radiometer data is not quality screened. Due to the rain flag misclassifications the whole time series is plotted including rain events. The quality screening will be done after the cruise. The time series of IWV (upper diagram, black symbols) and LWP (lower diagram) are displayed in Fig. 3.2. In the upper diagram the IWV from radiosonde ascents is added with red triangles. The IWV values from both instruments are in a good agreement. According to Fig. 3.1 the highest values occured during our passage of the equator region (16 to 21 March 2014). The LWP values vary with the occurrence of clouds. Larger shower clouds in the tropics lead to high values in the LWP whereas the lower non-zero values occur during we passed stratocumulus cloud fields or trade wind cumuli. Figures 3.3 and 3.4 show the height time displays of the temperature and absolute humidity along the ship track, respectively. As expected, the hottest region (reddish colors) is around the equator and around the March 26, 2014 the temperature inversion can be seen. Fig. 3.4 shows that the most humid region is around the equator (19 March 2014). After leaving the inner tropical convergence zone on 22 March 2014 *Polarstern* entered a dryer region.

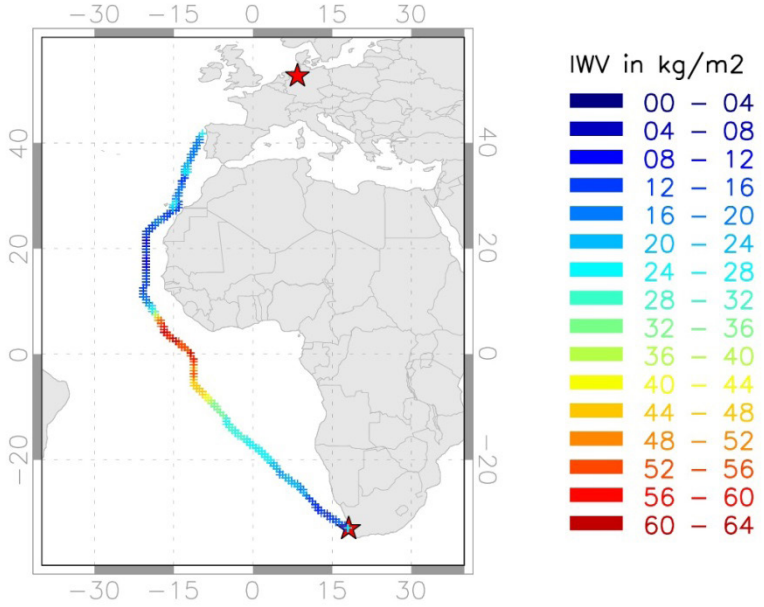

Fig. 3.1: Map of the ship track. The colours indicate the integrated water vapour (IWV) derived from microwave radiometer. The red stars mark Cape Town and Bremerhaven.

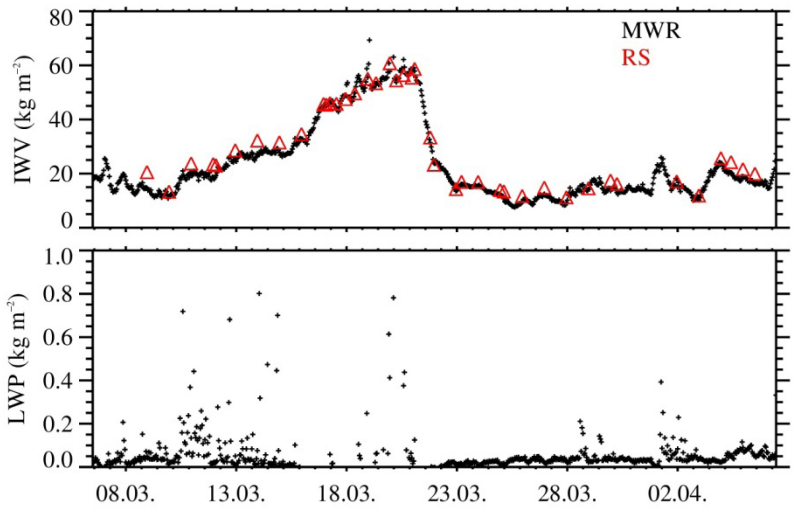

Fig. 3.2: Time series of IWV (upper diagram, black plus symbols) and LWP (lower diagram) from microwave radiometer. In the upper diagram the IWV from radiosonde ascents is also plotted in red triangles.

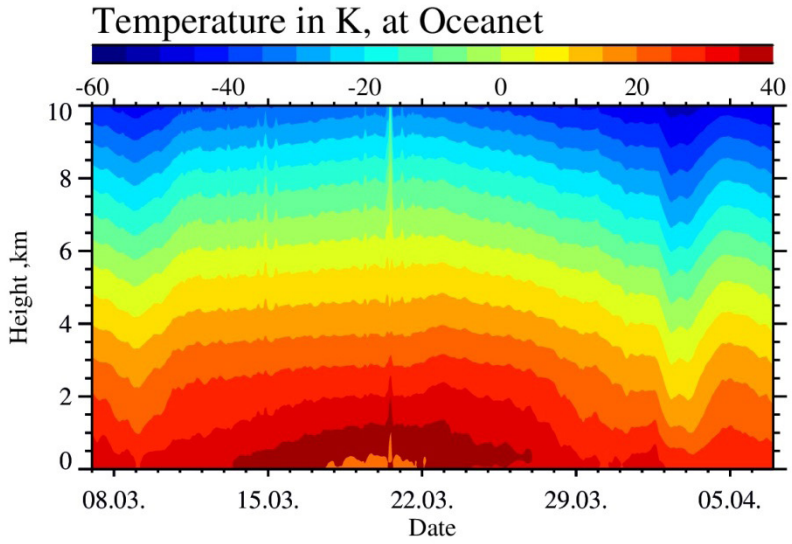

Fig. 3.3: Height time display of the temperature from microwave radiometer

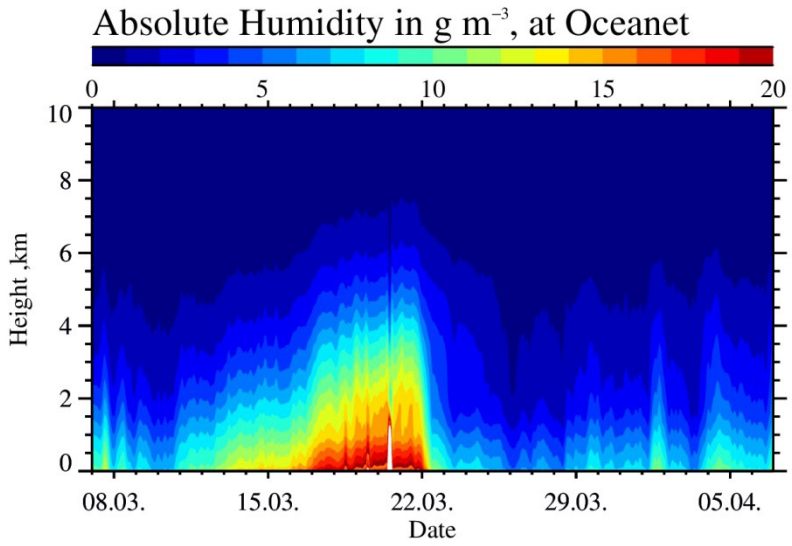

Fig. 3.4: Height time display of the absolute humidity from microwave radiometer

Fig. 3.5 shows the time series of the range corrected signal of the backscatter at the 1064 nm channel measured by the lidar along the *Polarstern* cruise PS83. Dark blue colours indicate low values whereas red colours illustrate strong signals. Most time of the cruise low boundary layer clouds occur within the lower 2 km. On March 19, the *Polarstern* had crossed the equator. In this period some very high cirrus clouds had been measured between 12 and 16 km height (Fig. 3.5). These results are consistent with radiosonde observations of the tropopause region conducted by the DWD and GEOMAR scientists. At the same time the aerosol forecast model MACC had predicted an advection of biomass-burning smoke and mineral dust from the

African continent. That could also be seen in the lidar signal and depolarization ratio. Further analysis has to be done after the cruise to flag regions without low clouds in order to quantify the aerosol optical depth (AOD). These results could then be compared to observations from the sun photometer microtops and from the rotating shadowband pyranometer.

For further investigations of this overview plot one should consider that this lidar system is not able to gain information from above low optically thick clouds.

As mentioned before, the course of *Polarstern* was adjusted to six overflights of the satellites Calipso and Cloudsat. The black vertical lines show the time (March 12, 15, 18, 21, 25, 31) of these overflights. Different weather conditions were covered by the satellite overflights, low cumulus clouds during the first cruise leg, some aerosol layers and high cirrus clouds around the equator as well as clear sky conditions in the subtropics. More analysis has to be done after the cruise for intercomparisons between the lidar and the instrument CALIOP.

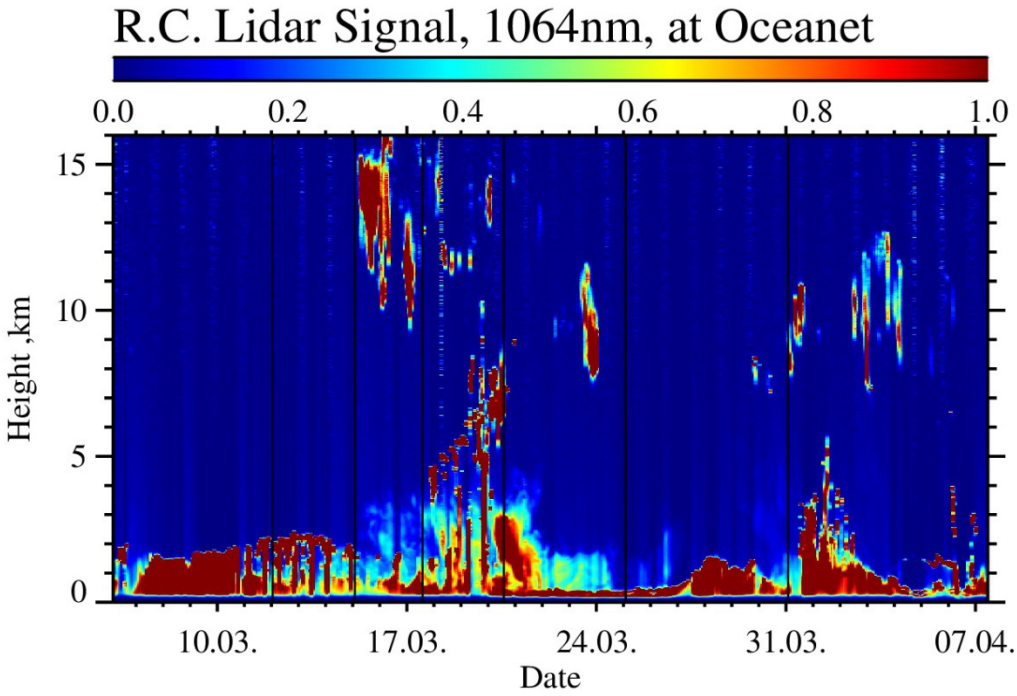

Fig. 3.5: Time series of the range corrected backscattered lidar signal of the 1064 nm channel. The colour scale is normalized to the maximum value of the time series. The black vertical lines show the time of the six Calipso overflights.

Data management

All data collected during this cruise will be available through the PANGAEA database after the cruise.

References

Althausen D, Engelmann R, Baars H, Heese B, Ansmann A, Müller D, Komppula M (2009) Portable Raman lidar PollyXT for automated profiling of aerosol backscatter, extinction, and depolarisation, Journal of Atmospheric and Oceanic Technology, 26, 2366-2378.

Boucher O, Randall D, Artaxo P, Bretherton C, Feingold G, Forster P, Kerminen V-M, Kondo Y, Liao H, Lohmann U, Rasch P, Satheesh S K, Sherwood S, Stevens B, Zhang X Y (2013) Clouds and Aerosols. In: Climate Change 2013: The Physical Science Basis. Contribution of Working Group I to the Fifth Assessment Report of the Intergovernmental Panel on Climate Change [Stocker, T.F., D. Qin, G.-K. Plattner, M. Tignor, S.K. Allen, J. Boschung, A. Nauels, Y. Xia, V. Bex and P.M. Midgley (eds.)]. Cambridge University Press, Cambridge, United Kingdom and New York, NY, USA.

Rose T, Crewell S, Löhnert, U (2005) A network suitable microwave radiometer for operational monitoring of the cloudy atmosphere, Atmospheric Research, 75, 183-200.

4. OCEANET: NOAA/ESRL/PSD W-BAND CLOUD RADAR

Sergio Pezoa NOAA ESRL/PSD

Objectives

The main objective of NOAA/PSD (National Oceanic and Atmospheric Administration / Physical Science Division) participation in OCEANET2014 is to examine the W-Band Radar reflectivity together with the OCEANET instruments, and to study the correlation between the satellite overpasses from the A-Train constellation, specifically with the CLOUDSAT cloud radar. A comparison will be examined between the CALIOP aerosol lidar and the TROPOS lidar. The ship course (see chapter 1) on its way to Bremerhaven was slightly modified on March 12, 15, 18, 21, 25 and 31 to matchup and lined up the ship course as accurate as possible with the satellite overpasses. W-Band Radar time series reflectivity, Ceilometer and TROPOS lidar backscatter data sets were created hourly and daily for further analysis during the period of March 9 – April 1, 2014 to display the cloud structure during the OCEANET 2014 campaign including the matchup satellites from the A-Train constellation.

Work at sea

The Physical Sciences Division (PSD) of the Earth System Research Laboratory (ESRL) W Band Radar was installed on the *Polarstern* on 5 March 2014 to participate in OCEANET2014. The W-Band radar sea container was installed in the helideck next to the TROPOS aerosol Lidar sea container near the port side. The cruise departed from Cape Town in March 8, 2014 with final destination Bremerhaven on April 13, 2014; there was a short stop for a few hours at the island of Las Palmas on April 1, 2014. The W-Band Radar operated continuously with the exception of restrictions imposed within 3 miles of the island of Las Palmas.

The radar was operated in the basic mode, an attempt was made to modify the radar setting in an effort to detect clouds at higher altitude during cruising the equatorial sector but the radar had problems with those setting. The basic Mode has the following parameters:

Number range gates=190; Range resolution=30 m; Distance to range gate(1)=60 m; Distance to range gate(190)=5870 m; Number Doppler velocity bins=128; Doppler Bin Resolution: 0.12 m/s; Number spectral averages=12; Minimum detectable SNR=-20; Minimum detectable dBZ @ 3 km=-30; Dwell=0.3 s; antenna diameter=12 “, 46 dB gain, 0.7 deg beamwidth; wavelength=3.17 mm.

The radar is a full Doppler Spectra processor. All Doppler spectra (1 mean spectrum every 0.3 s) are saved. The spectra are processed for standard first 3 moments (0th, 1st, 2nd) for reflectivity, mean Doppler velocity, and mean Doppler width.

A Vaisala CL31 and Radiometric 3000A microwave radiometer operated continuously in conjunction with the PSD W Band Radar adding information of the cloud base altitude and backscatter, while the microwave radiometer adds vertical temperature, humidity and water vapor concentration profiles to create a complete set of atmospheric information along the *Polarstern* course in an effort to understand the ocean surface-atmosphere radiation exchange. Microwave radiometer profiles are not analyzed in this report due a missing reference calibration file.

The ceilometer is an unsophisticated version of the lidar that measures the base of the clouds. It uses a laser diode and sends out a pulse (910 nm), which hits the bottom of the cloud and bounces back. Also, it can pick up rain events and virga (rain that falls but does not reach the ground). This instrument is useful because it gives the ceiling height, which can determine the top of the mixed layer, or where the lowest clouds start to form.

Preliminary Results

Rain and low clouds were observed during the beginning of the cruise with some precipitation in the southern part of the globe, very dry condition by the Equator and high cloudiness and low clouds in the north part of the globe with occasional showers. March 12 was characterized by cloudiness and some shower during the early morning, clear sky during mid-day and some cloudiness late afternoon. The W-Band Radar (Fig 4.1) showed occasional cloudiness with mostly clear sky during the satellite overpass at 13:40 UTC - Position: 23° 08.64'S , 5° 03.42'E. Fig. 4.2 shows the corresponding ceilometer backscatter. The TROPOS Lidar 532 nm wavelength time series (Fig 4.3) showed no clouds within the sat overpass.

March 25 (Fig 4.4-4.6) was characterized by scattered low clouds around 250 meters, clear sky by mid-day then low cloudiness during late afternoon. The W-Band Radar showed low clouds with no precipitation during the satellite overpass (Fig 4.4) at 14:57:55 UTC - Position: 15° 30.29'N , 20° 27.80'W. TROPOS Lidar 532 nm wavelength time series (Fig 4.6) showed low clouds about 400 meters.

Ceilometer Cloud Base Heights (Fig 4.7) history from March 9 until April 7 is shown with 1 hr and 10 min averages representing in general the cloud base formation from Cape Town to the entrance of the English Channel.

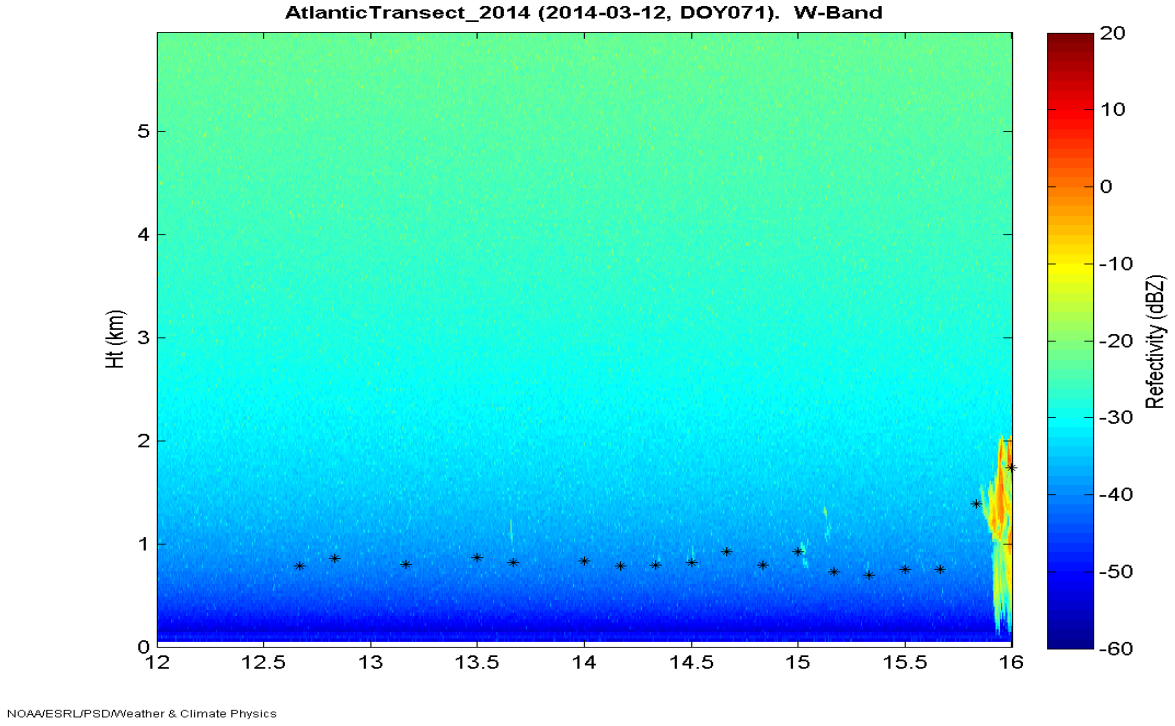

Fig 4.1: Time-height cross section shows the ESLR/PSD W-Band Radar reflectivity(dBZ) of 4 hours of data beginning at 12:00 UTC and ending at 16:00 UTC of March 12, 2014.

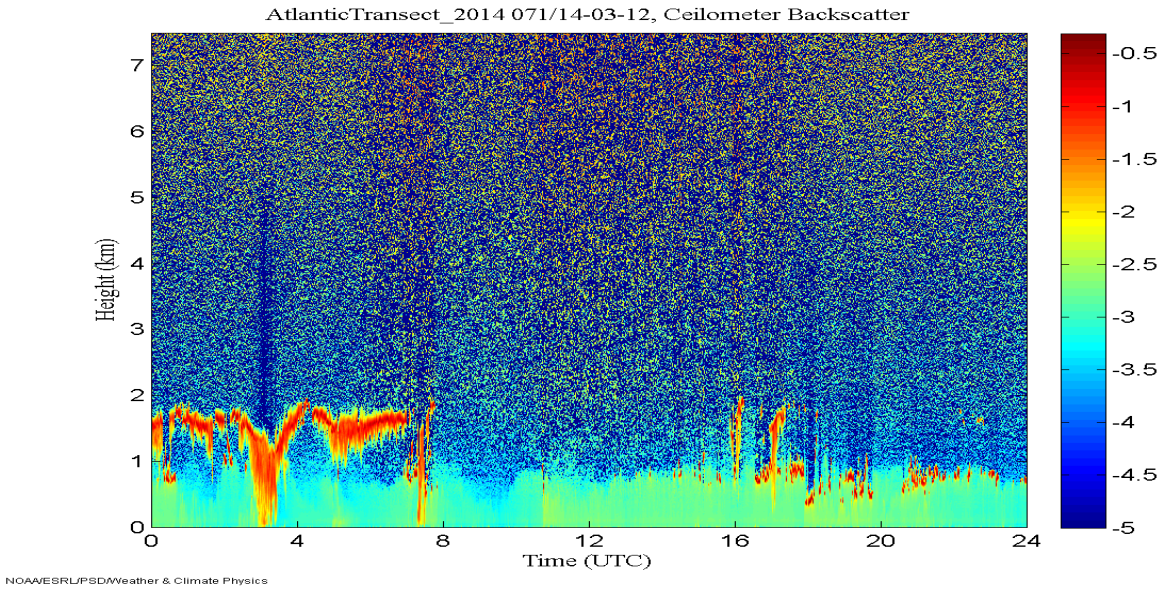

Fig. 4.2: Ceilometer CL31 Backscatter March 12, 2014 Day 71 (0 – 24hours)

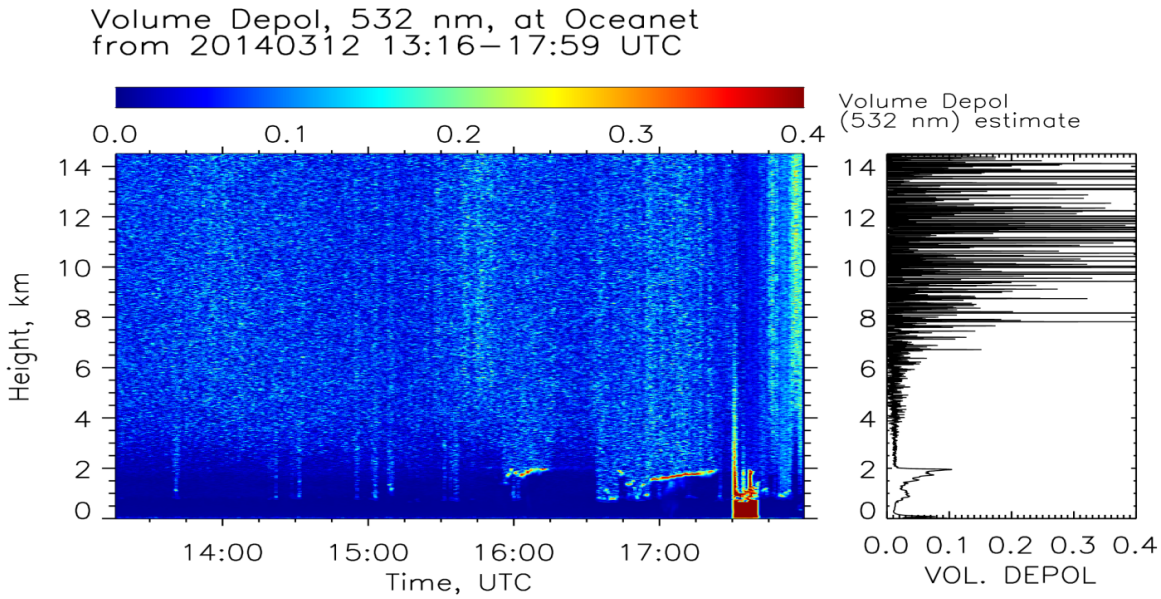

Fig. 4.3: TROPOS Lidar 532 nm wavelength March 12 2014 (13 – 18 hours)

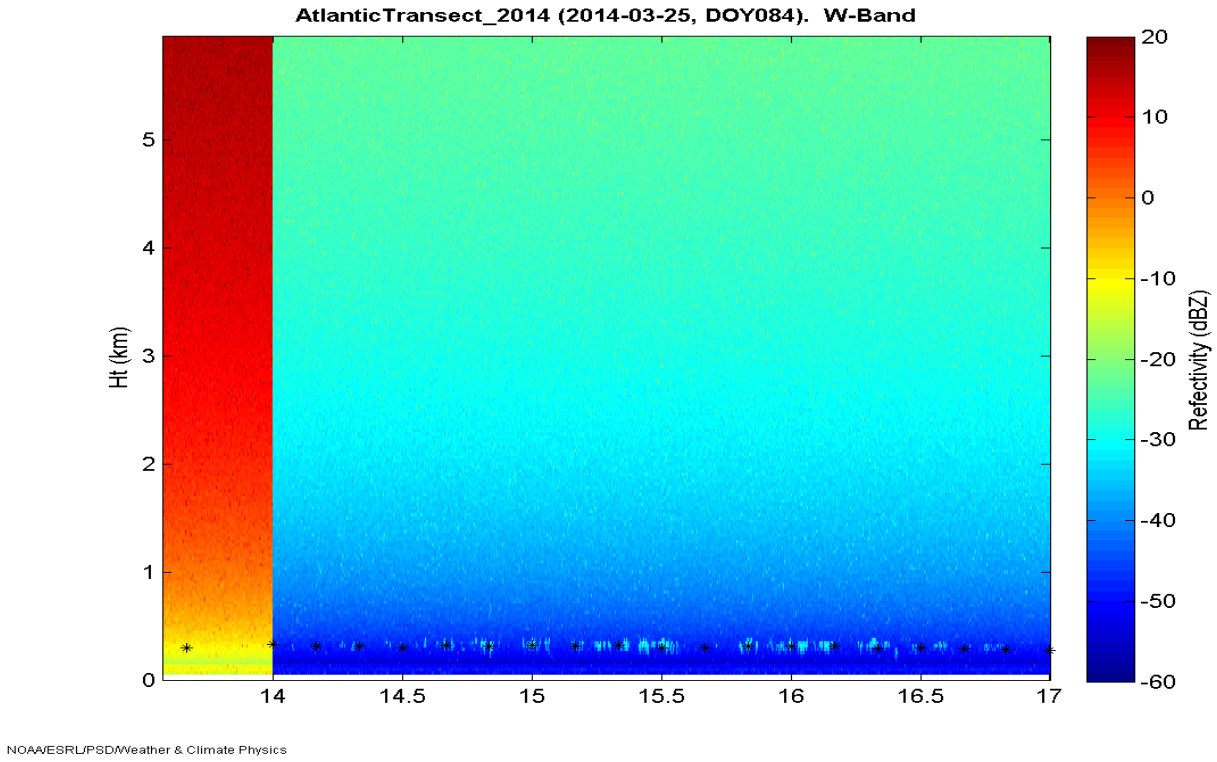

Fig. 4.4: Time-height cross section shows the ESLR/PSD W-Band Radar reflectivity (dBZ) of 4 hours of data beginning at 14:00 UTC and ending at 17:00 UTC of March 25, 2014.

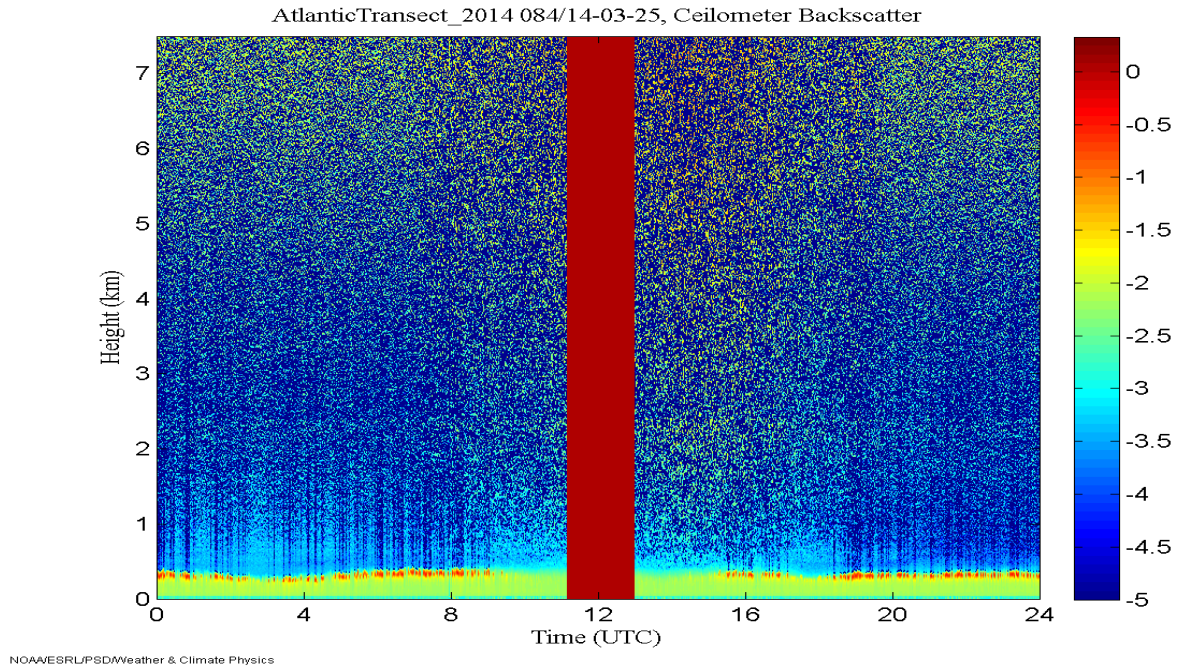

Fig. 4.5: Ceilometer CL31 Backscatter March 25, 2014 Day 84 (0 – 24hours)

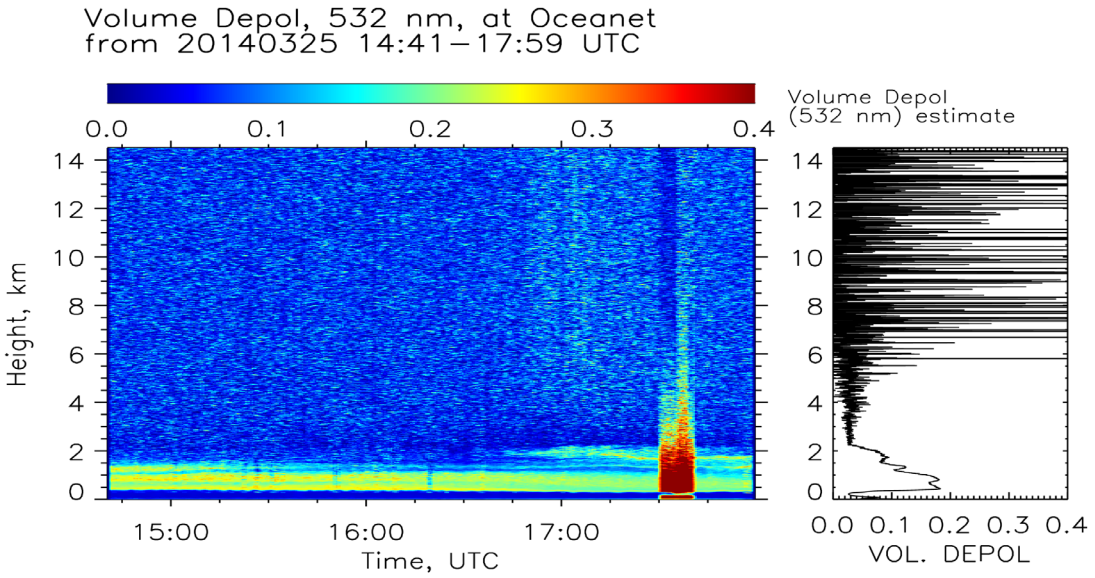

Fig. 4.6: TROPOS Lidar 532nm wavelength March 25 2014 (14:41 – 17:59 hours)

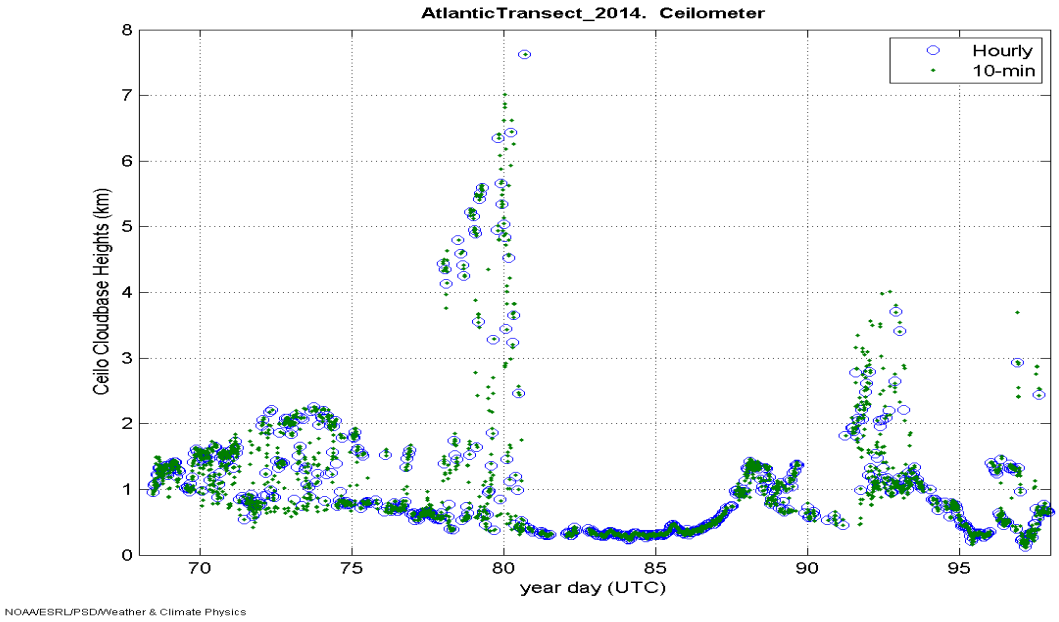

Fig. 4.7: Ceilometer CL31 Cloud base Heights March 9 – April 7, 2014

Data management

Data are available from NOAA ESRL on request.

References

Probert-Jones JR (1962) The radar equation in meteorology. Q J Roy Meteorol Soc 88:485–495

Rambukkange MP, Verlinde J, Eloranta EW, Flynn CJ, Clothiaux EE (2011) Using Doppler spectra to separate hydrometeor populations and analyze ice precipitation in multilayered mixed-phase clouds. IEEE Geosci Remote Sens Lett 8:108–112

Riddle AC, Gage KS, Balsley BB, Ecklund WL, Carter DA (1989) Poker Flat MST Radar Data Bases. NOAA Tech., Memorandum, ERL AL-11

Sekelsky SM, McIntosh RE (1996) Cloud observations with polarimetric 33GHz and 95GHz radar. Meteorol. Atmos Phys 59:123–140

Sekelsky SM, Ecklund WL, Firda JM, Gage KS, McIntosh RE (1999) Particle size estimation in ice-phase clouds using multi-frequency radar reflectivity at 95, 33, and 2.8GHz. J Appl Meteorol 38:5–28

Shupe MD, Kollias P, Matrosov SY, Schneider TL (2004) Deriving mixed-phase cloud properties from Doppler radar spectra. J Atmos Ocean Technol 21:660–670

Shupe MD, Daniel JS, de Boer G, Eloranta EW, Kollias P, Long CN, Luke EP, Turner DD, Verlinde J (2008) A focus on mixed-phase clouds. Bull Am Meteorol Soc 89:1549–1562

Stephens GL, Tsay SC, Stackhouse PW, Flatau PJ (1990) The relevance of the microphysical and radiative properties of cirrus clouds to climate and climate feedback. J Atmos Sci 47:1742–1752

Tucker SC, Brewer WA, Banta RM, Senff CJ, Sandberg SP, Law DC, Weickmann AM, Hardesty RM (2009) Doppler lidar estimation of mixing height using turbulence, shear, and aerosol profiles. J Atmos Ocean Technol 26(4):673–688

Vali G, Kelly R, Pazmany A, McIntosh RE (1995) Airborne radar and in-situ observations of a shallow stratus with drizzle. J Atmos Res 38:361–380

Vali G, Kelly R, French J, Haimov S, Leo D, McIntosh R, Pazmany A (1998) Fine-scale structure and microphysics of coastal stratus. J Atmos Sci 55:3540–3564

Webster PJ, Fairall CW, Hacker PW, Lukas R, Bradley EF, Godfrey S (2002) The Joint Air-Sea Monsoon Interaction Experiment (JASMINE) Pilot study. Bull Am Meteorol Soc 83:1603–1630

Woods R, 32 coauthors, (2011) The VAMOS Ocean-Cloud-Atmosphere-Land Study Regional Experiment (VOCALS-REx): goals, platforms, and field operations. Atmos Phys Chem Discuss 11:2627–654. doi:10.5194/acp-11-627-2011

5. OCEANET: CHEMICAL AND PHYSICAL CHARACTERIZATION OF MARINE AEROSOLS

Maik Merkel[1], Susanne Fuchs[1], Ronny Badeke[1], Manuela van Pinxteren[1] (not on board), Hartmut Herrmann[1] (not on board), Alfred Wiedensohler[1] (not on board)

[1]Leibniz Institute for Tropospheric Research (TROPOS) Leipzig, Germany

Objectives

The exchange of gases and aerosols between ocean and atmosphere has received considerable and intensive attention, but it is not well understood currently. Aerosol particles play an important role in the global climate change because of their effects on the radiation budget. This is particularly true for aerosols from marine environments. For this reason, the measurements on board *Polarstern* are to 1) better understand the formation mechanism of secondary fraction in marine aerosol particles, 2) investigate the interaction between sub-micron marine aerosols and water vapour under sub- and super-saturated as well as undercooling conditions, and 3) characterize the optical properties of marine aerosols. The export of organic compounds from the ocean to the atmosphere belongs to the manifold but unknown exchange processes between these two compartments. In this context, the sea surface microlayer (SML), the uppermost layer of the ocean plays an important role as it is the direct interface between air and sea (e.g. Wurl et al. 2011, van Pinxteren et al. 2012, Cunliffe et al. (2013). Current investigations show a different chemical composition of this layer, for example an enrichment of organic compounds (e.g. van Pinxteren et al. 2013). In order to receive a better understanding of these exchange processes, concerted sampling activities are performed to sample and investigate the SML and the corresponding aerosol particles during the *Polarstern* PS 83 cruise. Detailed chemical analysis of organic compounds in both compartments together with important algae pigments (as possible source) should help to elucidate formation and transfer pathways of especially atmospheric relevant organic compounds.

Work at sea

For achieving the foregoing objectives, the physical laboratory container of TROPOS equipped with a number of scientific instruments was operated by three scientists during the PS 83 (ANT-XXIX/10) leg from Cape Town to Bremerhaven.

Particle Number Size Distributions from 10 nm up to 1 µm in diameter were measured by a Scanning Mobility Particle Sizer (SMPS). This instrument has a time resolution of 5 minutes. The interaction between particles and water vapour under sub- and super-saturated conditions is respectively determined by a Cloud Condensation Nucleus Counter (CCNC; with relative humidities from 100.1 to 101 %). With this instrument the activation behaviour of the particles can be investigated, which is the probability of particles to form cloud droplets. Additionally, an Integrating Nephelometer and a Multi Angle Absorption Photometer (MAAP) as well as a Particle Soot Absorption Photometer (PSAP) were operated simultaneously to characterize the particle optical properties. They can measure the particle scattering and absorption coefficient and the black carbon concentration. Table 1 shows a summary of scientific equipment to determine the properties of the marine aerosol on board *Polarstern*.

The chemical compositions of marine aerosols were measured by the following off-line measurements and measurement techniques: (1) Sampling of aerosol particles on quartz fiber filters with a commercial High Volume Samples (2) Sampling of the sea surface microlayer with the glass plate technique and (3) sampling of bulkwater with a selfmade telescopic rod and (4) sampling of seawater for pigment analysis. The 24-hour DIGITEL filter sample will be analyzed in the lab to determine the elemental and organic carbon, and water soluble ions of particles below 10 mm.

Tab. 5.1: Scientific instruments on board *Polarstern*

Instruments	Time Resolution	Data availability
Scanning Mobility Particle Sizer (SMPS)	5 min	08.03. - 11.04.2014
Cloud Condensation Nucleus Counter (CCNC)	10 min	08.03. - 11.04.2014
Multi Angle Absorption Photometer (MAAP)	1 min	08.03. - 11.04.2014
Integrating Nephelometer	1 min	08.03. - 11.04.2014
Particle Soot Absorption Photometer (PSAP)	1 min	08.03. - 11.04.2014
Digitel – High Volume Filter Sampler	24 hours	08.03. - 11.04.2014
Denuder	24/48 hours	08.03. - 11.04.2014
Gas analyzers (Ozone, SO_2, NO_x)	1 min	08.03. - 11.04.2014

At the beginning of the cruise, the container was set up and all instruments were calibrated. The quality-control protocol was carried out to insure the high-quality data acquisition during the whole campaign.

For most of the time of the campaign the wind was coming from ahead and brought ship contamination-free air. Especially when the ship stopped at the daily station time, an influence of contamination from the ship exhaust could be seen frequently. Beside this, the measurements were successful until April 11, when the packing of the instruments started. A rough summary of data availability is given in the last column of Table 5.1. Water samples of the SML were taken 17 times in total for this cruise from Cape Town to Bremerhaven.

Preliminary (expected) results

Based on the on-line measurements, the size-dependent chemical and physical properties of near-surface marine will be obtained.

The measurements of particle activation can provide information about the formation of cloud condensation nuclei in a marine atmosphere. The light extinction at ambient humidity can be predicted from *in-situ* measurements of dry and humidified particle number size distributions, light scattering and absorption coefficients, and chemical composition. Optical properties of aerosol particles and *in-situ* physical and chemical measurements as well as columnar optical property measurements can be used to establish a connection between *in-situ* ground and columnar aerosol properties.

During the cruise PS 83 the ambient aerosol originated mainly from marine sources. Fig. 5.1 shows an example of the particle number size distribution as a function of time and particle

diameter, which was measured between March 18th and March 24th, 2014. Total particle number concentrations were in between 250 and 600 particles per cm³ representing marine aerosols. The number size distribution was bimodal for almost the whole time (Fig. 5.2).

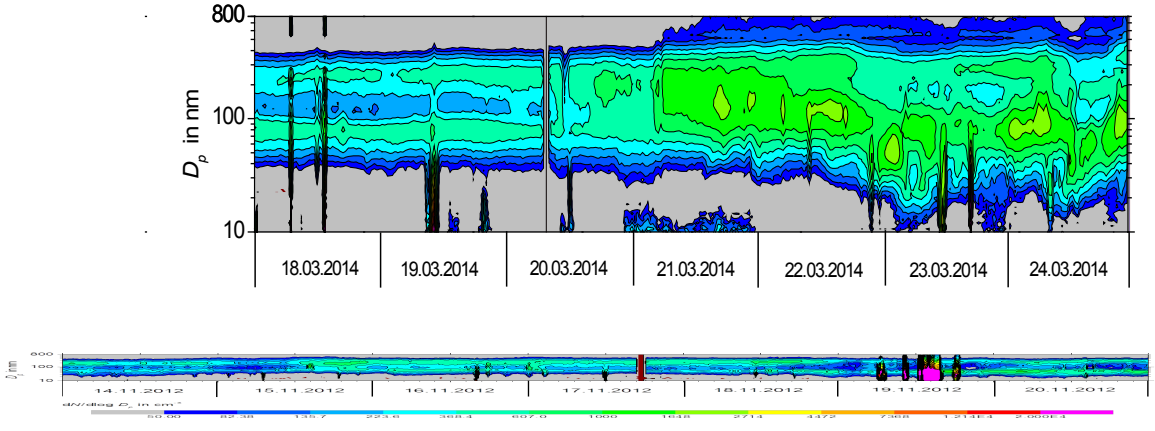

Fig. 5.1: Particle number size distribution measured by the SMPS for 7 days showing different aerosol particles and number concentrations.

Fig. 5.2 is showing the time series of total particle number concentration for two different days. The time series of the absorption coefficient determined by the Multi-Angle Absorption Photometer (MAAP) is also displayed in this plot. After passing the equator on March 19, the total particle number was rising. Especially particles larger than 100 nm in diameter occurred twice higher in concentration than before. The reason is the long range transport from the western African continent due to biomass burning on the one hand. But also the amount of particles larger than 400 nm was significantly higher. A small dust outbreak from the Saharan region might be responsible for those results. That influence was also detected by the Nephelometer. The measured total scattering coefficients for the three wave lengths 450, 550 and 700 nm are showing a sharp increase during the 21st of March (Fig. 5.3). High values for scattering are also a hint for mineral dust particles.

At the laboratories at TROPOS chemical analysis will be performed with focus on the organic content in the SML and in marine aerosols. Enrichment factors of organics in the SML will be calculated. Special emphasis is put on the analytical measurements of atmospheric relevant organic compounds in both: in the SML and in aerosol particles to find connections between these marine compartments.

Data management

All data processing will be carried out in the home laboratory at TROPOS. The online measurements of aerosol particles might need some months to insure the quality of the data set. As soon as the data are available they can be used by other cruise participants after request.

Results of project in the form of (1) Tables with the concentration of organic and inorganic constituents of seawater and marine aerosol particles and (2) publications resulting from these data will be stored on a data server accessible for other involved research groups.

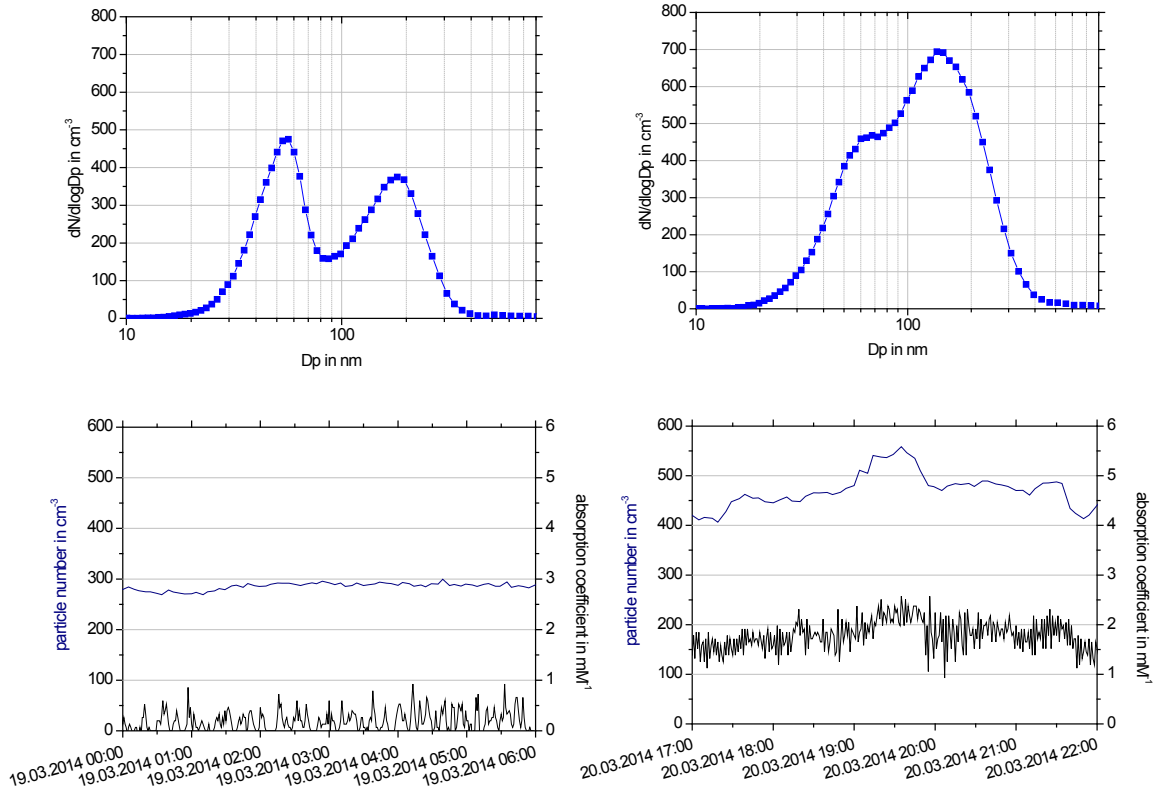

Fig. 5.2: Particle number size distribution and total particle number concentration measured by the SMPS as well as the calculated absorption coefficient for two days (while and after crossing the equator) showing different aerosol particles.

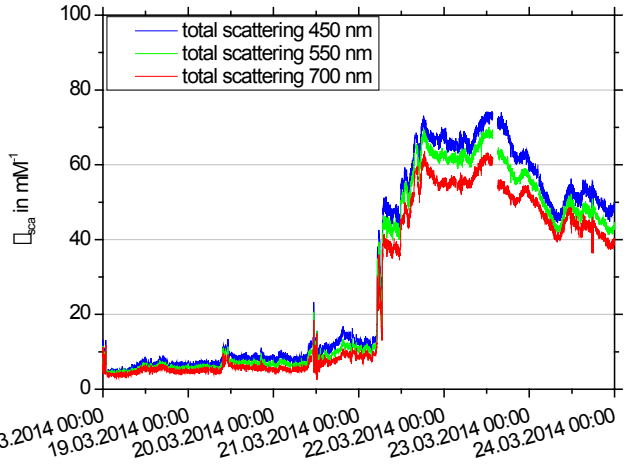

Fig. 5.3 Scattering coefficients for three different wave lengths for the time period from March 18 to March 24

References

Cunliffe M, Engel A, Frka S, Gašparović B, Guitart C, Murrell JC, Salter M, Stolle C, Upstill-Goddard R, Wurl O (2013) Sea surface microlayers: A unified physicochemical and biological perspective of the air–ocean interface. Progress in Oceanography. 109, 104-116.

Wiedensohler A, Birmili W, Nowak A, Sonntag A, Weinhold K, Merkel M, Wehner B, Tuch T, Pfeifer S, Fiebig M, Fjäraa AM, Asmi E, Sellegri K, Venzac H, Villani P, Laj P, Aalto P, Ogren JA, Swietlicki E, Roldin P, Williams P, Quincey P, Hüglin C, Fierz-Schmidhauser R, Gysel M, Weingartner E, Riccobono F, Santos S, Grüning C, Faloon K, Beddows D, Harrison R, Monahan C, Jennings SG, O'Dowd CD, Marioni A, Horn HG, Keck L, Jiang J, Scheckman J, McMurry PH, Deng Z, Zhao CS, Moerman M, Henzing B, Leeuw Gd, Löschau G and Bastian S (2012). Mobility Particle Size Spectrometers: Harmonization of Technical Standards and Data Structure to Facilitate High Quality Long-term Observations of Atmospheric Particle Number Size Distributions. AMT 5, 657–685.

van Pinxteren M, Müller C, Iinuma Y, Stolle C, Herrmann H (2012) Chemical characterization of dissolved organic compounds from coastal sea surface microlayers. Environ. Sci.Technol.,46, 10455−10462, DOI: 10.1021/es204492b.

van Pinxteren M, Herrmann H (2013) Glyoxal and methylglyoxal in Atlantic seawater and marine aerosol particles: method development and first application during the *Polarstern* cruise ANT XXVII/4. Atmos. Chem. Phys., 13, 1-12.

Wurl O, Wurl E, Miller L, Johnson K, Vagle S (2011) Formation and global distribution of sea-surface microlayers. BIOGEOSCIENCES, 8, 1, 121-135.

Fig. 5.4 Water sampling of the sea surface micro layer (© Hartwig Deneke)

6. OCEANET: ISOTOPE MEASUREMENTS FOR PARTICULATE AND GASEOUS MARITIME COMPOUNDS

Gode Gravenhorst[1], [1]Goettingen
Margarete Fricke[2], Wolfgang Fricke[2] [2]Hohenpeissenberg

Objectives

The Antarctic ice shield is a huge archive for information on environmental properties in the past and present. Water isotopes, gaseous , solid and dissolved constituents incorporated in Antarctic firn and ice indicate certain attributes and processes not only in Antarctica but also on the entire globe because the atmosphere can transport information from low latitudes to polar regions.

To narrow the characteristics of potential sources for particulate and gaseous- constituents incorporated in firn and ice of Antarctica, we have, therefore, taken samples on board *Polarstern* for analyzing size separated airborne particles and for C- , N- and S- containing gases of the atmospheric marine boundary layer. The focus of analyzing the marine trace substances was put on their stable isotopes. All samples were analyzed not on board but in laboratories at home.

Work at sea

Airborne marine particles were sampled on board *Polarstern* in two ways:

a) size separated via a high volume impactor and

b) as bulk particulate matter on membrane filters or teflon sheets.

Marine gas samples were taken in two ways:

a) as grab samples in evacuated containers for analyzing volatile organic compounds (VOC) and stable isotopes of N_2O and CO_2. The CO_2/N_2O samples of air in equilibrium with ocean surface water were taken from an equilibration system installed and run by St. v. Heuven, University Groningen, and M. Hoppema , AWI.

b) as integrated NH_3 samples collected on membrane filters doped with an acid. Airborne particles were separated by teflon membrane filters to minimize NH_4 interferences.

Information of atmospheric and sea water properties were gathered on board from other groups (DWD, AWI Bremerhaven, TROPOS Leipzig, MPI Hamburg, CIRES Boulder). We thank for the technical and analytical assistance given by H. Kreilein and D. Fellert, Department Bioclimatology, and the Kompetenz - Zentrum Stabile Isotope (KOSJ), all University Goettingen. The technical assistance of the crew, especially the repairs of electrical failures, are gratefully acknowledged.

Preliminary results

Airborne particles

The collected particles were analyzed by ionchromatography for Na as sea salt indicator, and for SO_4, NO_3, NH_4 for products of gaseous reaction in the atmosphere. The distribution of these four compounds on different particle size classes is shown in Fig. 6.1.

Sea salt emitted mechanically from the sea surface into the atmosphere is concentrated in Giant Particles larger than 1µm diameters mainly on impactor stages 2, 3 and 4. NO_3 ions are concentrated on the same size classes as the alkaline sea salt particles. We suggest that this is probably due to reaction of acidic HNO_3 and NOx. with alkaline sea salt. Non-sea-salt-sulfate (NSSS) is mainly found in the accumulation mode below 1µm diameter on the last impactor stage (back up filter) probably as a gas-to-particle-reaction product. The fraction of NSSS in the size spectrum of sea salt particles can be the result of SO_2 absorption on alkaline sea salt particles. NH_4 is associated with NSSS in the smallest size range, indicating an atmospheric reaction of alkaline gaseous NH_3 with airborne acidic sulfuric aggregates. NH_4 is not found associated with NSSS in Giant Particles indicating no coagulation of ammonium containing particles with sea salt particles or a volatilization of NH_3 from alkaline sea salt particles.

The airborne concentration of particles show marked differences with respect to regions they were sampled and to back trajectories of the respective air masses. The measured size distribution of the different components is rather characteristic for the background marine aerosol.

The aerosol samples were prepared for measurements of the ratio of stable N- and S isotopes in ammonium (NH_4) and in sulfate (SO_4). The results will be discussed with respect to sources, transport and reaction pathways of compounds involved.

Gaseous compounds

40 light VOCs were analyzed in 15 grab samples (1.5 liter) by A. Werner of Meteorological Observatory Hohenpeißenberg, German Weather Service. Pronounced differences between northern and southern hemispheric air masses could be found. For some compounds the mixing ratios are given in Fig. 6.2 and Fig. 6.3. A detailed interpretation of all VOC data is pending. The VOCs distributions will help to interpret the source and transport of the encountered air masses

The pCO_2 mixing ratio on the *Polarstern* track showed in general a supersaturation of the ocean surface water in the tropical South Atlantic. Whether this supersaturation is a sign of upwelling water will be investigated on the base of other water properties. On the North Atlantic the surface water encountered acts generally as a sink for atmospheric CO_2 (Fig.6.4). The CO_2 in the atmosphere is generally lighter by one promille in the ^{13}C / 12C ratio than the CO_2 in equilibrium with the ocean water (Fig. 6.5).

The N_2O does not show distinguished differences in its ratios of stable isotopes N and O between the atmospheric boundary layer and the gas samples in equilibrium with the ocean surface water. The ratios are rather similar (Fig. 6.6, Fig. 6.7).The atmospheric boundary and the upper oceanic reservoirs are in good exchange. The atmospheric N_2O has a lifetime of roughly hundred years. Thus atmospheric N_2O is well mixed. Which oceanic depth region contributes to the N_2O emitted into the atmosphere is still a matter of debate.

The gaseous NH_3 – particulate NH_4 samples indicate that ammoniacal compounds are strongly influenced by the source regions of the air masses with respect to geographical and oceanic properties and sampling conditions. This analysis is in progress.

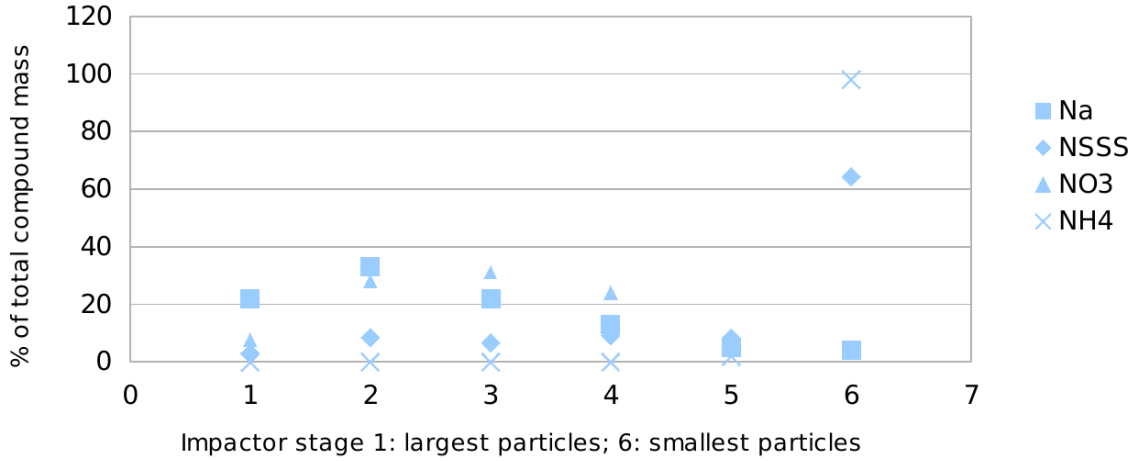

Fig. 6.1: Percent mass fraction of different size classes on their total mass for the soluble components Sodium, Non-Sea-Salt Sulfate, Nitrate and Ammonium. Na and NO_3 on the one side, and NSSS and NH_4 on the other side show similar distributions.

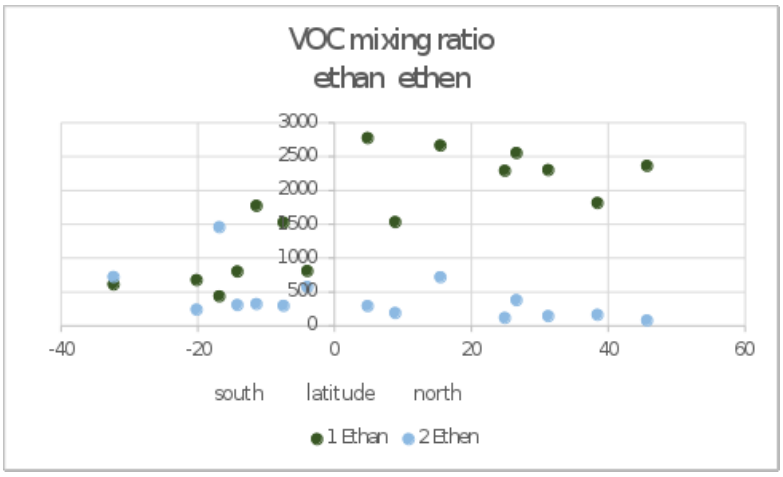

Fig. 6.2: Mixing ratios of ethan and ethen in the marine atmospheric boundary layer from Cape Town to Bremerhaven in grab samples.

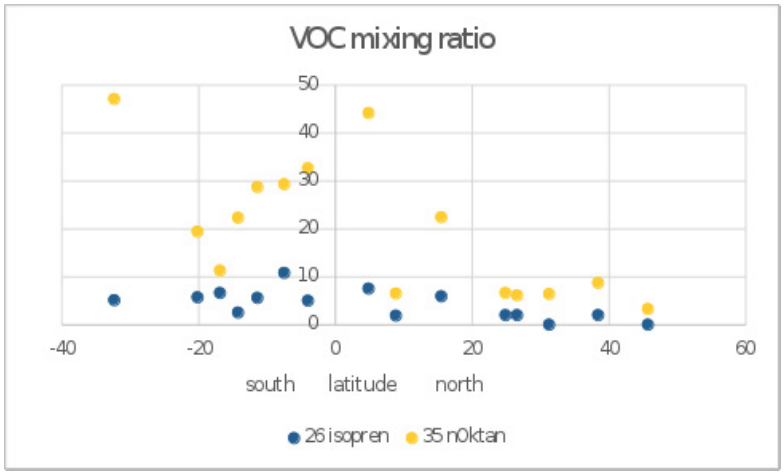

Fig. 6.3: Mixing ratio of Isoprene and nOktan in the marine atmospheric boundary layer from Cape Town to Bremerhaven (grab samples).

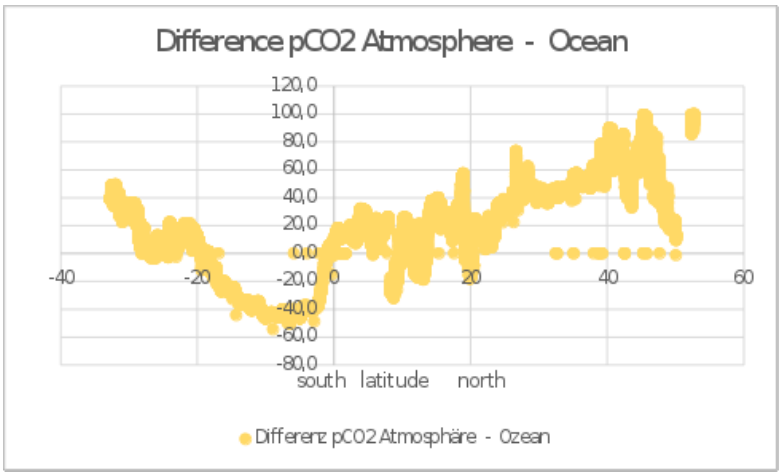

Fig. 6.4: pCO2 difference between atmosphere and equilibrium surface water on "Polarstern" track Cape Town - Bremerhaven, March 9. to April 13. 2014.

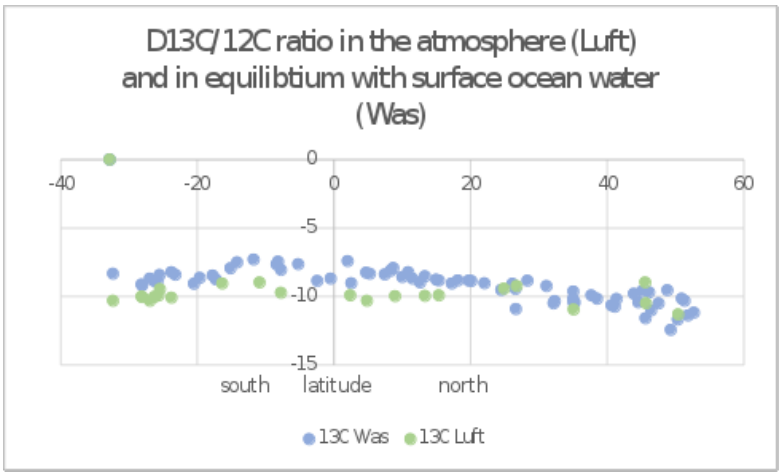

Fig. 6.5: Ratios of stable isotopes $^{13}C/^{12}C$ in CO_2 in the atmospheric marine boundary layer and in air equilibrated with ocean surface water along the track Cape Town Bremerhaven (March 9. to April 13. 2014) are rather similar. (Add as footnote: It seems that mainly for the water samples the $^{13}C/^{12}C$ ratio showed a trend along the track with highest values in the traversed tropical South Atlantic and decreasing to the north and south from there. For the atmospheric $C^{13}/^{12}C$ ratio a geographical trend is not really evident. The CO_2 in the atmosphere seems to be, however, 1 pro thousand lighter than the CO_2 in equilibrium with the surface oceanic water. Whether this is due to kinetic or equilibrium fractionation or to the oceanic C – source is not clear yet to us.)

Data management

Results will be reported in the scientific literature after completion of the analysis.

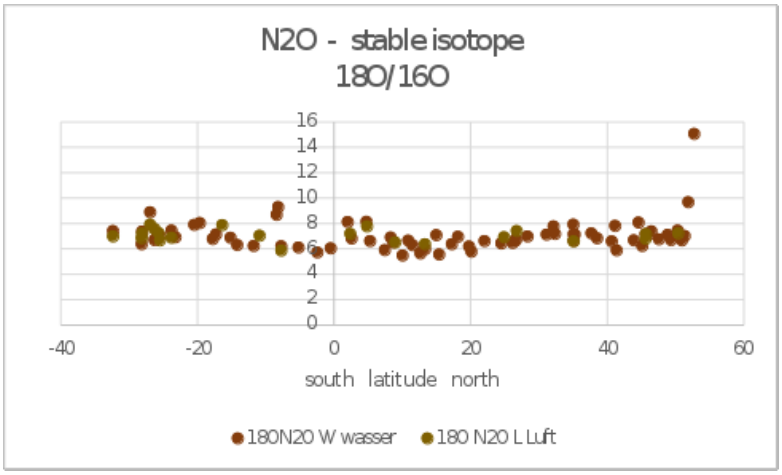

Fig. 6.6: The ratio $^{18}O/^{16}O$ in grab samples from the atmospheric marine boundary layer (L Luft) and in air in equilibrium with ocean surface water (W wasser). No differences between the two sample types could be detected. (For O ratios an internal standard was used).

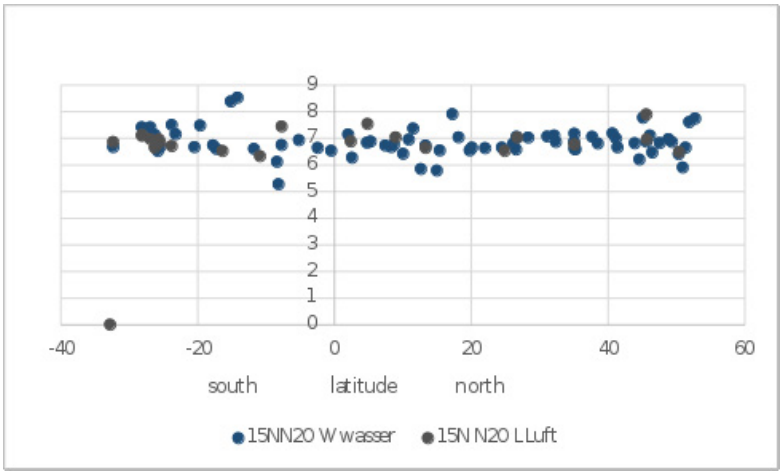

Fig. 6.7: The ratio $^{15}N/^{14}N$ in N_20 grab samples of the atmospheric marine boundary layer (L Luft) and of air in equilibrium with oceanic surface water (W wasser). No difference in the $^{15}N/^{14}N$ ratio in these two N_2O sample kinds could be detected. (Standard ratio was atmospheric N_2)

7. OCEANET: MEASUREMENTS OF AEROSOL OPTICAL DEPTH

Dagmar Popke[1], Gaby Rädel[1], Jonas Walther[2] [1]MPI
Stefan Kinne[1] (not on board) [2]TROPOS

Objectives

During PS83 (ANT-XXIX/10), aerosol optical depth was again measured within the context of the Marine Aeronet (MAN). This cruise was exceptionally interesting because it allowed the comparison of Aerosol Optical Depth (AOD) data sets from the two different instruments, the Microtops II and the Shadowband Radiometer. In the following we will describe the three instruments and their respective advantages and present first preliminary results of an intercomparison of them different instruments.

Work at Sea

Microtops Aerosol and Water vapour survey

During cloud-free conditions at daytimes, direct solar attenuation samples with handheld Microtops instruments offered data on atmospheric aerosol amount, aerosol size and atmospheric water vapor.

In collaboration with NASA-GSFC, Microtops measurements are conducted worldwide on an opportunity basis on (research) vessels in order complement continental aerosol monitoring at AERONET sites. In order to increase the data volume for aerosol reference data over oceans (e.g. for evaluations of satellite retrievals or model simulations) calibrated Microtops instruments are provided along with a GPS unit. The Microtops instrument, when directed towards the sun, captures the solar intensity at five selected sub-spectral solar wavelengths. As with the location and time information of the GPS the incoming solar intensity in these sub-spectral regions at the top of the atmosphere is known, the (smaller) measured value on the ship quantifies the atmospheric attenuation. Since the attenuation can be caused by particles and trace-gases, trace-gas poor sub-spectral regions are selected to attribute the solar attenuation to atmospheric particles. Under cloud-free conditions (thus sun-views contaminated by clouds must be avoided) the attenuation causing particles are aerosol and air molecules. Once the impacts of air-molecules, which are proportional to the surface pressure, are removed, the remaining aerosol attenuation is quantified by the vertically normalized decay exponent, the aerosol optical depth (AOD). With AOD values determined simultaneously at different solar wavelengths, this spectral AOD dependence offers information on aerosol size. Hereby the negative AOD slope with wavelength (in the context of log/log coordinates) is called the Angstrom parameter (AnP). AnP serves as a general indicator for particle size, because larger (super-micron) aerosol particles display little spectral dependence (AnP ~ 0.5 to 0), whereas smaller (sub-micron) aerosol particles have a stronger spectral dependence (AnP ~ 1 to 2). Dust and sea-salt are mainly contributing as super-micron sizes to the AOD, while pollution or wild-fires aerosol mainly contributes to sub-micron AOD. Thus, AnP indirectly offers some insights on aerosol type. In addition to aerosol also atmospheric water vapor is addressed, as one of the five solar sub-bands of the Microtops intentionally samples in band with water vapor

absorption, so that by difference to a sample without trace-gas absorption (and after vertical normalization) the atmospheric water vapor content can be determined.

The Microtops measurements are labor-intensive handheld operations, as the instrument has to be directed into the position of the sun (hereby the highest transmission signal of 20 measurements within a 8-second sample period is selected in order to eliminate the chance of pointing errors). Although these samples are repeated 10 times to identify and exclude by variability the presence of optically thicker and low clouds, these labor intensive measurement methods are rewarded by high quality data with the assurance of cloud-screened data, as visually identified cloud-cases, including especially cases containing high altitude cirrus clouds, are removed as bad samples.

Fig. 7.1: Microtops and GPS unit provided by the Marine Aerosol Network of AERONET at NASA-GSFC.

The instrument (which can be carried in a suitcase is shown in Fig. 7.1)

Shadowband Radiometer

As a fully automated alternative to the sun photometer, additional radiation measurements were provided by TROPOS with two shadowband radiometers.

The first radiometer from Biospherical Instruments Inc. measures the global irradiance in 18 different wavelengths and also the broadband irradiance. The second one is a self-built instrument from TROPOS, it measures only the broadband irradiance. The self-built radiometer is on board for evaluating low cost alternatives and compare the measurements to those of the Biospherical Instruments Inc radiometer.

A shadowband is mounted on both instruments. The shadowband moves continuously to produce a defined shadow on the sensor. The sensors sample measurements from the irradiance at high frequencies. It is thus possible to identify the measurement when the sun is blocked, and the direct component of solar radiation can be retrieved.

Despite the ship movement using a dynamic shadowband promises to block the sun at least once on every sweep, therefore no geometrical corrections will be necessary. Nevertheless, to achieve high accuracy the radiation data should be corrected for the ship's attitude. For this purpose the ships own inertial navigation system can be used to retrieve the roll and pitch angle.

From the ratio of the measured direct irradiance at the ship and the calculated irradiance at the top of the atmosphere, the optical thickness of the atmosphere along the way of the direct solar beam can be retrieved.

Both instruments have been operated by TROPOS for the first time on a ship. For this cruise, we will specifically focus on the Microtops wavelengths and the derivation of aerosol properties in comparison to the MAN observations.

Fig. 7.2: The shadowband radiometers. The radiometer from Biospherical Instruments Inc. on the left and the self-build one at the right side

Preliminary Results

Preliminary results for Aerosol Optical Depth (AOD) measured by the two different instruments, the Microtops II and the Shadowband Radiometer from Biospherical Instruments Inc. is given in Fig. 7.3, which portrays the time series of daily mean AOD from leaving the port in Cape Town on March 8 to roughly the Canary Islands on April 3.

Generally our data along the meridional cross section can be separated into three different aerosol categories: maritime background, mineral dust, and finally a mixture of mineral dust and biomass burning aerosol.

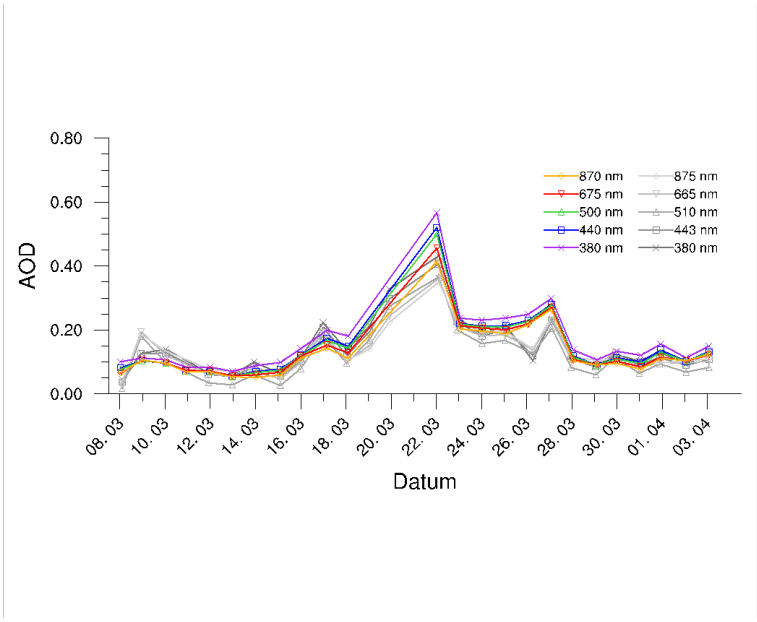

Fig. 7.3: Aerosol Optical Depth (AOD) as a function of time. Microtops II data is depicted in colors, and shadowband radiometer data in grey shades.

The maritime background (aerosols consist mainly of sea salt particles) with very clean air (AODs smaller than 0.2) was observed on the Southern Hemisphere (09/03- 16/03/2014) as well as on the Northern Hemisphere (28/03.-03/04/2014). On the Northern Hemisphere the AODs are slightly higher which may be due closer proximity of *Polarstern* to land.

Due to large-scale atmospheric transport higher AODs could be observed. Backward trajectories showed that mineral dust was transported from West Africa towards the location of '*Polarstern*' from 17/03 – 27/03/2014, which lead to AODs of about 0.2. The greater dust loading from 22/03-27/03/2014 lead to AODs larger than 0.2.

At about 8ºN, 19ºW '*Polarstern*' crossed an area that was influenced by biomass burning aerosol which had been transported towards the sea from West Africa. This event caused very hazy conditions on 22/03/2014 with AODs of 0.4 to 0.5 depending on the wavelength. The large spectral dependence on this day was a further hint at the presence of the small biomass burning aerosol in addition to the larger mineral dust particles in the atmospheric column.

Overall the daily mean values, separately measured with the Microtops II and the shadowband radiometer, exhibit commensurate AODs in the three different aerosol categories. Larger disagreement, however, is apparent on days when measuring conditions were imperfect. The presence of clouds, for example, limited the number of measurements taken on 09/03/2014 and complicated the screening for useable data from the shadowband radiometer. The largest absolute deviations in Aerosol Optical Depth between both instruments are found on March 22 and March 26 which are probably also caused by data availability of the Microtops II (almost 100 % overcast situations, thus almost no measurements) and cloud screening issues of the shadowband radiometer. Generally the shadowband radiometer measures slightly lower AODs which may be caused by the early stage of calibration development. Further research cruises with the presence of both instruments may aid in improving the cloud screening process and the calibration method for different aerosol types.

Since during PS83 (ANTXXIX/10) the ship's track could be matched with several satellite overflights of Calipso, the AOD data will be used for ground based validation of satellite data in ongoing analysis. Further comparisons will be undertaken with AOD data measured on board by the OCEANET Lidar.

The 935 nm channel of the Microtops II uni offers also the possibilty to measure the atmospheric water vapor column. The measurements as a function of latitude are shown in Fig. 7.4. As to be expected the highest values for water vapor are observed in the tropics with a maximum around the equator. Particularly low values were observed around 25°S 7ºE.

Data management

The measured Microtops data are transferred via internet to the central NASA location, where the data are available at http://aeronet.gsfc.nasa.gov/new_web/maritime_aerosol_network.html within days.

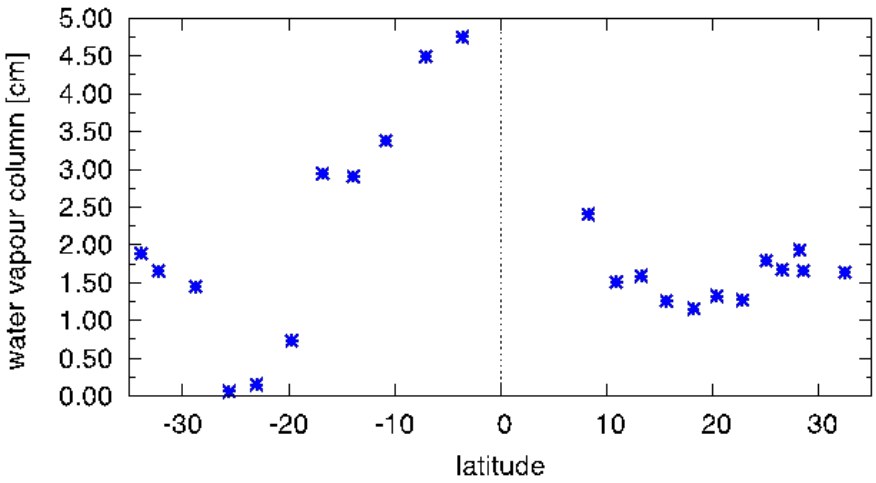

Fig. 7.4: Atmospheric water vapor column measured by the Microtops II as a function of latitude.

8. OCEANET: AEROSOL FORECAST

Stefan Barthel TROPOS

Objectives

The quality of current aerosol models is good enough for use in forecast mode to get reliable results on the aerosol situation to be expected within the near future. The idea was to improve the understanding of the current aerosol situation and that of the next hours along the cruise track by using a daily forecast of an aerosol model. This should help analysing the measurements by knowing which aerosol types should be there and in which altitudes they should be. Due to those thoughts it was tested whether an on-board aerosol forecast models is beneficial for the whole campaign.

Work at sea

Since aerosol forecast models are computational expensive, it was not possible to do the model runs on board. That's why we used the results of the global model MACC (Monitoring Atmospheric Composition & Climate) (Benedetti et al. 2009, Morcette et al. 2009), which works operational at the ECMWF (European Centre for Medium-Range Weather Forecast). The modelled aerosol data was supported in a three day forecast and only in data files. So the plots had to be produced on board. The normal weather forecast at the daily seminar was added with an additional talk on the aerosol situation. That included an overview on the general aerosol situation based on the newest forecast data as well as a special analysis of the situation for *Polarstern*. Since we also had the data of the aerosol forecast model, we were able to compare the model results nearly online to the measurement results and interpret both with the help of each other.

Preliminary results

Aerosol forecast

During the cruise a daily aerosol forecast was done and presented within the seminar. Therefore the modelled AOD (Aerosol Optical Depth) at a wavelength of 550 nm was used to get an imagination about regions with higher aerosol load in the atmosphere due to higher AODs. Some of the plots shown during these presentations are displayed in Fig. 8.1. While Fig. 8.1a) and 8.1b) show the Atlantic and Africa, Fig. 8.1c) is already shifted northwards to include Europe, which was the more relevant Region at the end of the cruise. At all three plots dust outbreaks with higher AODs (red) could be seen. While those shown in the first two figures were transported towards the eastern Mediterranean Sea, Fig 8.1c) shows the dust event which was reported over London as well as over big parts of Germany (Süddeutsche Zeitung). Most of the time on the southern hemisphere the ship track went through clean marine air with low AODs. A typical situation for that is illustrated by the blue colour in Fig. 8.1a). On March the 21st and the 22nd the track crossed the biomass-burning plume, which originated at the southern part of West Africa. This is shown by Fig 8.1b). This biomass-burning event was always of interest during the aerosol forecast presentations up to that date.

Fig. 8.1c) shows a typical situation for *Polarstern* regarding the detection of mineral dust. Except a small and weak dust event and the mineral dust within the biomass-burning plume

no stronger dust event could be detected during the cruise. This situation lasted all the time. In contrast to that Germany and even London got mineral dust from the Sahara. The dust concentrations in these regions were much higher than that detected by the ship. The corresponding dust outbreak is also visible on Fig. 8.1c).

With the help of the forecast the on board interpretation of the measured data was slightly easier than without. Knowing the exact sources was very helpful. It was even good to know when the measurements should detect which aerosol types. This was very beneficial especially for the high-volume-sampling by Gode Gravenhorst and Magarete and Wolfgang Fricke.

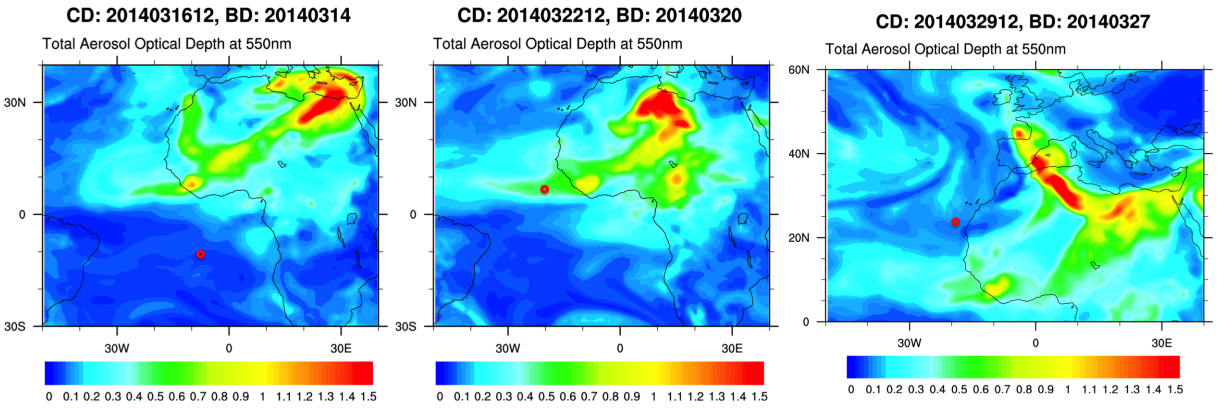

Fig. 8.1: Modelled AOD forecast for 12 UTC at the a) 16.12.2014, b) 22.3.2014 and c) 29.3.2014 with the start date of the model forecast simulation at 00UTC of the date given with BD

Model comparison to the Microtops measurements

Measurements of the AOD using MICROTOPS sun-photometers (see chapter 7) were done during the cruise. Since we got the modelled data on board, we got the opportunity to have a quicklook on the comparison of the measured and the modelled AOD. This is displayed in Fig. 8.2. There the blue points stand for the measurements and the coloured lines for the one day (grey), the two day (green) and the three day (pink) forecast.

The displayed time series lasts until the ship was near the latitude of Gibraltar and shows all the time from leaving the port of Cap Town. With the low values it is nicely visible that *Polarstern* travelled within clean marine air during the time on the Southern Hemisphere. The strong increase of the modelled AOD on 21 March is due to the entrance into the biomass-burning plume, which could not be captured by the measurements due to clouds. At the next day the ship already started to leave that region and entered a region with lower AODs, which are still higher than these of clean marine air. This is because the air mass is still affected by older material of the plume and also some older mineral dust. At the 27th one last weak dust transport to the ocean could be detected, which was a very local event. On the next day the track left the region with mineral dust influence. Then clean marine air occurs within the last days until the end of this plot.

In general the model results fits quite well to the measurements. Only on 17 March the measured AOD had a local maximum, which was not predicted by any of the three forecast types.

One could believe that the one day forecast is closer to the measurements than the two or three day forecast. But this is not judgeable based on this data. While there are points and times where the one day forecast fits best to the measurements (ex: 23.4. to 26.3.), there are also points where it misses the measurements compared to the other forecasts (ex: 10.3, 27.3.).

This may have different reasons, which are highly speculative for now. For a final conclusion on that and an analysis of some misses of the model further analysis after the cruise is needed, which should also contain the reanalysed MACC-data. The plot also does not include the errors of the measurements. But these could also affect the conclusions.

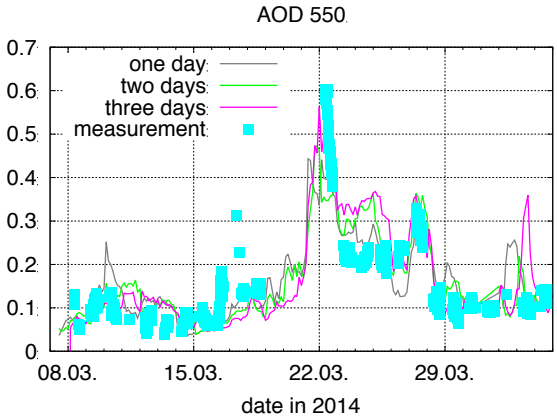

Fig. 8.2: Time series on the measured AOD at 500 nm compared to the modelled AODs at 550 nm for the one day, two days and three day forecast

Model comparison to LIDAR-measurements

Using a LIDAR (chapter 3) vertical information about the aerosols could be gained. This measurement data could also be compared to the model. Therefore the morning of 22 March is presented here. On that day the ship was within the plume of biomass-burning aerosol, which was one of the most interesting cases during the cruise. The LIDAR-signal in the 1,064 nm and 532 nm band is show in Fig. 8.3. The backscatter signal at 1,064 nm retrieves information whether there are reflecting objects like aerosols or cloud droplets in the atmosphere, while the depolarisation signal at 532 nm retrieves information about the aerosol typ. Since there is further work on this data needed the results presented here are only rough estimations. The 1064 nm-band shows an aerosol layer up to roughly 4,000 m. This layer consists of 2 maxima. The layer with the uppermost maxima is descending during the day. Since mineral dust retrieves a strong depolarisation signal at 532 nm, how it is visible in the depolarisation plot (Fig. 8.3b), this layer contains mineral dust, which is typical for that region. Due to the knowledge that the ship crossed the biomass-burning plume on that day, it must also contain black carbon and organic carbon. The lowermost maximum is the sea salt enriched boundary layer. This is also visible on the depolarisation at 532 nm (Fig. 8.3b), where sea salt retrieves no signal. The signal between 1 and 4 a.m. is due to downward mixed mineral dust.

Now it is possible to compare this data to the modelled profiles shown in Fig. 8.4 for 00UTC, 3UTC and 6UTC. The vertical scale of the modelled plots is in pressure units, because we did have the need data for the conversion into a metric scale. That's why the extinction coefficient contains the unusual unit of 1/hPa. Due to that reason, and the fact that there is still work needed to get the extinction coefficients from the LIDAR, only a qualitative comparison can be done. The model predicted the two aerosol layers seen in the LIDAR. It also captures the downward mixing leading to the upper maxima in lower altitudes. The different aerosol types are summed to anthropogenic (red line) and natural (blue line) in the model. While mineral dust and sea salt represent the natural aerosols, organic carbon, black carbon and sulphate form the anthropogenic class. With this information on could say that the model get the change in the dominating aerosol types within the upper layer. The modelled extinction coefficient is

affected by natural and anthropogenic aerosols at 00UTC and 3UTC. In contrast to mineral dust is dominating within the upper layer at 6UTC. In the 532 nm depolarisation the layer with the signal increases towards 6UTC, so one could conclude that there is relatively more mineral dust in this layer at the end than at the beginning. But this is just a rough guess based on unprocessed data.

Finally the model creates the upper aerosol layer onto a high of 400hPa, which is roughly 6,500 m. The comparison with the LIDAR shows that this too high.

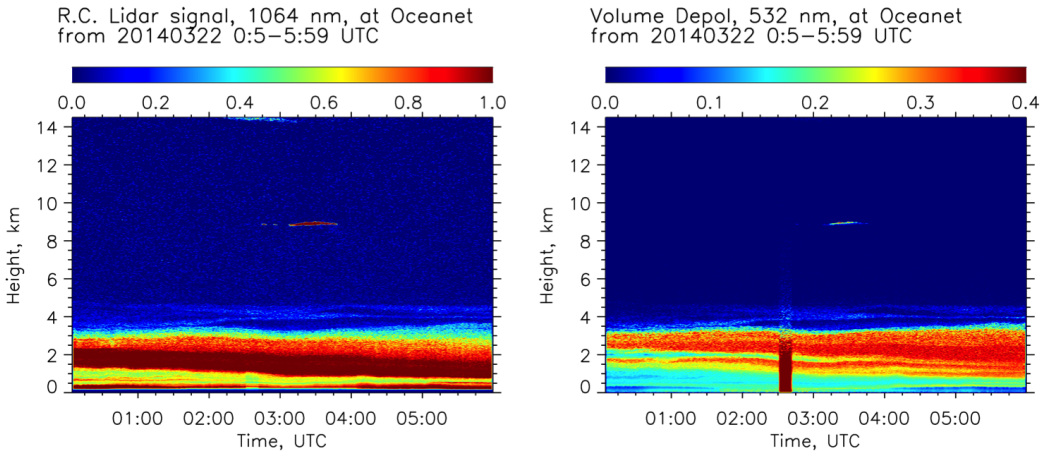

Fig. 8.3: LIDAR-signal containing the information on a) backscattering at 1,064 nm and b) depolarisation at 532 nm

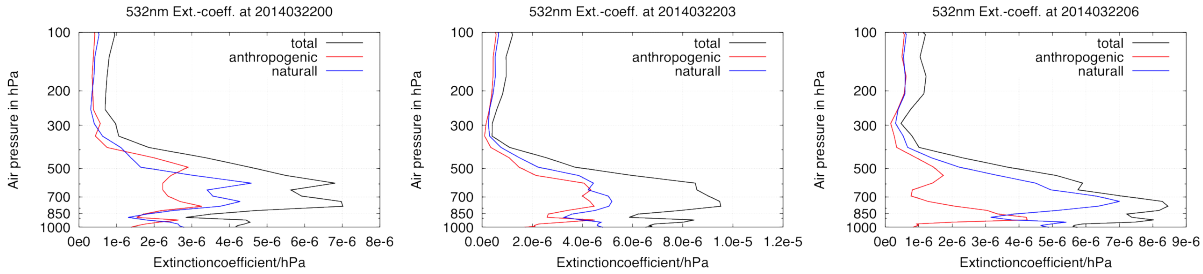

Fig. 8.4: Modelled vertical profiles at a wavelength of 532nm for a) 00UTC, b) 3UTC and c) 6UTC

References

Benedetti A, Morcette J -J, Boucher O, Dethof A, Engelen R J, Fisher M, Flentje H, Huneeus N, Jones L, Kaiser J K, Kinne S, Mangold A, Razinger M, Simmons A J and Suttie M, 2009 Aerosol analysis and forecast in the European Centre for Medium-Range Weather Forecasts Integrated Forecast System 2: 2 Data assimilation J Geophys Res 114 D13205 doi: 10 1029/2008JD011115.

Morcette J -J, Boucher O, Jones L, Salmond D, Bechtold P, Beljaars A, Benedetti A Bonet A, Kaiser J W, Razinger M, Schulz M, Serrer S, Simmons A J, Sofiev M, Suttie M, Tompkins A M and Untch A, 2009 Aerosol analysis and forecast in the European Centre for Medium-Range Weather Forecasts Integrated Forecast System: Forward modeling J Geophys Res 114 D06206 doi:10 1029/2008JD011235

Süddeutsche de - Wissen 2 April 2014 17:41

9. OCEANET: REMOTE SENSING OF ATMOSPHERIC GREENHOUSE GAS CONCENTRATIONS (REMOTEC)

Friedrich Klappenbach[1], Julian Kostinek[1], Marco Bertleff[1]
not on board: Andre Butz[1], Frank Hase[1], Matthias Schneider[1]

[1]KIT-Karlsruhe

Objectives

The man made release of carbon dioxide (CO_2) and methane (CH_4) to the atmosphere drives an enhanced greenhouse effect that is considered responsible for climate change (IPCC, 2011). Our research group at KIT develops and operates robust and versatile spectrometers that allow for measuring total column CO_2 and CH_4 concentrations in the Earth's atmosphere. We generally aim at determining the target concentrations with an accuracy better than 0.3 % in order to validate coinciding satellite measurements and to extract information on sources and sinks that control the atmospheric concentrations. While total column greenhouse gas concentrations are monitored on a regular and long-term basis by several land-based stations around the world, only a few measurements are conducted close to the oceans or on research vessels and ships. Deployment of our instruments on *Polarstern* aims at demonstrating that the instrumentation is sufficiently robust for ship deployments while achieving the accuracy required for satellite validation and source/sink estimation. The observational technique relies on absorption spectroscopy in the shortwave infrared spectral range where telluric absorption of the target species can be observed in direct sunlight. Building on solar absorption spectroscopy, our approach requires a sun-tracking device that compensates movements of the measurement platform. Two instruments had been taken on board: A miniature Fourier Transform Infrared spectrometer (FTIR), Bruker EM27 as well as the infrared grating spectrometer G-RemoteC (GRC). The GRC is a custom-built instrument still under development. It is designed to operate under harsh environmental conditions, whereas the EM27 basically is designed for the laboratory. Both instruments have been operated simultaneously in order to guarantee data quality by comparing the two data records. In preparation of the cruise the greenhouse gases observing satellite (GOSAT) extended its measurement schedule for achieving more matchups with the ship cruise.

Work at sea

As long the weather conditions allowed for the two instruments have been deployed on the Peildeck measuring absorption spectra every other minute. During the whole measurement period, both instruments were under surveillance for instrumental failure or changing illumination conditions. Changes in the ship track often resulted in shadowing of the instruments which require direct sunlight to operate. Measurements at 14:00 are the most important ones because of GOSAT-overpasses. At the end of a measurement day, the instruments were examined for damage and fatigue and maintenance measures were undertake to guarantee operability for the next day. Onboard instrument adjustments reached from an additional peltier-cooling-system for the GRC or a vibration-sensor for the EM27 as well as cleaning the optical parts from sea salt and applying changes in the measurement-script.

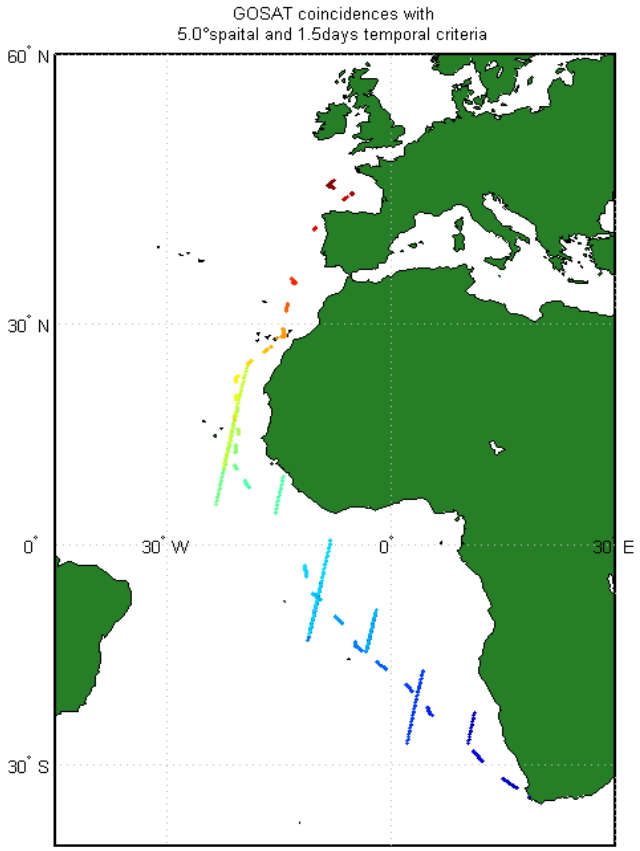

Fig 9.1: Measurements taken during the cruise. The color code has a temporal meaning: Blue is at the beginning of the campaign, red at the end. The vertical stripes in the plot are satellite-measurements that coincide with the measurements taken on board.

Preliminary results

The two instruments operated for the whole campaign and recorded together more than 150.000 spectra. It can be expected, that this will result in approximately 100 CO_2 and CH_4 data points per day in average along the ship track. Both instruments have been improved in their robustness as well as their performance during the cruise. In the first part of the cruise from Cape Town to the Canary Islands we were able to get several GOSAT coincidences with a coincidence-criteria of 5 degrees latitude longitude spatially and 1.5 days temporally (Fig. 9.1).

The concentrations of the trace gases need to be obtained in a retrieval process that will be performed in the months after the cruise. Beside the comparison with satellite data the two instruments EM27 and GRC will be compared with each other. The observations of the ground-based observatory at Izana on Tenerife will serve as a valuable reference measurement. Furthermore, we expect to exploit the CO_2 and CH_4 data record for interhemispheric gradients caused by the non-uniform distribution of sources.

Data management

Data will be made available to interested parties upon request. Upload of the data to the PANGAEA database is planned.

References

Edenhofer O, Pichs-Madruga R, Sokona Y, Seyboth K, Matschoss P, Kadner S, Zwickel T, Eickemeier P, Hansen G, Schloemer S, von Stechow C (Eds.) (2011) Intergovernmental Panel on Climate Change, Cambridge University Press, Cambridge, United Kingdom and New York, NY, USA, 1075 pp

10. OCEANET: HEAT FLUX MEASUREMENTS AND TROPOPAUSE STUDY

Robin Pilch Kedzierski [1] , Wuke Wang [1] [1]GEOMAR

Objectives and Work at sea

Heat flux measurements

There are two instruments mounted on the crow's nest of Polarstern (see Fig. 10.1): Licor, to measure CO_2 and water vapor concentrations at 10Hz frequency; and Sonic, to measure the 3D components of the wind and the temperature at 30Hz frequency.

The variability of these parameters at ~1/10 second timescale will be analyzed after the cruise to retrieve sensible and latent heat fluxes. Together with the solar and long-wave radiation data measurements from the ship, an estimate the air-sea energy budget can be obtained (for method, see Bumke et al. 2014).

Fig. 10.1: Sonic (top left) and Licor (top, centre) mounted on the crow's nest of Polarstern.
© Robin Pilch Kedzierski, GEOMAR.

Tropopause study

Available are 20 radiosondes to release during the cruise. They are the same Vaisala model that the Deutscher Wetter Dienst releases every day around noon. They obtain vertical profiles (up to around 30km) of temperature, humidity and horizontal wind.

The focus is made on the Tropopause region (the boundary between the troposphere and the stratosphere). Of interest is the release of extra radiosondes when it is possible to capture special features like a strong temperature inversion, or a double Tropopause. In Fig. 10.2, the release of one radiosonde is shown.

Preliminary results

The graphic in Fig. 10.3 shows all the temperature profiles obtained during the cruise. The coldest, highest, and also the sharpest tropopause can be observed around the Equator (< -80ºC, about 17km altitude). The sharpness of the tropopause decreases gradually towards the subtropics and mid-latitudes, where temperatures so cold are not reached.

Fig. 10.2: Radiosonde release. © Friedrich Klappenbach, KIT

A secondary (relative) temperature minimum above 10km altitude gradually appears from 20ºN northwards. At around 35ºN several profiles show clearly two peaks of minimum temperature (around 12 and 17km altitude), meaning that a double Tropopause is present. In this latitude range, the temperature peak around 17 km gradually disappears northwards.

North of 40ºN, only the minimum temperature peak (<-60ºC) at 10-12km altitude remains, which corresponds to the extratropical Tropopause.

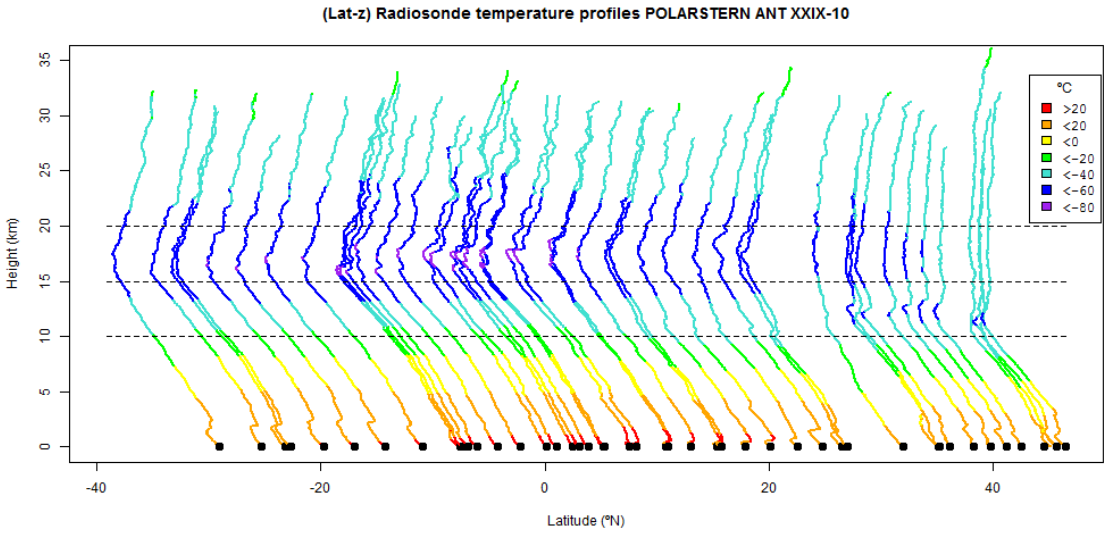

Fig. 10.3: meridional cross section of all observed temperature profiles. © Robin Pilch Kedzierski, GEOMAR

Data management

Radiosonde data are available through the PANGAEA archive. The flux data will be made available to other cruise participants upon request after completion of the post processing.

Acknowledgments

Special thanks to Juliane Hempelt (DWD) for sharing the data from the DWD radiosondes as well as for her help when showing us the release process.

References

Bumke K, Kalisch J, Macke A, Kleta H (2014) Measured and parameterized Energy Fluxes estimated for Atlantic Transects of R/V Polarstern. Journal of Physical Oceanography, vol44, 482-491.

11. OCEANET: CLOUD COVER MEASURED WITH INFRA-RED CAMERAS

Gaby Rädel[1] and Wolfgang Fricke[2]

[1] MPI
[2] formerly DWD

Objectives

During the expedition two different infra-red cameras were installed on board with the objective to continuously measure cloud base temperatures and thus derive cloud cover. The two instruments had very different horizontal and temporal resolutions which makes an intercomparison of the measurements interesting. In the following we will briefly describe the two cameras and then present very preliminary first comparisons of low-cloud covers.

Work at sea

MPI Infra-Red Camera

During the whole expedition pictures of the sky were taken with an infra-red camera that was mounted on the upper deck, starboard side, next to the aerosol OCEANET container on which a fish-eye cloud camera was mounted.

The camera is a commercial product, VarioCAM®, manufactured by Jenoptic, ESW, GmbH and the data acquisition software is provided by InfraTec, GmbH, Dresden.

The sensitive area of the camera consists of a micro bolometer focal plane array with 384 x 288 pixels. This leads to a field of view of 30 x 23° or a visible area of about 1,000 m x 800 m at 1 km height. The spectral range covered is 7.5 to 14 µm.

Pictures were taken every 5s from about 18h00 until 10h00 the next day, in order to avoid the exposure to direct sun light. The 5s were a compromise to achieve a good temporal resolution and keeping the data volume manageable.

These high horizontal and temporal resolutions provide information complementary e.g. to large-scale cloud measurements from satellites which are not able to measure temporal development of small scale cloud structures.

Nubiscope

A NubiScope manufactured by IMK was measuring cloud cover and the cloud base height and temperature during the whole cruise. It was mounted on top of the AERONET container on the Helideck's portside (Fig. 11.1). This position minimized influences from the ship's body on the measurements. The instrument consists of an infrared sensor contained in a weather tight metal tube and mounted to a pan and tilt unit programmed for scanning the full sky hemisphere. The Heitronics KT15D infrared sensor has a field of view of 3°. It covers the wavelength range of 8 to 14 µm and measures temperatures between -100° and +50°C. A control unit contains an interface board, the power supply and a computer for controlling the instrument and storing the data. The NubiScope can also be controlled remotely through a serial RS232 interface.

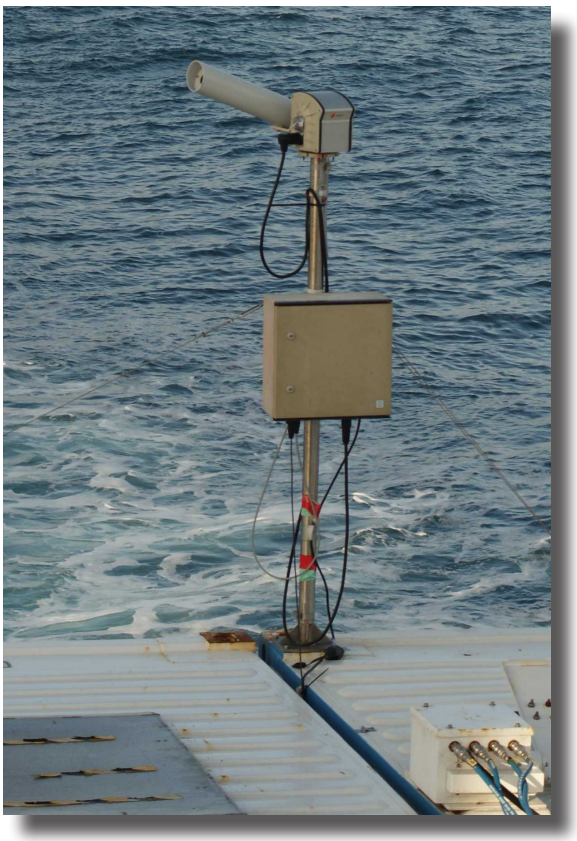

Fig. 11.1: Nubiscope as mounted on Polarstern'

A scan of the sky is made every 10 minutes and takes about 6 minutes each. It is performed in azimuth steps of 10°, and 3° for the zenith angle. An example of the resulting graphs is given in Fig. 11.2. North has been set to the ship's bow. The different cloud heights are represented by different shades of grey, clear sky is shown in blue. Cloud coverage at different elevations is given in percent, Tzero is the ground temperature being measured during the scan. It can be set to any position. The horizon in this example had been set to 69° zenith angle; however, measurements are made down to 90° and can, if necessary, be considered for the cloud cover calculation.

Preliminary results

The low-level cloud covers measured by the two instruments were initially inter-compared. The data taken during the two nights when the ship followed the track of the A-Train satellite constellation and was positioned directly under the Calypso satellite were analysed. These dates were the 17/18 March 2014 (02:27UTC overflight) and 20/21 March 2014 (02:55UTC overflight). Low-cloud cover as a function of time is plotted for these two nights in Figs 11.3 and 11.4 for the two instruments, respectively.

Here it must ne noted that the definition of low clouds is different for the two cases. While for the NubiScope low clouds are defined as cloud base to be lower than 3km, a temperature cut of Tbase > 15°C has been applied. This cut is valid in the tropics and subtropics but has to be adjusted for higher latitudes. Furthermore the field of view of the NubiScope is extending to higher angles than the about 30° of the IR-camera. In a future, more refined comparison of the two instruments we plan to restrict the field of view of the NubiScope to an area more similar to that of the IR-camera.

Given these differences and the very preliminary nature of the data treatment the agreement between the two measurements is remarkably good, especially for the first of the two nights. The second night shows reasonable qualitative agreement but quantitatively the NubiScope shows more often overcast situations.

In addition to these comparisons the results of the MPI camera have also been compared to the NOAA ceilometer and W-band radar and to the OCEANET 1064nm Lidar, and a very good qualitative agreement was observed.

Furthermore we could check the consistency of our measurements with the space borne Lidar on Calypso for two points: 18th March 2:27 UTC and 21st March 2:55UTC. For the first night both devices measured a clear sky case, while for the second night, the MPI cloud camera found 100% low-cloud cover while the Calypso Lidar signal got fully attenuated at about 10km height and hence no measurement can be made for lower altitudes.

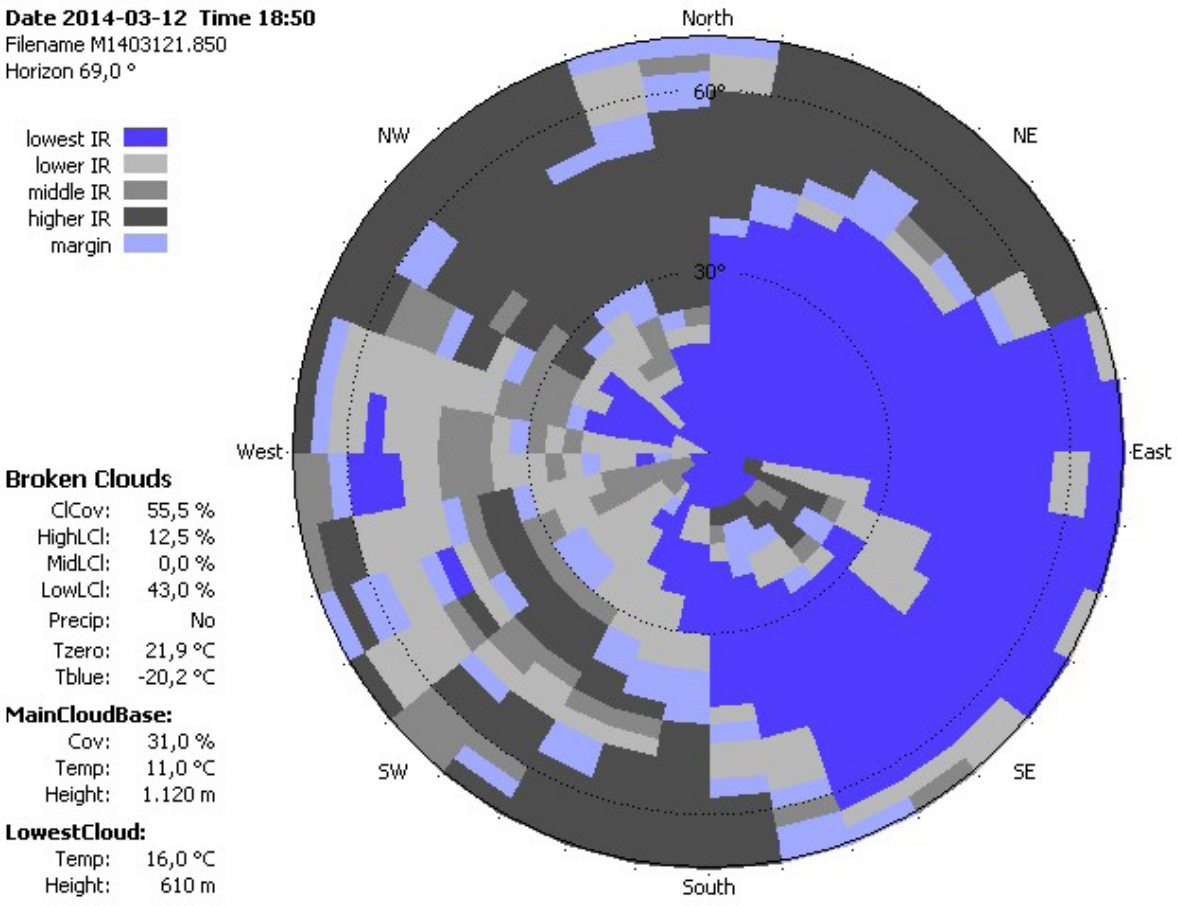

Fig. 11.2: Graph of the cloud cover on the 12th of March at 18:50 UTC

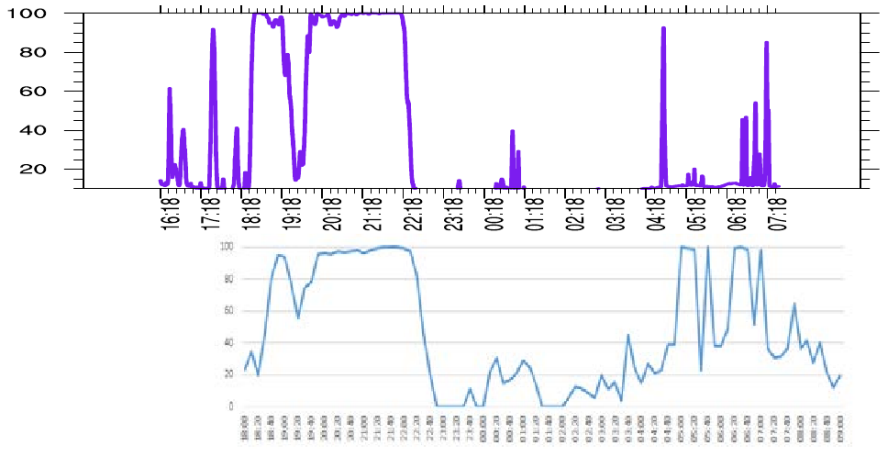

Fig. 11.3: Low-cloud cover for the night of 17 March to 18 March measured by the MPI infra-red camera (top) and by the NubiScope (bottom) Data management

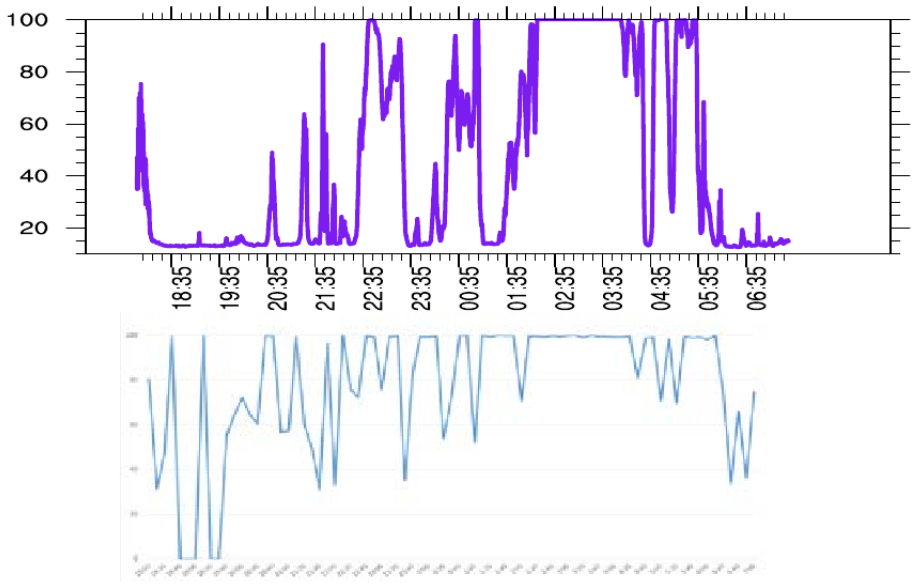

Fig. 11.4: Low-cloud cover for the night of 20 March to 21 March measured by the MPI infra-red camera (top) and by the NubiScope (bottom)

Data management

The Nubiscope data are undergoing a detailed analysis, quality control and reprocessing following the 'Polarstern' cruise. This is a prerequisite for storing them in the AWI data base and making them accessible to other cruise participants and research groups. In addition to the comparison with the MPI infrared camera it is intended to compare the NubiScope measurements with other data like

- Cloud radar measurements by NOAA,
- Ceilometer data from NOAA,
- Data from the weather station ceilometer on board 'Polarstern',
- Eye observations by the weather observers
- Cloud camera pictures from TROPOS
- TROPOS lidar measurements

or with other measurements on request.

These comparisons take some time and can then be used for common publications. Data from the MPI infra-red camera can be obtained on request from the MPI for Meteorology, Hamburg.

12. OCEANET: SATELLITE OVERFLIGHTS

Hartwig Deneke TROPOS

Objectives and work at sea

As a novel aspect of the OCEANET project, a comparison of the ship-based aerosol and cloud observations – in particular the lidar and W-band cloud radar measurements described in chapters 3 and 4 – to measurements from the CLOUDSAT and CALIPSO satellites, which fly in orbit as part of the A-Train satellite constellation, was planned.

An investigation of the consistency of satellite and ship-based estimates of aerosol and cloud properties are the motivation for this comparison. Due to the orbital height of 705 km of the satellites, the signal-to-noise ratio of the satellite observations is significantly lower than that for the ship-based instruments. It is important to understand and quantify the resulting differences including their implications for the scientific interpretation of the data in more detail. In particular the first-time availability of cloud radar observations during the cruise through the participation of NOAA's Earth System Research Laboratory served as motivation for this plan.

Towards this goal, a flexible route planning strategy was adopted, to achieve an optimal collocation between the ship track of *Polarstern* and the satellite ground track. As accurate estimates of the satellite orbits, and thus the satellite ground track, are only available 1-2 weeks in advance, the exact position of the intended satellite overflights had to be determined en route in close coordination between the master of *Polarstern* and the chief scientist. This strategy was supported by direct communication with the ground control centers of the CLOUDSAT and CALIPSO satellite missions, which advised on planned interruptions of the satellite observations, and even provided special orbit predictions for the purpose of route planning in case of CALIPSO.

All in all six such satellite overpasses could be achieved during this cruise, yielding an interesting dataset comprising a variety of atmospheric conditions, and made this strategy a full success. For an overview of the approximate locations of the overpasses, see the positions marked in Fig. 1.1 of this report.

Preliminary results

An important prerequisite for the comparability of the satellite and ship observations is the accuracy of collocation. In Figure 12.1, the ship and satellite ground tracks are shown for the six overpasses. For the overflights, the following strategy was adopted: 1-2 hours before the overpass, *Polarstern* reached the predicted ground track and followed it for 3-5 hours. During this period, the A-Train satellites passed directly above the ship. Thus, in the absence of significant temporal development, vertical cross-sections of about 30-40 sea miles in length can be compared between satellite and ground, assuming a typical cruise speed of *Polarstern* of about 10,5 knots.

In Table 12.1, the date/time, the position, and the distance between *Polarstern* and the satellite ground tracks at the time of the overflight are given. As basis for these calculations, the two-line elements (TLE) published at [1] have been used for CLOUDSAT, while predictions provided by the ground control team where used in case of CALIPSO. It can be seen that the achievable

accuracy of the collocation is roughly about 50 m. This accuracy has been realized relative to the CALIPSO ground track, whose orbital predictions have been used for the planning of the first 5 overflights. Collocation with CLOUDSAT is mostly significantly worse, due to relatively large deviations in the ground track of the CLOUDSAT and CALIPSO instruments. For planning the last overflight, the CLOUDSAT two-line elements have been used. Here, some relatively large changes in the predicted orbit were observed during the last days prior to the overpass. The final, rather large deviation is thus a consequence of the omission to update the position based on the most recent TLE for final planning, and the fact that *Polarstern* had to keep a minimum distance of 3,5 sea miles to the coast of Fuerte Ventura. This fact motivated the choice of the CLOUDSAT ground track for planning the overflight in the first place.

It also has to be realized that the satellite ground track shown here is based on orbital predictions, which are updated by a more accurate navigation once the final version of the satellite products are released. It is therefore expected that the accuracy of the final collocation will change, and is limited by the accuracy of the orbital predictions, which is an aspect which will be investigated in the time following the cruise.

As two examples for the planned comparisons, time-height cross-sections obtained from the OCEANET lidar, NOAA PSD radar, and from the CLOUDSAT and CALIPSO instruments are given in Figs. 12.2 and 12.3. A more thorough analysis will be carried out after the cruise.

In summary, the concept of obtaining accurately collocated measurements from ship and active satellite instruments has been successfully demonstrated during the cruise PS83 (ANT-XXIX/10). The coordination of the overpasses with the ship's crew, and other works carried out on board was possible with minor effort. Only minimal delays resulted from the overflights, which could easily be accounted for in the overall cruise planning. We therefore hope to be able to collect valuable scientific data from additional overpasses on future cruises of *Polarstern* made within the framework of OCEANET, and contribute to the validation of active satellite instruments through this effort.

Data management

Not applicable.

References

[1] http://www.CLOUDSAT.cira.colostate.edu/dpcstatusElements.php

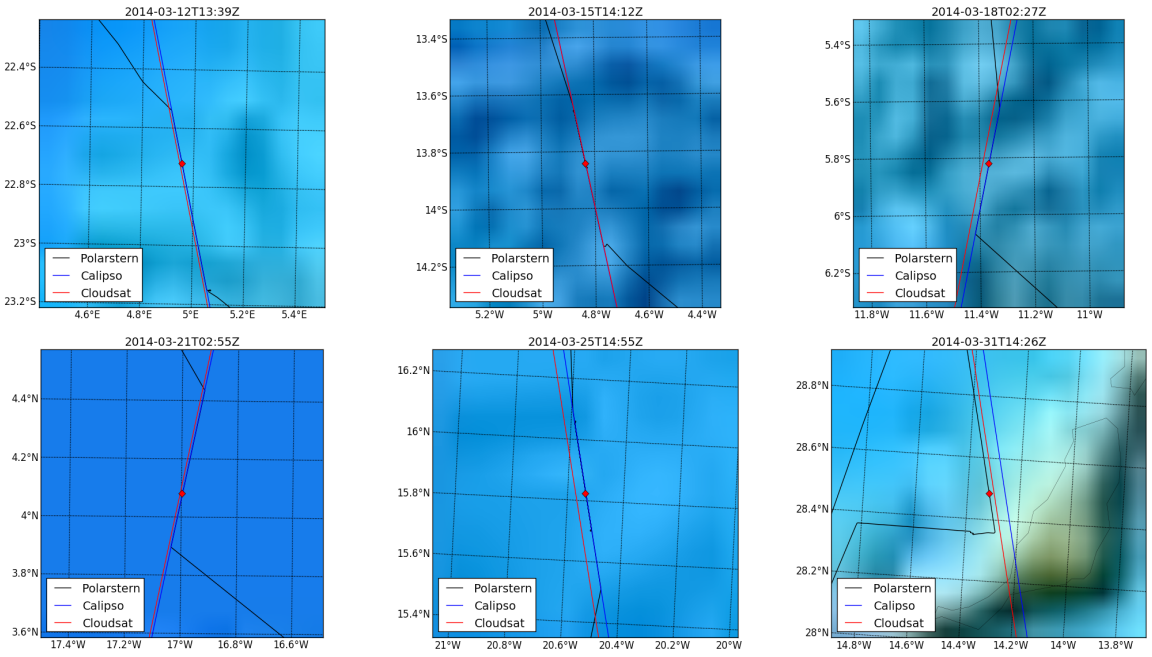

Fig. 12.1: Overview plots for the 6 satellite overflights realized during PS83 (ANT-XXIX/10)

Tab. 12.1: Date/time, location, and geolocation accuracy with the CLOUDSAT and CALIPSO satellites calculated for the time of overflight.

Date/Time	Latitude [°]	Longitude [°]	d(CLOUDSAT) [m]	d(CALIPSO) [m]
2014-03-12T13:39Z	-22.721	4.956	878	50
2014-03-15T14:12Z	-13.843	-4.834	55	49
2014-03-18T02:27Z	-5.821	-11.366	2549	36
2014-03-21T02:55Z	4.080	-16.996	927	2
2014-03-25T14:55Z	15.822	-20.535	3840	7
2014-03-31T14:26Z	28.483	-14.316	1778	7936

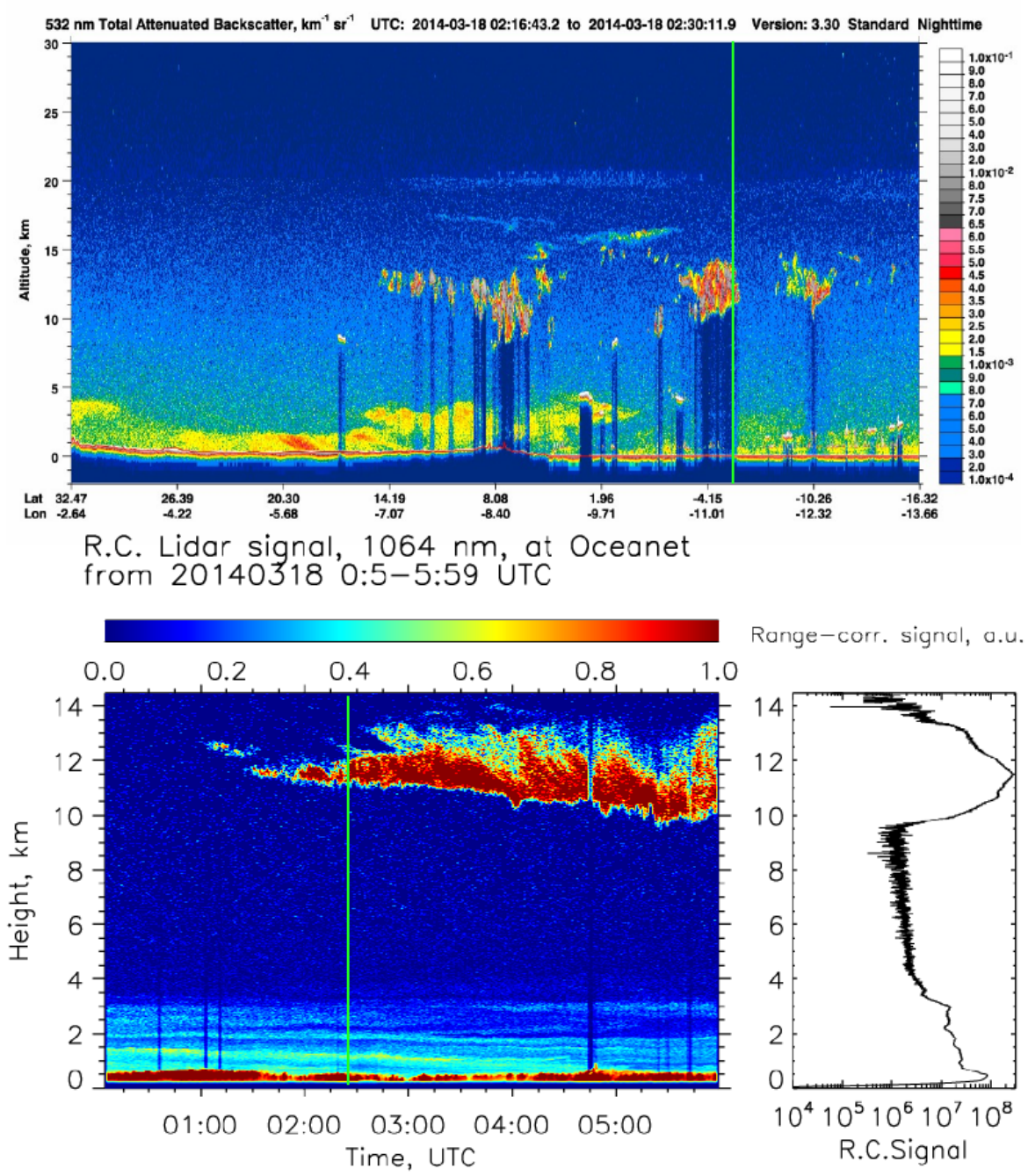

Fig. 12.2: Comparison of backscatter signal from CALIPSO (top) and OCEANET lidar (bottom) on 2014-03-18 around the time of the overflight (2:27Z). The corresponding time is marked by a green line. During the overpass, both lidars observed a dust layer ranging up to 3km in height, as well as a cirrus cloud in a height of 12 km.

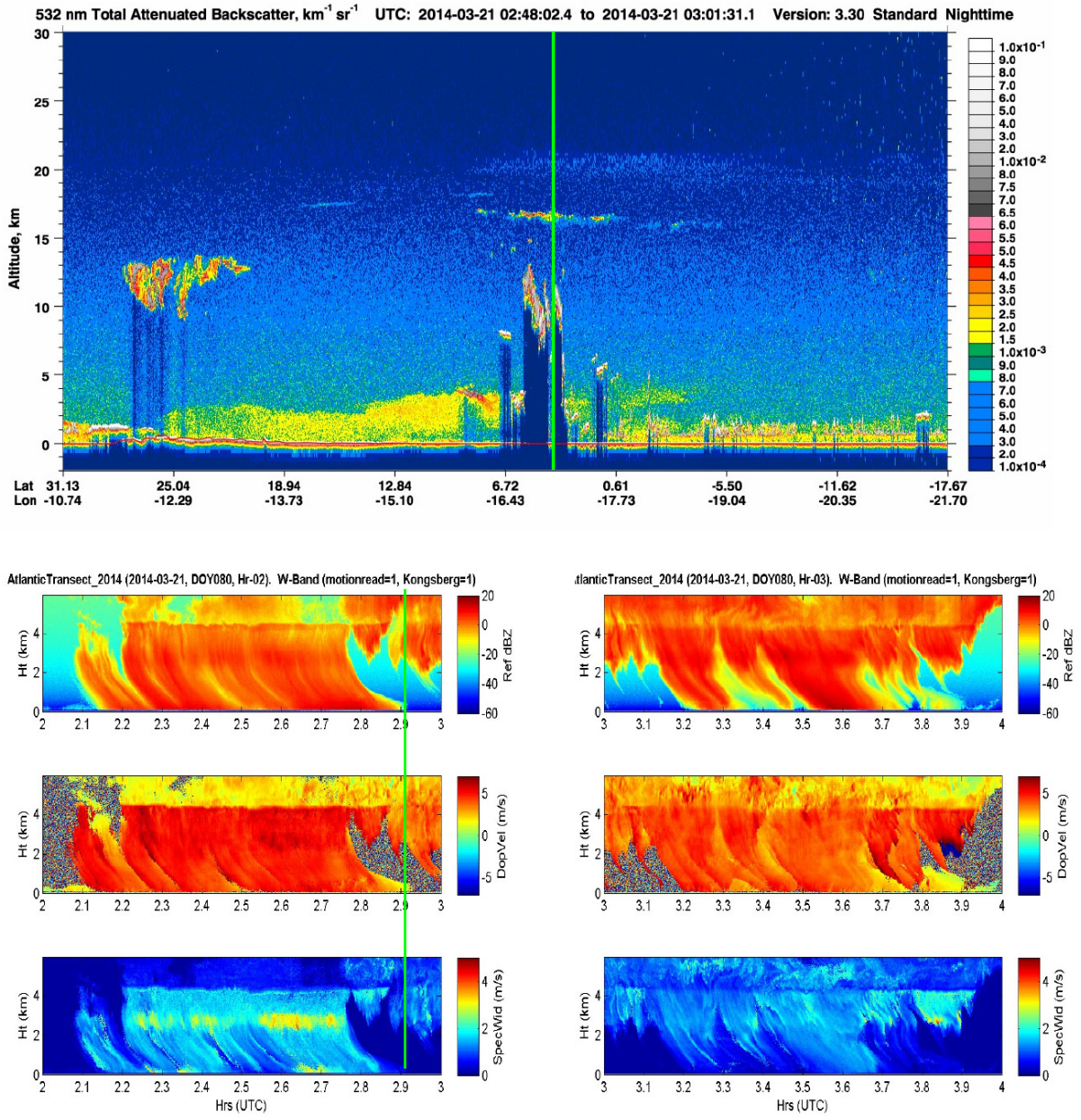

Fig. 12.3: Comparison of backscatter signal from CALIPSO (top) and NOAA PSD W-Band radar (bottom) on 2014-03-21 around the time of the overflight (2:55Z). The corresponding time is marked by a green line. During the overpass, the lidar observed a deep convective system ranging up to 13km in height, while the radar observed the corresponding heavy precipitation, including a bright-band at a height above 4 km ASL.

13. GENETIC & METABOLIC PROFILING AND ECOPHYSIOLOGY OF ANTARCTIC FISHES

Christian Bock[1], Astrid Böhmer[1], Guido Krieten[1], Maj Wetjen[1], Rainer Knust[1+], Chiara Papetti[1+], Magnus Lucassen[1+]

[1]AWI, [+]not on board

Objectives

It is believed that increasing temperatures and CO_2 concentrations, also known as ocean warming and acidification, will have their biggest impact in polar areas (Pörtner 2008, IPCC 2007). Antarctic fishes are exceptional for their high specialization to live under constant conditions near the freezing point of sea water and are believed to be highly stenothermal. Temperatures are expected to increase up to plus 2-3°C in Antarctic waters until the end of this century. This scenario may have dramatic effects on the physiology of these specialists with unknown consequences for the biodiversity of the Antarctic ecosystem itself. Recent approaches like genetic and metabolic profiling will help to understand the climate-induced response of ecological relevant performance parameters such as growth of Antarctic marine fishes. For such studies alive animals have to be transported to the Alfred Wegener Institute, Helmholtz Centre for Polar and Marine Research in Bremerhaven.

Work at sea

More than 150 high Antarctic fish specimens, caught on the previous leg, were kept in special aquarium containers at natural and defined conditions at temperatures around -0.5°C. Regular daily water exchanges were performed by an onboard sea water cooling tank with an integrated UV lamp to keep the water quality as optimal as possible. Fishes were further characterized; the number of individuals of a single species was counted and a rough size distribution was conducted on board. In order to get some information about the condition status of the fishes, ventilation frequency was measured on the most frequent fish species *Trematomus eulepidotus*. Ventilation rate was visually calculated by counting the opercular movement rates of fishes from different size classes to address for potential allometric effects.

Results

In total 111 alive fish specimens were managed to be transferred to the aquarium of the institute in Bremerhaven (Tab. 13.1). No signs of stress or flight reactions were observed during the entire cruise leg indicating sufficient maintenance conditions for the animals in the aquarium containers.

Tab. 13.1: Number of individuals per species maintained in the aquarium container on board *Polarstern*.

Species	Number
T. eulepidotus	71
T. bernacchii	4
T. hansoni	3
Trematomus sp.	2
D. longedorsalis	11
A. orianae	14
A. shackeltoni	3
A. loennbergi	1
Artedidraco sp.	1
P. borchgrevinki	1
Octopus sp.	5

Ventilation frequency measurements were performed on individuals of *T. eulepidotus* of different size classes. The overall mean ventilation rate was 25 beats per minute, which is well in the range in comparison to literature values of a closely related Antarctic fish species *T. bernacchii* (Jayasundara et al. 2013). This indicates stress less conditions of the fishes during transportation. The biggest individuals showed the lowest opercular movements and a clear negative linear relationship of the ventilation rate with body size could be observed. The observed allometric effect on the ventilation rate is in line with a decrease in oxygen consumption per gram wet weight with an increase in body size of fishes. Smaller individuals have higher heart rates resulting in elevated energy requirements for their cardio-vascular performance. The later may explain the observed relationship between ventilation rate and body size (Yamamoto 1992).

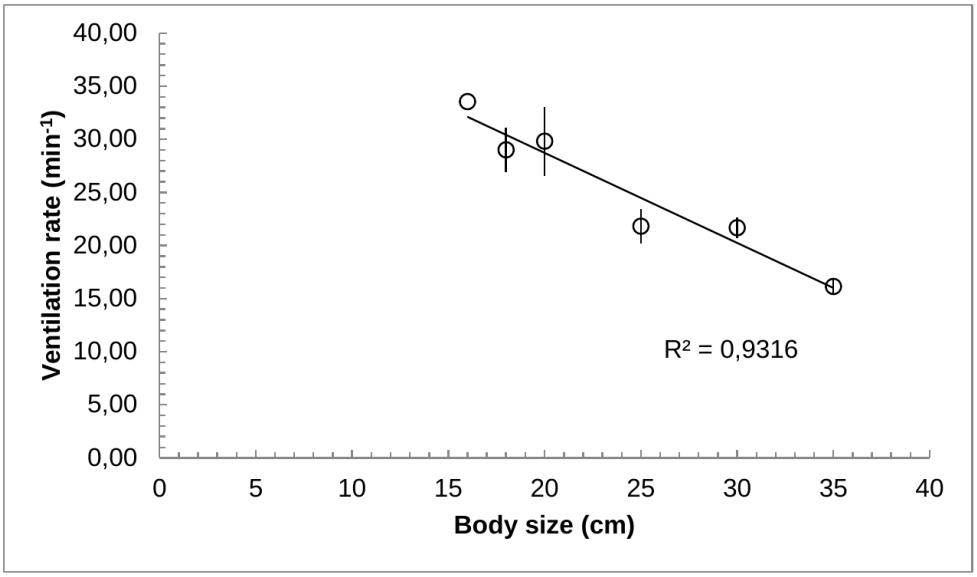

Fig. 13.1: Relationship between ventilation rate and body length of the high-Antarctic fish Trematomus eulepidotus caught on the previous leg (PS 82).

Data management

All data collected during this cruise will be available through publications or reports.

References

IPCC Fourth Assessment Report: Climate Change 2007 (AR4) https://ipcc.ch/report/ar4/

Jayasundara N, Healy TM, Somero GN (2013). Effects of temperature acclimation on cardiorespiratory performance of the Antarctic notothenioid Trematomus bernacchii. Polar Biol 36:1047-1057.

Pörtner HO (2008). Ecosystem effects of Ocean acidification in times of Ocean warming: a physiologists view. Mar Ecol Prog Ser 373:203-217.

Yamamoto K (1992). Relationship of respiration to body weight in the tilapia Oreochromis niloticus under resting and normoxic conditions. Comp Biochem Physiol 103:81-83.

14. AT-SEA DISTRIBUTION OF SEABIRDS AND MARINE MAMMALS

Simon Jungblut[1], Dominik Nachtsheim[1], Claude R. Joiris[1] (not on board) [1]PolE

Objectives

In the course of long-term observations to study the at-sea distribution of marine top predators the icebreaking research vessel RV *Polarstern* is used regularly by the PolE group (Laboratory for Polar Ecology, Head: Prof. Claude R. Joiris) to record marine birds and mammals in polar regions. Operating in Arctic and Antarctic, the vessel crosses the Atlantic Ocean frequently, leading to a large north-south transect for each transfer. The main aim of participating in PS83 (ANT XXIX/10) is to deepen the understanding of factors determining the at-sea distribution of seabirds and marine mammals across the Atlantic Ocean. This expedition is one of four trans-equatorial expeditions of RV *Polarstern* used to collect bird and mammal observation data for this area. Additionally, these “long time surveys” ensure a solid baseline for later comparisons of geographical distributions and densities of single species which may alter in the future due to climate change effects.

On such large scale, very different biogeographical zones can be recognized with differences in ecological structure, in prey availability and thus in upper level predator abundance. The main water masses and fronts can be defined on the basis of hydrological factors registered on board *Polarstern* on a continuous basis: salinity, water temperature and depth.

Work at sea

Half-hour transect counts were conducted continuously from the bridge (approx. 18 m above sea level) without width limitation during daylight and travelling speed of the vessel (see Methods in Joiris & Falck 2011). Observations covered a 90° angle from bow to one side since the bridge is too broad for simultaneous counts of both sides by one observer. Species were identified with naked eye, following confirmation using binoculars (8 – 10 fold magnification). Photographic documentation helped in retrospective recognition of rare or difficult to identify specimens.

Water temperature and salinity were recorded continuously and automatically by a thermo-salinometer installed at the keel of *Polarstern* (approx. 10 m below sea level). Depth data are achieved by either the vessel´s echosounder or hydrosweep. Data were extracted from the DShip data system on board.

Preliminary results

Transect counts

Counts were done during times the ship was moving at travelling speed and light allowing, usually between 20 and 23 counts per day. Fig. 14.1 shows crosses for coordinates of the starting points of half-hour counts. Big gaps between counts along the expedition transect are due to night time.

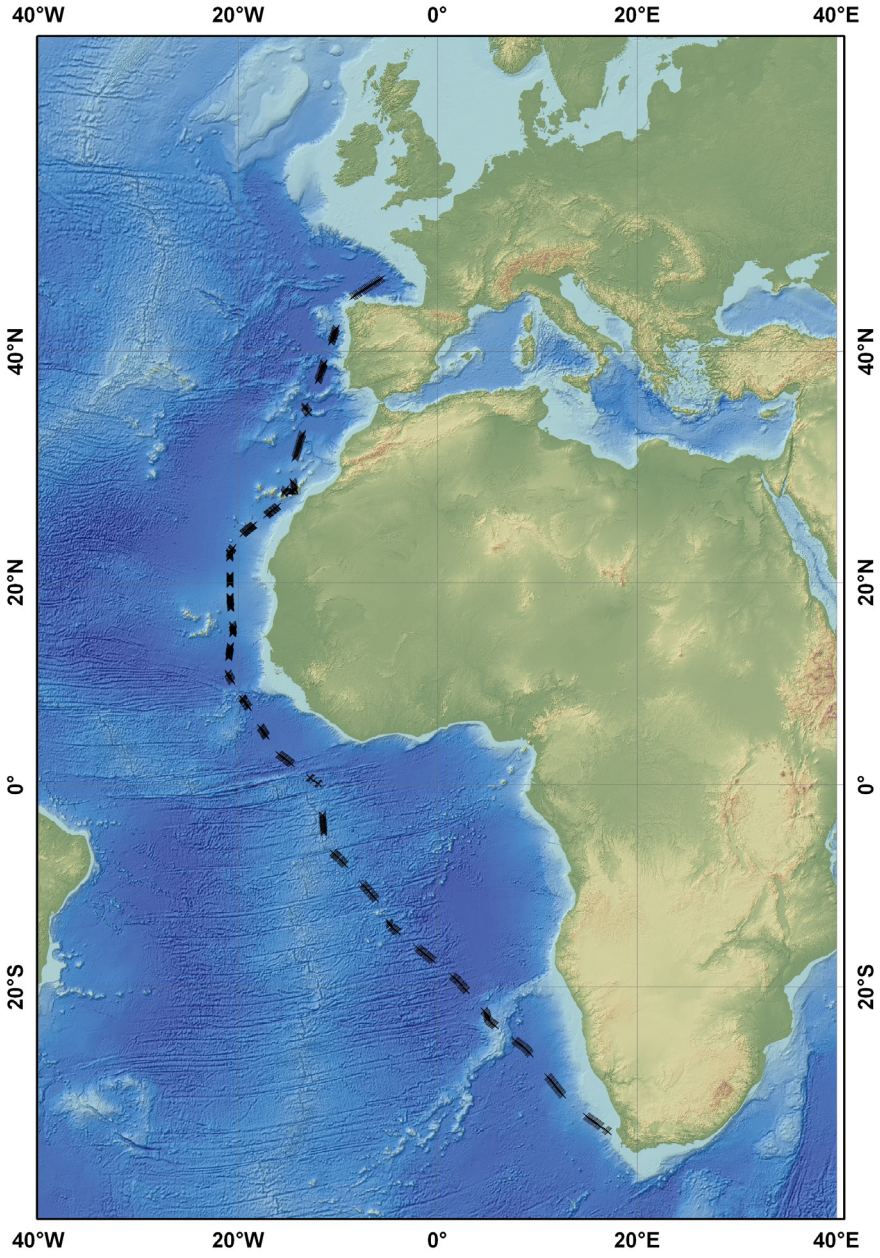

Fig. 14.1: Map of the Atlantic Ocean. Each cross represents one half-hour count, big gaps are due to night time.

Sampling results

This report includes preliminary counting results ranging from our departure in Cape Town on 8 March 2014 until 7 April 2014 passing the Bay of Biscay. In total 538 counts, representing 269 hours of observation were done. About 2,103 birds of 33 species and 309 cetaceans of 11 species were observed. Table 14.1 gives a summary of species and total numbers of individuals per species over all counts. Additionally to the target species, 39 sea turtles, six sharks, one ray and two sunfishes were detected.

Tab. 14.1: Species list and total numbers of seabirds and marine mammals observed during PS83 (ANT XXIX/10)

species		total no.
seabirds		
Black-browed albatross	*Thalassarche melanophris*	11
Shy albatross	*Thalassarche cauta*	90
Albatross sp.		3
Great-winged petrel	*Pterodroma macroptera*	10
Bulwer's petrel	*Bulweria bulwerii*	9
White-chinned petrel	*Procellaria aequinoctialis*	76
Petrel sp.		300
Cory's shearwater	*Calonectris diomedea*	861
Great shearwater	*Puffinus gravis*	31
Sooty shearwater	*Puffinus griseus*	34
Manx shearwater	*Puffinus puffinus*	18
Macaronesian shearwater	*Puffinus baroli*	2
Shearwater sp.		59
White-faced storm-petrel	*Pelagodroma marina*	7
Madeiran storm-petrel	*Oceanodroma castro*	88
Leach's storm-petrel	*Oceanodroma leucorhoa*	7
Storm-petrel sp. (Mad./Leach.)	*Oceanodroma sp*	2
European storm-petrel	*Hydrobathes pelagicus*	10
Storm-petrel sp.		47
Red-billed tropicbird	*Phaeton aethereus*	1
Tropicbird sp.		14
Ascension frigate-bird	*Fregata aquila*	5
Northern gannet	*Sula bassana*	22
Cape gannet	*Sula capensis*	31
Red-footed booby	*Sula sula*	2
Brown booby	*Sula leucogaster*	1
Great skua	*Catharacta skua*	16
Skua sp.		1
Herring gull	*Larus argentatus*	1
Lesser black-backed gull	*Larus fuscus*	4
Yellow-legged gull	*Larus michahellis*	2
Great black-backed gull	*Larus marinus*	1
Gull sp.		2
Tern sp.		252
Alcidae sp.		1
Unidentified birds		22

species		total no.
bird vagrants		
Peregrine falcon	*Falco peregrinus*	1
Collared dove	*Streptopelia decaocto*	2
European turtle dove	*Streptopelia turtur*	1
Laurel pigeon	*Columba junoniae*	1
Feral pigeon	*Columba livia f. domestica*	52
Pigeon sp.		2
Barn swallow	*Hirundo rustica*	1
sum birds		**2103**
cetaceans		
Sperm whale	*Physeter macrocephalus*	3
Fin whale	*Balaenoptera physalus*	5
Sei whale	*Balaenoptera borealis*	1
Minke whale	*Balaenoptera acutorostrata*	2
Large whale		14
Long-finned pilot whale	*Globicephala melas*	10
Short-finned pilot whale	*Globicephala macrorhynchus*	20
Common dolphin	*Delphinus delphis*	65
Atlantic spotted dolphin	*Stenella frontalis*	22
Striped dolphin	*Stenella coeruleoalba*	8
Bottlenose dolphin	*Tursiops truncatus*	117
Risso's dolphin	*Grampus griseus*	5
Dolphin sp.		37
sum cetaceans		**309**

The density of seabirds was quite low in the open ocean. Fig. 14.2 shows a map of the observed area and includes circles representing the daily mean abundance of birds per replicate. Open ocean values are generally low and higher closer to land masses. High numbers in offshore areas are mainly due to sightings of great swarms which lead to high mean values. Swarms, if travelling, have to be matter of discussion as they may not be correlated to the respective water mass. Thus, care has to be taken, if extremely high mean abundance values occur in offshore areas.

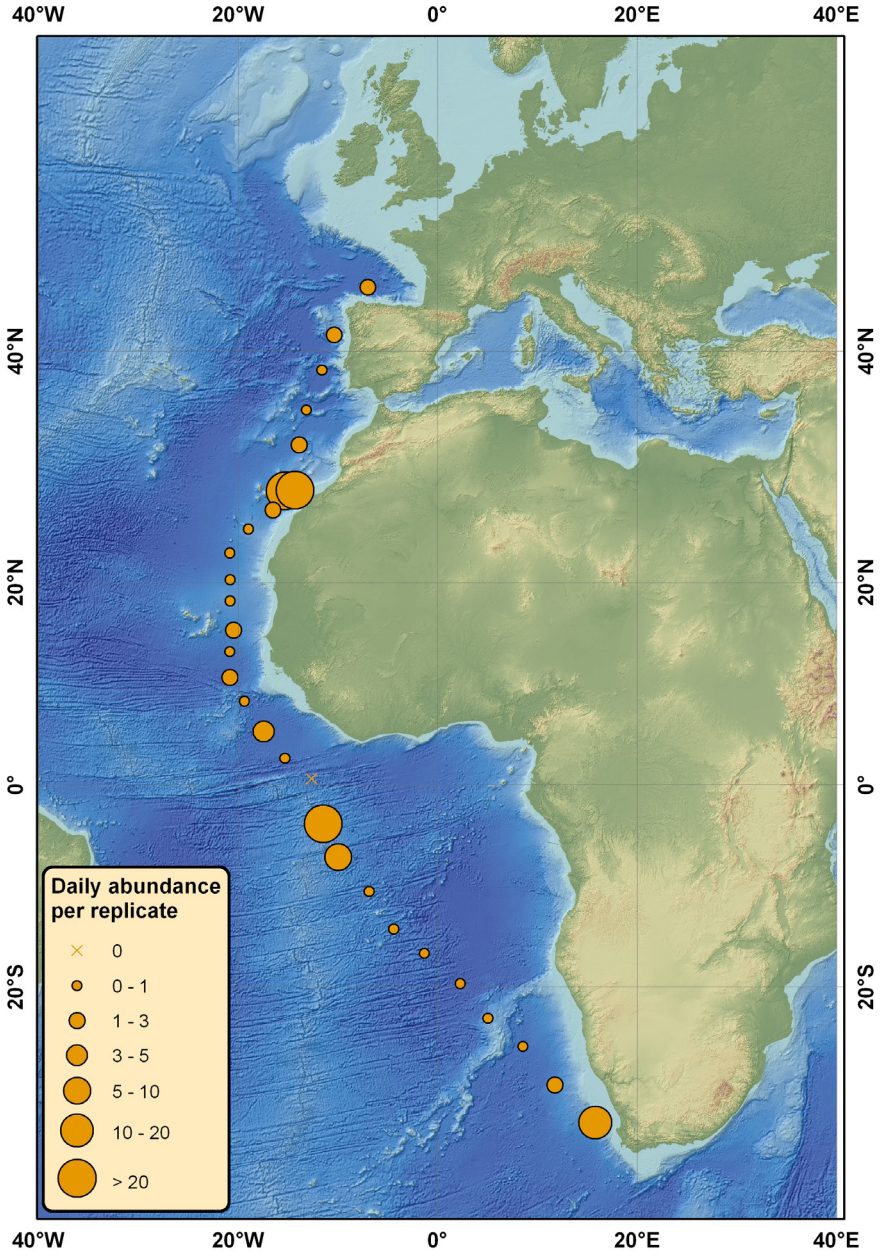

Fig. 14.2: Daily mean abundance per replicate of seabirds during PS83 (ANT XXIX/10)

The long south-north expedition of *Polarstern* covers the distributional areas of a lot of different bird and mammal species. Only three days after leaving Cape Town we reached the northern distribution limit of albatrosses. The most frequent species of this family was the shy albatross *Thalassarche cauta (*Fig. 14.3 left). The seabird showing the largest south-north distribution was Cory´s shearwater *Calonectris diomedea* (Fig. 14.3 right top) from 33° South to 38° North. Occasionally vagrants appear quite far offshore and utilize ships as resting places. Amongst others we observed a juvenile peregrine falcon *Falco peregrinus* travelling a few days with *Polarstern* (Fig. 14.3 right bottom).

Fig. 14.3: (left) Shy albatross Thalassarche cauta, (right top) Cory´s shearwater Calonectris diomedea, (right bottom) peregrine falcon Falco peregrinus. © Simon Jungblut, PolE.

Cetaceans were sighted relatively rarely. Especially larger whales, usually not attracted by sailing ships, were detected only in larger distances from the vessel and are thus sometimes difficult to identify. As body parts were often not visible and blows in many cases did not allow species identification, a large proportion goes into the category of unidentified “large whales” (Tab. 14.1). However, dolphins are sometimes attracted by sailing ships and thus relatively easy to observe. Some examples for sighted cetaceans are given in Fig. 14.4.

Outlook

Water temperature and salinity will be plotted in dependence to latitude. Limits of latitudinal zones and thus water masses will defined by sharp changes of temperature and salinity allowed the allocation of subsequent replicates exactly to one zone or the other.

Observation data of seabirds and marine mammals of the current PS83 (ANT-XXIX/10) and three previous expeditions (ANT-XXVIII/1, ANT-XXVIII/5 and ANT-XXIX/1) will be analysed together for the importance of hydrological parameters regarding the at-sea distribution of these animals.

Fig. 14.4: (left) Long-finned pilot whale Globicephala melas, (middle top) Risso´s dolphin Grampus griseus, (middle bottom) fin whale Balaenoptera physalus, (right) common dolphin Delphinus delphis. © Simon Jungblut & Dominik Nachtsheim, PolE.

Data management

All seabird and marine mammal data are available in the PolE dataset (contact: crjoiris@gmail.com).

References

Joiris CR, Falck E (2011) Summer at-sea distribution of little auks *Alle alle* and harp seals *Pagophilus (Phoca) groenlandica* in the Greenland Sea: impact of small-scale hydrological events. Polar Biology 34: 541 – 548.

15. SEA TRIALS AND SYSTEM APPROVAL OF THE MULTIBEAM SONAR "HYDROSWEEP DS III"

Boris Dorschel[1)], Ralf Krocker[1)], Joachim Reuter[3)], Johannes Rogenhagen[2)]

[1]AWI
[2]RFL
[3]ATLAS Hydrographic

Objectives

In 2010, ATLAS HYDROSWEEP DS 2 was updated to the new version ATLAS HYDROSWEEP DS3 (HS-DS3). The objectives during PS83 (ANT XXIX/10) were to perform a patch test in order to update the calibration of the constant installation offsets of the HS-DS3 and to perform a Sea Acceptance Test (SAT) for the HS-DS3.

The Patch test included:

- a time latency calibration
- a pitch calibration
- a roll calibration
- a heading calibration.

For the SAT, the HS-DS3 was operated under expedition conditions. In addition to general operational tests, the SAT included:

- a performance test for the depth range 100 - 1,000 m water depth
- a performance test for the depth range 1,000 - 5,000 m water depth
- a test of the automatic mean sound velocity (c-mean) calculation feature
- a 48 hour operational test

Work at sea

The HS-DS3 calibration and SAT were performed at the Ampére Seamount (Fig. 15.1), in the Bay of Biscay abyssal plain (Fig. 15.2) and on the Celtic Shelf (Fig. 15.3). At all survey sites, sound velocity profiles were recorded for accurate depth calculations during data acquisition and post-processing (tab. 15.1, Fig. 15.1-3).

At the Ampére Seamount, the work at sea started with the time latency calibration on 3 April at 05:48 UTC. For the time latency calibration, a transect on the northwest flank was surveyed with 10 kn from the foot of the seamount to the summit. This transect was repeated with 3 kn again from the foot of the mount to the summit. On the same transect, the pitch calibration was performed. For the pitch calibration, the transect was recorded twice with a constant speed of 5 kn but in opposite directions. After this, the roll calibration was performed along a transect in the flat area to the north of the Ampére Seamount (Fig. 15.1). This transect was recorded twice with 5 kn in opposite directions. Finally, for the heading calibration, a small obstacle to the North of the Ampére Seamount was surveyed. This obstacle was covered by 2 transects with 5

kn in opposite direction with an offset of 2.5 nm (Fig. 15.1). In addition, a comparison transect was recorded with 10 kn along the track of an existing line and 2 slope-parallel transects were recorded with 5 kn for data quality control from northern flank of the Ampére Seamount. In order to overlap centre beams with outer beams, these transects were offset by approximately 2 nm. On 4 April at 14:43 UTC, the work at the Ampére Seamount site was completed.

During the transit to the 2nd survey area in the Bay of Biscay, the 48 hour operational test was performed as part of the SAT. The test started on 4 April at 16:00 UTC and ended on 6 April at 16:00 UTC.

In the Bay of Biscay, the work at sea started on 7 April at 23:24 UTC with the test of the automatic mean sound velocity (c-mean) calculation feature. The results of the c-mean test were compared to a sound velocity profile measured with the ship's Valeport® sound velocity probe. After the c-mean test, the performance test for a higher depth range (1,000 - 5,000 m water depth) was conducted as part of the SAT. For this test, a previously mapped area was surveyed along 5 north-south, 5 east-west and 2 diagonal transects (Fig. 15.2). The work in the Bay of Biscay was finished on the 8 April at 20:00 UTC.

The last part of the SAT, the performance test for a lower depth range (100 - 1,000 m water depth), was performed on the Celtic Shelf at approximately 200 m water depth. In this area, the work started on 9 April at 20:15 UTC. For the SAT, 2 cross lines of 2 nm each and a sound velocity water column profile were recorded (Fig. 15.3). The work in the survey area on the Celtic Shelf and also the working programme during this cruise was completed on 9 April at 22:17 UTC.

Preliminary (expected) results

The calibration of the HS-DS3 and all tests of the SAT were performed successfully.

Data management

The data collected during the cruise will be stored in the AWI data repository and can be made available by the AWI Bathymetry group.

Images caption

Tab. 15.1: Valeport SVP casts

Station	Date time (begin) [UTC]	Position	Depth
PS83/383	2014/04/03 02:05	34°50.0′ N 013°00.0′ W	1970 m
PS83/387	2014/04/04 10:58	35°10.5′ N 012°49.5′ W	2454 m
PS83/394	2014/04/08 20:21	45°37.0′ N 005°17.0′ W	2992 m
PS83/398	2014/04/09 20:15	47°34.3′ N 006°59.7′ W	195 m

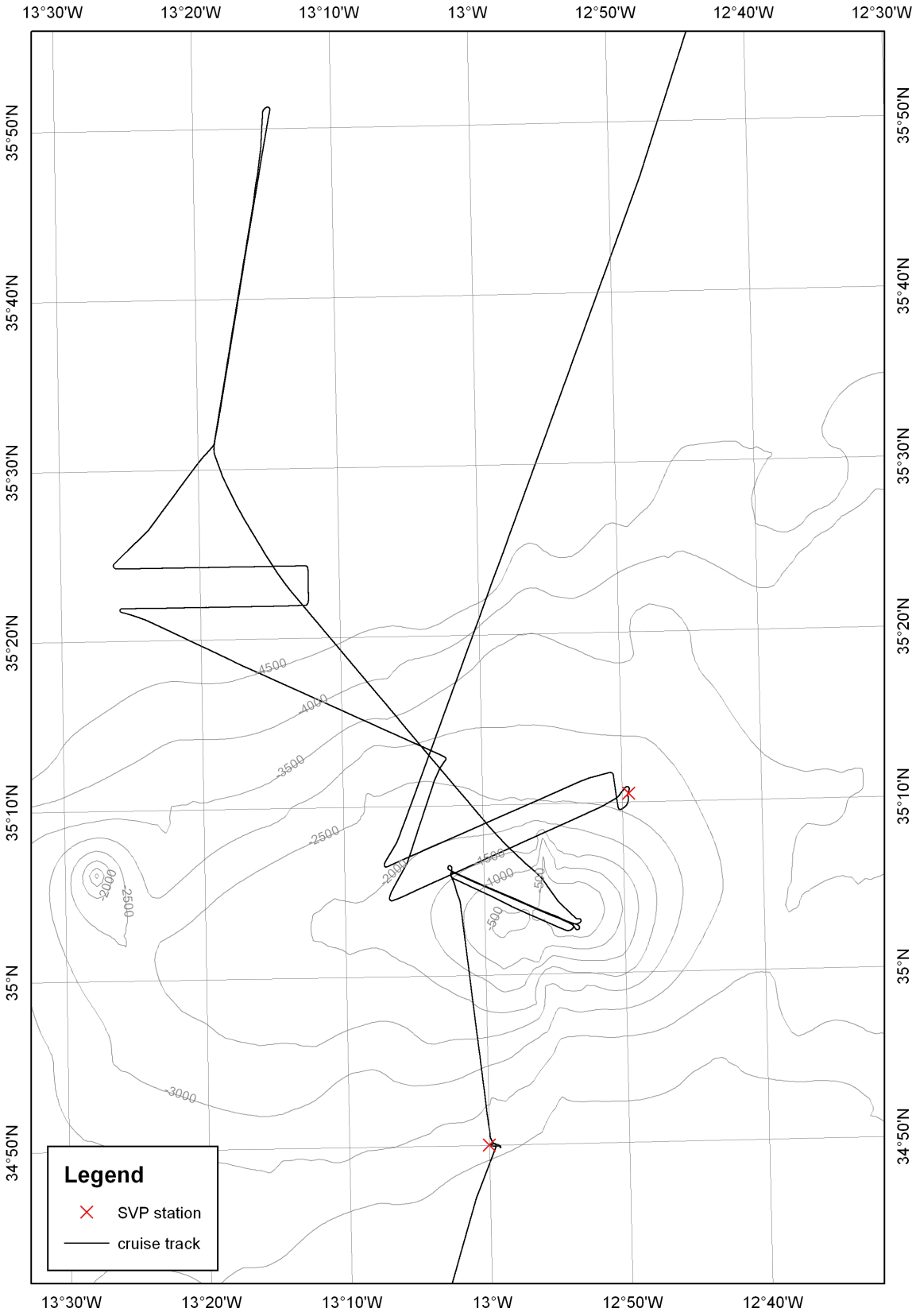

Fig. 15.1: Survey area at the Ampére Seamount

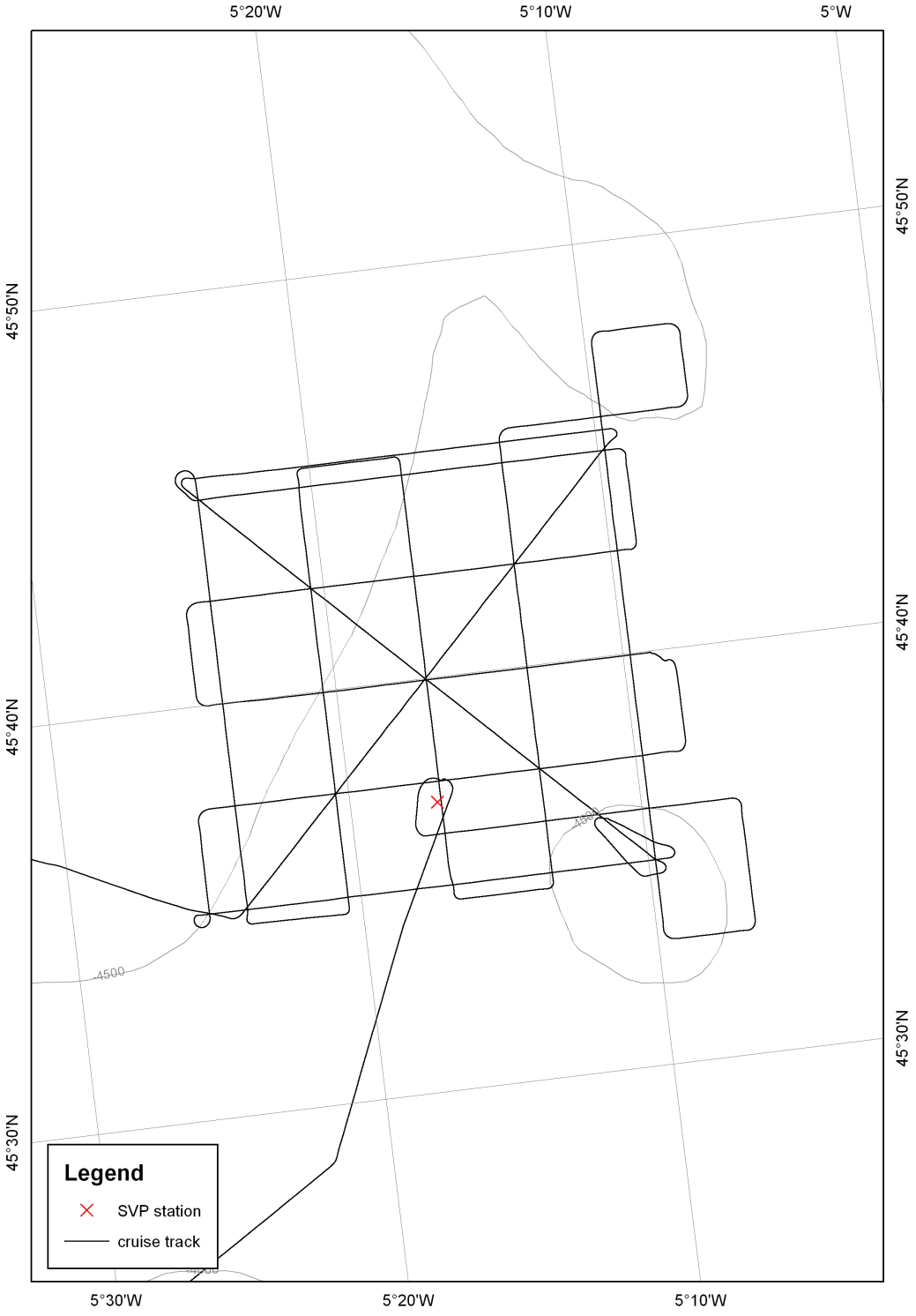

Fig. 15.2: Survey area in the Bay of Biscay

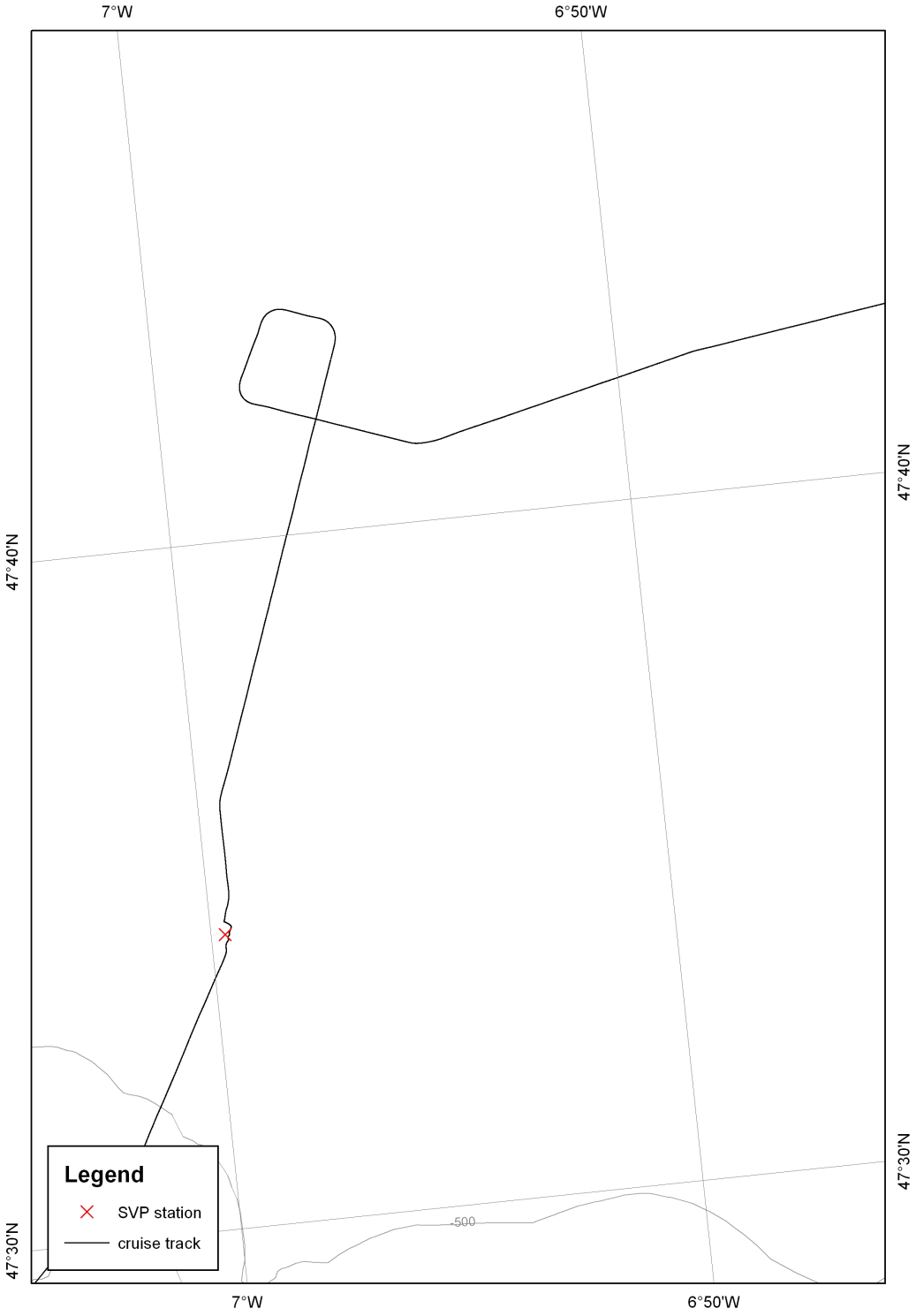

Fig. 15.3: Survey area on the Celtic shelf

16. SEA TRIALS OF THE TOWED UNDULATING VEHICLE TRIAXUS

Sören Krägefsky[1], Daniel Stepputtis[2], Volker Strass[1], Ulf Böttcher[2],
Andriy Martynenko[3], Alexander Davidov[4],
Heiko Lilienthal[5] (not on board)

[1] AWI
[2] Thünen-Institut f. Ostseefischerei
[3] Thünen-Institut f. Seefischerei
[4] MBT GmbH
[5] ISITEC

Objectives

The coupling between the atmosphere and the ocean, the exchange of momentum and heat as well as of gases such as oxygen and carbon dioxide, is mediated by turbulent motions in the – typically tens of metres thick – upper ocean mixed layer. Since the mixed layer also is the best sun-lit layer, it supports most of the phytoplankton photosynthesis hence primary production of the ocean. The primary production constitutes the basis of the whole marine food web, which not only sustains fisheries but also the biological pump of carbon that sequesters CO_2 from the atmosphere. Upper ocean mixing is modulated by the mesoscale dynamics associated with ocean eddies and fronts. The mesoscale – extending over horizontal scales from about 1 Km to a few 100s of Km - represents the most energetic scale of the ocean. Mesoscale upwelling events can enhance primary production by supply of nutrients from below the mixed layer.

The interaction of physical, chemical and biological processes at this wide range of horizontal scales, and the interdependency of marine species at different trophic levels, such as phytoplankton, zooplankton, fishes and top predators, creates a highly complex system that is only marginally understood. However, better understanding is needed for projecting future changes which the marine ecosystems might face during the course of climate change and because of other anthropogenic pressures, such as the harvesting of marine living resources.

Obtaining in-situ data which provide a better insight into this complex system on the relevant spatial and temporal scales represents a challenge. It requires near-synoptic measurements of physical, chemical and biological variables with a high temporal and spatial coverage and resolution. Towed vehicles that undulate vertically are well suited carrier systems allowing for synergistic integration of multi-disciplinary instruments and sensors.

Especially promising among the family of towed undulating vehicles is the TRIAXUS, recently developed by MacArtney, Denmark, because it has been designed to carry a wide range of sensor payload. Additionally, it allows for towing with some horizontal offset from the ship's track – and thus for sampling the important near-surface layer outside the propeller wash in undisturbed water. The main objective of the work during PS83 (ANT-XXIX/10) was rigorously testing the performance of a TRIAXUS at sea. The tested TRIAXUS system, complete with vehicle, cable, winch and control computers, was provided by the Thünen-Institute for Baltic Sea Fisheries Research, Rostock and Thünen-Institute of Sea Fisheries, Hamburg.

Work at sea

Work at sea began immediately after embarking *Polarstern* in the harbour of Las Palmas, Gran Canaria, with the procedure of buoyancy adjustment of the TRIAXUS. These adjustments

were conducted in the harbour because it provided a calm environment without high waves. The purpose of this procedure was to make the vehicle slightly buoyant, so that it rests well levelled at the sea surface if no other forces act on it. While levelling helps to improve the flight characteristics, assuring slightly positive buoyancy is aimed at preventing the loss of the vehicle in case the towing cable breaks just in front of it during deployments at sea. The buoyancy adjustment procedure was carried out for the different configurations of payload that were planned to be included in the tests. The weights in water of the different instruments were compensated by changing the numbers of hard foam buoyancy elements included within the TRIAXUS body tubes. The number of buoyancy elements needed for the different payload configurations was noted for the later changes of instruments during the sea trials. For testing, three different payload configurations were foreseen: 1. the basic instrumentation ('naked' TRIAXUS) including EdgeTech side scan sonar transducers on each lower tube, 2. basic configuration plus a SeaBird 911 CTD with one T-C pumped sensor duct and a Brooke's LOPC (Laser Optical Particle Counter), 3. configuration 2 plus an image-based optical plankton detection and enumeration system type ISITEC LOKI.

During the sea trials, TRIAXUS was deployed and towed using the A-frame. The winch holding the 10.2 mm diameter towing cable was fixed mid-ship on the aft deck. Sea conditions during the tests were characterized by weak to fresh winds (generally below 6 Bft) and moderate swell heights of maximum 3 m. The tests were conducted by systematically changing parameters that are expected to influence the performance of the vehicle. Towing speeds were varied between 4 and 10 knots, length of towing cable paid out between 350 and 2,500 m, vertical speeds of the vehicle during descents and ascents between 0.5 and 1 m s^{-1}, horizontal offset angles (flap angles) up to 5 degrees, and maximum allowed cable tension loads between 19.200 and 21.000 N.

The achieved horizontal offset was monitored using ultra-short baseline (USBL) acoustic positioning of the vehicle relative to the ship. However, this test was carried out at maximum ship speeds of 4 and 6 knots only, limited by the specification of the acoustic receiver that was mounted in the ship's moon pool.

Preliminary results

Seeking a balanced compromise between towing as fast as possible and achieving an as large as possible vertical profiling range of the vehicle at high horizontal resolution, the best performance was found at a towing speed of roughly 8 knots, with a length of paid out cable of 1500 m, an ascent/descent velocity of 0.8 m s^{-1} and a tension limit of 20.000 N. With this parameter setting, the vehicle profiled between less than 10 m and almost 300 m depth. This corresponds to a horizontal resolution of roughly 1,500 m at the upper and lower turning points, respectively, or 750 m at mid-depth between ascending and descending tracks of the vehicle along its sawtooth-like path through the water column.

A detrimental influence of the payload on the vehicles flight performance could not be identified, at least not by comparison of the configurations basic and basic plus LOPC. However, we did not test a payload configuration including LOKI. Unfortunately, the bandwidth of the two optic fibres in the cable, needed to transmit the images taken by LOKI via GBit-Ethernet, apparently were partly damaged in one of the lower cable layers on the winch, causing significantly reduced communication performance. Since this damage could not be repaired by on-board means, LOKI was not deployed.

The USBL positioning test confirmed the ability of TRIAXUS to profile in offset mode, sheared out to the side of the ship track. At a towing speed of 4 knots, a cable length of 350 m and an offset angle of 5°, the vehicle was monitored profiling 114 m aside of the track line of the ship's centre or approximately 100 m outside of the propeller wash. This suggests TRIAXUS

indeed makes possible to take measurements in the mixed layer that are widely undisturbed by influences from the ship.

Our sea trials also yielded some suggestions for further improvements of the TRIAXUS system, regarding the vehicle itself (relative mount of rear wings and flaps for up and downward motion), the cable termination, the winch (e.g. tension meter) and the control software. These suggestions are communicated to the manufacturer for consideration.

Data management

Does not apply.

Fig. 16.1: TRIAXUS at rest on the aft deck of Polarstern after towing

APPENDIX

A.1 PARTICIPATING INSTITUTIONS

A.2 CRUISE PARTICIPANTS

A.3 SHIP'S CREW

A.4 STATION LIST

A.1 BETEILIGTE INSTITUTE/ PARTICIPATING INSTITUTIONS

	Adresse **Address**
ATLAS	ATLAS Elektronik GmbH Sebaldsbrücker Heerstr. 235 28309 Bremen/Germany
AWI	Alfred-Wegener-Institut für Polar- und Meeresforschung Am Handelshafen 12 27570 Bremerhaven/ Germany
DWD	Deutscher Wetterdienst Hamburg Abteilung Seeschifffahrt Bernhard-Nocht Str. 76 20359 Hamburg / Germany
GEOMAR	Leibniz-Institut für Meereswissenschaften GEOMAR Düsternbrooker Weg 20 24105 Kiel/ Germany
KIT Karlsruhe	Karlsruhe Institute of Technology Kaiserstraße12 76131Karlsruhe/Germany
MBT Kiel	Meerestechnisches Büro Turla Wischhofstrasse 1-3 24148 Kiel/Germany
MPI-MET	Max-Planck-Institut für Meteorologie Bundesstraße 53, 20146 Hamburg/Germany
NOAA ESRL	NOAA/ESRL/PSD 325 Broadway Boulder, CO 80305-3328 USA
TI Rostock	Thünen –Institut für Ostseefischerie Alter Hafen Süd 2 18069 Rostock/Germany
PolE	Laboratory for Polar Ecology (*PolE*) rue du Fodia 18 B-1367 Ramillies, Belgium

	Adresse **Address**
TROPOS	Leibniz-Institut für Troposphärenforschung e.V. Permoserstraße 15 D-04318 Leipzig/Germany
Uni Göttingen	Georg-August-Universität Göttingen Wilhelmsplatz 1 37073 Göttingen
Uni Leipzig	Universität Leipzig P.O. Box 100920 D-04009 Leipzig/Germany

A.2 FAHRTTEILNEHMER / CRUISE PARTICIPANTS

	Name/ Last name	Vorname/ First name	Institut/ Institute	Beruf/ Profession
1	Arnhold	Tilo	TROPOS Leipzig	Journalist
2	Badeke	Ronny	TROPOS Leipzig	Student, Geo Sciences
3	Barthel	Stefan	TROPOS Leipzig	Meteorologist
4	Bertleff	Marco	KIT Karlsruhe	Scientist, Geo Sciences
5	Bley	Sebastian	TROPOS Leipzig	Student, Geo Sciences
6	Bock	Christian	AWI	Physicist
7	Böhmer	Astrid	AWI	Biologist
8	Böttcher	Ulf	TI Rostock	Engineer
9	Davidov	Alexander	MBT Kiel	Engineer
10	Deneke	Hartwig	TROPOS Leipzig	Scientist, Geo Sciences
11	Dorschel	Boris	AWI	Scientist, Geo Sciences
12	Foth	Andreas	Uni Leipzig	Meteorologist
13	Fricke	Margarete	./.	Technician
14	Fricke	Wolfgang	./.	Meteorologist
15	Fuchs	Susanne	TROPOS Leipzig	Technician
16	Gerchow	Peter	AWI	Engineer
17	Gravenhorst	Gode	Uni Göttingen	Chemicist
18	Hempelt	Juliane	DWD	Technician
20	Jungblut	Simon	PolE Ramilliers	Student, Biology
21	Klappenbach	Friedrich	KIT Karlsruhe	Scientist, Geo Sciences
22	Kostinek	Julian	KIT Karlsruhe	Scientist, Geo Sciences
23	Krägefsky	Sören	AWI	Scientist, Bio Sciences
24	Krieten	Guido	AWI	Engineer
25	Krocker	Ralf	AWI	Engineer
26	Martynenko	Andriy	TI Hamburg	Engineer
27	Merkel	Maik	TROPOS Leipzig	Scientist, Geo Sciences
28	Miller	Max	DWD	Meteorologist
29	Nachtsheim	Dominik André	PolE Ramilliers	Student, Bio Sciences
30	Pezoa	Sergio	NOAA ESRL	Engineer
31	Pilch Kedzierski	Robin Norbert	Geomar Kiel	Scientist, Geo Sciences
32	Popke	Dagmar	MPIMET-HH	Scientist, Geo Sciences
33	Rädel	Gaby	MPIMET-HH	Scientist, Geo Sciences
34	Reuter	Joachim	Atlas El. Bremen	Engineer
35	Rogenhagen	Johannes	Reederei Laeisz	Engineer
36	Stepputtis	Daniel	TI Rostock	Oceanographist
37	Strass	Volker	AWI	Oceanographist
38	Walther	Jonas	TROPOS Leipzig	Student, Geo Sciences
39	Wang	Wuke (Mr.)	Geomar Kiel	Student, Geo Sciences
40	Wetjen	Maj	AWI	Biologist.

A.3 SCHIFFSBESATZUNG/SHIP'S CREW

No.	Name	Rank
1	Wunderlich, Thomas	Master
2	Spielke, Steffen	1st Offc.
3	Ziemann, Olaf	Ch.Eng.
4	Hering, Igor	2nd Offc.
5	Kentges, Felix	2nd Offc.
6	Lauber, Felix	2nd Offc.
7	Spilok, Norbert	Doctor
8	Fröb, Martin	Comm. Elo
9	Herde, Bernd	2nd Eng.
10	Kotnik, Herbert	2nd Eng.
11	Westphal, Henning	2nd Eng.
12	Brehme, Andreas	Elec. Eng.
13	Dimmler, Werner	ELO
14	Feiertag, Thomas	ELO
15	Ganter, Armin	ELO
16	Winter, Andreas	ELO
17	Schröter, Réné	Boatsw.
18	Neisner, Winfried	Carpenter
19	Burzan, Gerd-Ekkeh.	A.B.
20	Clasen, Nils	A.B.
21	Gladow, Lothar	A.B.
22	Hartwig-Lab., Andreas	A.B.
23	Kreis, Reinhard	A.B.
24	Kretzschmar, Uwe	A.B.
25	Moser, Siegfried	A.B.
26	Schröder, Norbert	A.B.
27	Beth, Detlef	Storek.
28	Dinse, Horst	Mot-man
29	Fritz, Günter	Mot-man
30	Krösche, Eckard	Mot-man
31	Plehn, Markus	Mot-man
32	Watzel, Bernhard	Mot-man
33	Fischer, Matthias	Cook
34	Tupy, Mario	Cooksmate
35	Völkse, Thomas	Cooksmate
36	Dinse, Petra	1. Stwdess
37	Westphal, Kerstin	Stwdss/N.
38	Chen, Quan Lun	2. Steward
39	Hischke, Peggy	2. Steward
40	Sun, Yong Sheng	2. Steward
41	Streit, Christian	2. Steward
42	Wartenberg, Irina	2. Steward
43	Ruan, Hui Guang	Laundrym.

A.4 STATIONSLISTE/STATION LIST PS83

Station	Date	Time	Gear	Action	Pos. Lat.	Pos. Lon	Depth
PS83/0367-1	11.03.2014	11:15	ZODIAK	profile start	25° 29,86‘ S	8° 29,63‘ E	4750,5
PS83/0368-1	12.03.2014	11:08	ZODIAK	profile end	23° 8,61‘ S	5° 3,43‘ E	2683,2
PS83/0368-1	12.03.2014	14:40	SATP	on ground/ max depth	22° 32,78‘ S	4° 54,85‘ E	3597,2
PS83/0369-1	13.03.2014	12:17	SATP	on ground/ max depth	19° 35,56‘ S	2° 10,75‘ E	5467,2
PS83/0370-1	14.03.2014	12:05	ZODIAK	profile start	16° 50,06‘ S	1° 19,49‘ W	4968,0
PS83/0370-2	14.03.2014	12:22	ZODIAK	profile end	16° 50,09‘ S	1° 19,53‘ W	4969,0
PS83/0371-1	15.03.2014	12:04	SATP	on ground/ max depth	14° 7,75‘ S	4° 45,62‘ W	4336,0
PS83/0372-1	15.03.2014	12:40	SATP	on ground/ max depth	14° 6,40‘ S	4° 46,54‘ W	4061,2
PS83/0372-1	15.03.2014	16:30	SVP	on ground/ max depth	13° 51,06‘ S	4° 49,98‘ W	4110,0
PS83/0373-1	16.03.2014	12:04	HS_PS	profile start	10° 45,54‘ S	6° 50,87‘ W	4057,2
PS83/0374-1	17.03.2014	12:01	HS_PS	profile end	7° 23,15‘ S	9° 54,11‘ W	3262,5
PS83/0375-1	18.03.2014	1:01	HS_PS	on ground/ max depth	6° 3,99‘ S	11° 25,05‘ W	2862,5
PS83/0375-1	18.03.2014	3:30	HS_PS	on ground/ max depth	5° 38,49‘ S	11° 19,64‘ W	2523,0
PS83/0376-1	18.03.2014	12:03	HS_PS	profile start	3° 58,77‘ S	11° 28,14‘ W	2858,0
PS83/0377-1	20.03.2014	12:08	HS_PS	profile end	2° 34,78‘ N	15° 13,08‘ W	4722,7
PS83/0378-1	21.03.2014	1:51	HS_PS	on ground/ max depth	3° 53,84‘ N	17° 2,09‘ W	4952,0
PS83/0378-1	21.03.2014	4:56	HS_PS	profile start	4° 26,00‘ N	16° 55,19‘ W	4974,5
PS83/0379-1	21.03.2014	12:05	HS_PS	profile end	5° 18,44‘ N	17° 27,48‘ W	4972,2
PS83/0380-1	22.03.2014	12:05	HS_PS	profile start	8° 18,17‘ N	19° 18,95‘ W	4361,2
PS83/0381-1	23.03.2014	12:02	HS_PS	profile end	10° 58,88‘ N	21° 0,25‘ W	5047,2
PS83/0382-1	25.03.2014	13:00	HS_PS	profile start	15° 30,80‘ N	20° 27,90‘ W	3756,2
PS83/0382-1	25.03.2014	18:30	HS_PS	profile end	15° 42,60‘ N	20° 30,57‘ W	3735,2
PS83/0383-1	30.03.2014	12:12	HS_PS	profile start	26° 35,31‘ N	16° 37,84‘ W	3592,7
PS83/0384-1	31.03.2014	12:06	HS_PS	profile end	28° 21,28‘ N	14° 22,73‘ W	1701,2
PS83/0385-1	31.03.2014	13:41	HS_PS	profile start	28° 21,69‘ N	14° 17,16‘ W	210,2
PS83/0385-1	31.03.2014	18:54	HS_PS	profile end	29° 22,26‘ N	14° 32,60‘ W	3481,0
PS83/0386-1	03.04.2014	3:18	HS_PS	profile start	34° 49,95‘ N	12° 59,26‘ W	3950,8
PS83/0387-1	03.04.2014	5:48	HS_PS	profile end	35° 6,01‘ N	13° 1,99‘ W	1808,0
PS83/0387-1	03.04.2014	6:31	HS_PS	profile start	35° 3,04‘ N	12° 54,09‘ W	161,6

Station	Date	Time	Gear	Action	Pos. Lat.	Pos. Lon	Depth
PS83/0387-1	03.04.2014	7:26	SVP	profile end	35° 6,00‘ N	13° 1,91‘ W	1767,2
PS83/0387-1	03.04.2014	9:45	ZODIAK	profile start	35° 2,99‘ N	12° 53,99‘ W	139,4
PS83/0387-1	03.04.2014	10:01	HS_PS	profile end	35° 3,02‘ N	12° 53,92‘ W	136,9
PS83/0387-1	03.04.2014	11:33	HS_PS	profile start	35° 6,05‘ N	13° 2,05‘ W	1792,1
PS83/0387-1	03.04.2014	11:45	ZODIAK	profile end	35° 6,03‘ N	13° 2,04‘ W	1823,9
PS83/0387-1	03.04.2014	13:12	TRIAXUS	profile start	35° 3,05‘ N	12° 54,04‘ W	137,5
PS83/0387-1	03.04.2014	17:29	TRIAXUS	profile end	35° 31,78‘ N	13° 18,76‘ W	4856,4
PS83/0387-1	03.04.2014	19:21	ZODIAK	on ground/ max depth	35° 46,51‘ N	13° 15,45‘ W	4875,7
PS83/0387-1	03.04.2014	20:32	TRIAXUS	on ground/ max depth	35° 46,56‘ N	13° 15,53‘ W	4867,3
PS83/0387-1	03.04.2014	22:25	TRIAXUS	profile start	35° 31,72‘ N	13° 18,78‘ W	4871,0
PS83/0387-1	03.04.2014	23:16	SVP	profile end	35° 24,29‘ N	13° 25,68‘ W	4870,7
PS83/0387-1	04.04.2014	1:24	HS_PS	profile end	35° 24,29‘ N	13° 12,73‘ W	4894,5
PS83/0387-1	04.04.2014	1:46	HS_PS	profile start	35° 21,95‘ N	13° 12,96‘ W	4919,4
PS83/0387-1	04.04.2014	3:52	HS_PS	profile end	35° 21,94‘ N	13° 25,53‘ W	4870,0
PS83/0387-1	04.04.2014	4:34	HS_PS	profile start	35° 18,59‘ N	13° 17,36‘ W	4759,1
PS83/0387-1	04.04.2014	5:55	HS_PS	profile end	35° 12,98‘ N	13° 2,86‘ W	2569,0
PS83/0387-1	04.04.2014	6:47	HS_PS	profile start	35° 4,56‘ N	13° 6,36‘ W	1931,8
PS83/0387-1	04.04.2014	9:26	SVP	profile end	35° 9,73‘ N	12° 51,61‘ W	2462,5
PS83/0388-1	04.04.2014	10:59	ZODIAK	on ground/ max depth	35° 9,83‘ N	12° 49,68‘ W	2653,1
PS83/0389-1	04.04.2014	11:05	HS_PS	on ground/ max depth	35° 9,80‘ N	12° 49,73‘ W	2642,3
PS83/0387-1	04.04.2014	12:20	HS_PS	profile start	35° 11,36‘ N	12° 52,72‘ W	2714,4
PS83/0387-1	04.04.2014	14:50	ZODIAK	profile end	35° 6,51‘ N	13° 6,86‘ W	2092,4
PS83/0390-1	05.04.2014	11:00	TRIAXUS	on ground/ max depth	38° 15,29‘ N	11° 44,37‘ W	5063,5
PS83/0391-1	05.04.2014	17:23	TRIAXUS	profile start	38° 58,84‘ N	11° 24,85‘ W	3533,2
PS83/0391-1	06.04.2014	8:30	ZODIAK	profile end	40° 52,38‘ N	10° 34,14‘ W	4394,1
PS83/0392-1	06.04.2014	11:05	TRIAXUS	on ground/ max depth	41° 10,26‘ N	10° 25,64‘ W	4077,9
PS83/0393-1	06.04.2014	12:03	TRIAXUS	profile start	41° 9,41‘ N	10° 25,25‘ W	4104,6
PS83/0393-1	06.04.2014	13:24	SVP	profile end	41° 13,16‘ N	10° 23,38‘ W	3865,1
PS83/0394-1	07.04.2014	21:41	HS_PS	on ground/ max depth	45° 37,54‘ N	5° 16,70‘ W	4611,3
PS83/0395-1	07.04.2014	22:58	HS_PS	profile start	45° 36,24‘ N	5° 17,60‘ W	4612,9
PS83/0395-1	08.04.2014	0:28	HS_PS	profile end	45° 34,93‘ N	5° 9,78‘ W	4559,5

Station	Date	Time	Gear	Action	Pos. Lat.	Pos. Lon	Depth
PS83/0395-1	08.04.2014	0:28	HS_PS	profile start	45° 34,93‘ N	5° 9,78‘ W	4559,5
PS83/0395-1	08.04.2014	1:31	HS_PS	profile end	45° 45,44‘ N	5° 9,78‘ W	4551,5
PS83/0395-1	08.04.2014	2:42	HS_PS	profile start	45° 45,00‘ N	5° 13,37‘ W	4587,1
PS83/0395-1	08.04.2014	3:43	HS_PS	profile end	45° 35,08‘ N	5° 13,37‘ W	4572,7
PS83/0395-1	08.04.2014	4:04	HS_PS	profile start	45° 34,97‘ N	5° 16,82‘ W	4572,9
PS83/0395-1	08.04.2014	5:04	HS_PS	profile end	45° 44,94‘ N	5° 16,88‘ W	4606,2
PS83/0395-1	08.04.2014	5:26	HS_PS	profile start	45° 44,97‘ N	5° 20,44‘ W	4617,3
PS83/0395-1	08.04.2014	6:26	HS_PS	profile end	45° 35,08‘ N	5° 20,47‘ W	4586,4
PS83/0395-1	08.04.2014	6:47	HS_PS	profile start	45° 34,92‘ N	5° 23,99‘ W	4591,7
PS83/0395-1	08.04.2014	7:45	SVP	profile end	45° 44,57‘ N	5° 23,98‘ W	4623,4
PS83/0395-1	08.04.2014	7:57	ZODIAK	profile start	45° 45,26‘ N	5° 24,48‘ W	4632,9
PS83/0395-1	08.04.2014	8:57	HS_PS	profile end	45° 44,98‘ N	5° 10,14‘ W	4561,7
PS83/0395-1	08.04.2014	9:15	HS_PS	profile start	45° 42,76‘ N	5° 9,08‘ W	4565,8
PS83/0395-1	08.04.2014	10:18	ZODIAK	profile end	45° 42,51‘ N	5° 23,98‘ W	4627,1
PS83/0395-1	08.04.2014	10:38	TRIAXUS	profile start	45° 40,01‘ N	5° 24,14‘ W	4624,3
PS83/0395-1	08.04.2014	11:37	TRIAXUS	profile end	45° 39,98‘ N	5° 10,05‘ W	4572,9
PS83/0396-1	08.04.2014	11:50	ZODIAK	on ground/ max depth	45° 39,93‘ N	5° 8,96‘ W	4568,9
PS83/0395-1	08.04.2014	12:40	TRIAXUS	profile start	45° 37,52‘ N	5° 9,75‘ W	4565,8
PS83/0395-1	08.04.2014	13:40	TRIAXUS	profile end	45° 37,51‘ N	5° 24,01‘ W	4616,1
PS83/0395-1	08.04.2014	14:14	SVP	profile start	45° 34,99‘ N	5° 24,07‘ W	4593,4
PS83/0395-1	08.04.2014	15:14	HS_PS	profile end	45° 34,99‘ N	5° 9,83‘ W	4559,0
PS83/0395-1	08.04.2014	16:01	HS_PS	profile start	45° 35,01‘ N	5° 9,81‘ W	4542,7
PS83/0395-1	08.04.2014	17:25	HS_PS	profile end	45° 45,04‘ N	5° 24,02‘ W	4610,0
PS83/0395-1	08.04.2014	17:31	HS_PS	profile start	45° 45,51‘ N	5° 24,00‘ W	4612,6
PS83/0395-1	08.04.2014	18:30	HS_PS	profile end	45° 45,49‘ N	5° 9,80‘ W	4539,2
PS83/0395-1	08.04.2014	18:36	HS_PS	profile start	45° 45,04‘ N	5° 9,76‘ W	4538,2
PS83/0395-1	08.04.2014	20:00	HS_PS	profile end	45° 35,08‘ N	5° 23,92‘ W	4579,4
PS83/0397-1	08.04.2014	20:15	TRIAXUS	profile start	45° 35,05‘ N	5° 25,52‘ W	4563,8
PS83/0397-1	09.04.2014	12:49	TRIAXUS	profile end	46° 29,62‘ N	8° 28,19‘ W	4723,1
PS83/0398-1	09.04.2014	20:22	SVP	on ground/ max depth	47° 34,32‘ N	6° 59,64‘ W	198,4
PS83/0399-1	09.04.2014	21:26	HS_PS	profile start	47° 40,65‘ N	6° 57,15‘ W	170,2
PS83/0399-1	09.04.2014	21:41	HS_PS	profile end	47° 42,56‘ N	6° 56,12‘ W	155,7
PS83/0399-1	09.04.2014	22:03	HS_PS	profile start	47° 42,07‘ N	6° 58,12‘ W	158,7

Station	Date	Time	Gear	Action	Pos. Lat.	Pos. Lon	Depth
PS83/0399-1	09.04.2014	22:19	HS_PS	profile end	47° 41,29‘ N	6° 55,15‘ W	168,2
PS83/0400-1	10.04.2014	11:04	ZODIAK	on ground/ max depth	49° 21,45‘ N	4° 6,46‘ W	86,8

Die **Berichte zur Polar- und Meeresforschung** (ISSN 1866-3192) werden beginnend mit dem Band 569 (2008) als Open-Access-Publikation herausgegeben. Ein Verzeichnis aller Bände einschließlich der Druckausgaben (ISSN 1618-3193, Band 377-568, von 2000 bis 2008) sowie der früheren **Berichte zur Polarforschung** (ISSN 0176-5027, Band 1-376, von 1981 bis 2000) befindet sich im electronic Publication Information Center **(ePIC)** des Alfred-Wegener-Instituts, Helmholtz-Zentrum für Polar- und Meeresforschung (AWI); see http://epic.awi.de. Durch Auswahl “Reports on Polar- and Marine Research“ (via “browse”/”type”) wird eine Liste der Publikationen, sortiert nach Bandnummer, innerhalb der absteigenden chronologischen Reihenfolge der Jahrgänge mit Verweis auf das jeweilige pdf-Symbol zum Herunterladen angezeigt.

The **Reports on Polar and Marine Research** (ISSN 1866-3192) are available as open access publications since 2008. A table of all volumes including the printed issues (ISSN 1618-3193, Vol. 1-376, from 2000 until 2008), as well as the earlier **Reports on Polar Research** (ISSN 0176-5027, Vol. 1-376, from 1981 until 2000) is provided by the electronic Publication Information Center **(ePIC)** of the Alfred Wegener Institute, Helmholtz Centre for Polar and Marine Research (AWI); see URL http://epic.awi.de. To generate a list of all Reports, use the URL http://epic.awi.de and select “browse”/ ”type” to browse ”Reports on Polar and Marine Research”. A chronological list in declining order will be presented, and pdf-icons displayed for downloading.

Zuletzt erschienene Ausgaben:

Recently published issues:

683 (2014) The Expedition PS83 of the Research Vessel POLARSTERN to the Atlantic Ocean in 2014, edited by Hartwig Deneke

682 (2014) Handschriftliche Bemerkungen in Alfred Wegeners Exemplar von: Die Entstehung der Kontinente und Ozeane, 1. Auflage 1915, herausgegeben von Reinhard A. Krause

681 (2014) Und sie bewegen sich doch …Alfred Wegener (1880 – 1930): 100 Jahre Theorie der Kontinentverschiebung – eine Reflexion, von Reinhard A. Krause

680 (2014) The Expedition PS82 of the Research Vessel POLARSTERN to the southern Weddell Sea in 2013/2014, edited by Rainer Knust and Michael Schröder

679 (2014) The Expedition of the Research Vessel ‘Polarstern’ to the Antarctic in 2013 (ANT-XXIX/6), edited by Peter Lemke

678 (2014) Effects of cold glacier ice crystal anisotropy on seismic data, by Anja Diez

677 (2014) The Expedition of the Research Vessel “Sonne” to the Mozambique Ridge in 2014 (SO232), edited by Gabriele Uenzelmann-Neben

676 (2014) The Expedition of the Research Vessel “Sonne” to the Mozambique Basin in 2014 (SO230), edited by Wilfried Jokat

675 (2014) Polarforschung und Wissenschaftsutopien: Dargestellt und kommentiert am Beispiel von zehn Romanen aus der Zeit von 1831 bis 1934, von Reinhard A. Krause

674 (2014) The Expedition of the Research Vessel ‘Polarstern’ to the Antarctic in 2013 (ANT-XXIX/7), edited by Bettina Meyer and Lutz Auerswald

673 (2014) Airborne Measurements of Methane Fluxes in Alaskan and Canadian Tundra with the Research Aircraft ‘Polar 5’, by Katrin Kohnert, Andrei Serafimovich, Jörg Hartmann, and Torsten Sachs

ALFRED-WEGENER-INSTITUT
HELMHOLTZ-ZENTRUM FÜR POLAR-
UND MEERESFORSCHUNG

BREMERHAVEN

Am Handelshafen 12
27570 Bremerhaven
Telefon 0471 4831-0
Telefax 0471 4831-1149
www.awi.de

HELMHOLTZ
GEMEINSCHAFT